HYDROGEN SULFIDE ADSORPTION/OXIDATION ON CARBONACEOUS SURFACES AND ITS APPLICATION IN VAPOR PHASE MERCURY CONTROL

by

Wenguo Feng

B. E., Environmental Engineering, Dalian University of Technology, 1996

M. A. Sc., Chemical Engineering, University of Toronto, 2002

Submitted to the Graduate Faculty of

The School of Engineering in partial fulfillment

of the requirements for the degree of

Doctor of Philosophy

University of Pittsburgh

2005

UNIVERSITY OF PITTSBURGH

SCHOOL OF ENGINEERING

This dissertation was presented

by

Wenguo Feng

It was defended on

November 21st, 2005

and approved by

J. Karl Johnson, Professor, Department of Chemical Engineering

Leonard W. Casson, Associate Professor, Department of Civil and Environmental Engineering

Robert Ries, Assistant Professor, Department of Civil and Environmental Engineering

Eric Borguet, Associate Professor, Department of Chemistry, Temple University

Dissertation Director: Radisav D. Vidic, Professor, Department of Civil and Environmental Engineering

HYDROGEN SULFIDE ADSORPTION/OXIDATION ON CARBONACEOUS SURFACES AND ITS APPLICATION IN VAPOR PHASE MERCURY CONTROL

Wenguo Feng, PhD

University of Pittsburgh, 2005

Based on the concept of industrial ecology, this study investigated the interaction between hydrogen sulfide and carbonaceous surfaces, and the application of the resulting sulfur impregnated material for vapor phase mercury control. A fixed bed reactor system was used to study adsorption and oxidation of hydrogen sulfide and mercury uptake by carbonaceous materials. The carbon surface chemistry was characterized using state of the art techniques before and after sulfur impregnation.

Adsorption of hydrogen sulfide onto carbonaceous surfaces at low temperatures and under dry and anoxic conditions included both reversible and irreversible components. Reversible adsorption was affected mainly by pore structure and pore filling is likely the dominating mechanism. On the other hand, hydrogen sulfide retention (or irreversible adsorption) was affected by surface chemistry.

Retention of hydrogen sulfide occurred through strong and possibly dissociative surface interactions. The retained amount of hydrogen sulfide increased with an increase in the surface area. The retained amount of H_2S correlates well with the density of basic surface groups,

especially those derived from basic oxygen containing surface groups. Therefore, hydrogen sulfide retention was enhanced by surface treatments, such as heat treatment and ammonia treatment.

Sulfurization at temperatures between 200-800 ˚C resulted in high sulfur content and very stable sulfur forms such as organic sulfur. Higher temperatures also led to more uniform sulfur distribution inside the sorbent pores. Uptake of hydrogen sulfide under these conditions occurs as a result of substitution of the surface oxygen or active carbon atoms. The most effective mercury sorbents were produced by the reaction between H_2S and carbonaceous surface at 600 °C. The presence of H_2S during the cooling process increased the amount of relatively unstable species like elemental sulfur, and sorbents produced under these conditions also showed effective mercury uptake. It was found that sulfur forms are important parameters affecting mercury uptake; the amounts of elemental sulfur, thiophene, and sulfate showed good correlation with mercury uptake capacity, with active elemental sulfur species being the most effective.

Keywords: Hydrogen Sulfide (H_2S), Mercury (Hg), Activated Carbon, Activated Carbon Fiber, Adsorption, Sulfurization, Oxidation

TABLE OF CONTENTS

LIST OF TABLES ix

LIST OF FIGURES x

GLOSSARY xiii

ACKNOWLEDGEMENTS xiv

1.0 INTRODUCTION 1

1.1 MERCURY 1

1.1.1 Toxicity and Regulations 1

1.1.2 Sources and Discharge Conditions 2

1.2 HYDROGEN SULFIDE 4

1.2.1 Toxicity and Regulations 4

1.2.2 Sources and Discharge Conditions 5

1.3 MERCURY CONTROL BY HYDROGEN SULFIDE ADSORPTION/OXIDATION 6

1.4 OBJECTIVES AND SCOPE 7

2.0 LITERATURE REVIEW 9

2.1 ADSORPTION AND CATALYSIS 9

2.1.1 Physical and Chemical Adsorption 9

2.1.2 Surface Catalysis 11

2.1.3 The Micropore Filling Theory and DR Equation 12

2.2 CARBON SURFACE CHEMISTRY 14

2.2.1 Structure of Carbonaceous Materials 14
2.2.2 Oxygen Containing Functionalities 16
2.2.3 Characterization 17
2.2.4 Oxidation of Carbon Surface 18
2.2.5 Adsorption Properties 19
2.2.6 Nitrogen Containing Functionalities and Other Functionalities 21
2.2.7 Carbon Acidity and Basicity 23
2.2.8 Decomposition of Oxygen Containing Functionalities 25
2.2.9 Summary 28
2.3 MERCURY REMOVAL BY ADSORPTION 30
2.3.1 Mercury Control Technologies 30
2.3.2 Mercury Removal by Activated Carbon Injection 31
2.3.3 Sulfur Impregnated Activated Carbons 31
2.4 HYDROGEN SULFIDE ADSORPTION ON CARBON SURFACE 35
2.5 SULFURIZATION OF CARBON SURFACES 39
2.6 OXIDATION OF HYDROGEN SULFIDE ON ACTIVATED CARBON 43
3.0 MATERIALS AND METHODS 48
3.1 CARBON MATERIALS 48
3.1.1 Activated Carbon Fibers 48
3.1.2 Activated Carbons 50
3.2 EXPERIMENTAL SETUP AND PROCEDURE 51
3.2.1 Sample Preparation 51
3.2.2 H_2S Adsorption, Sulfurization, and Oxidation 52
3.2.3 Hg Uptake Test 57
3.3 SORBENT CHARACTERIZATION 58

3.3.1 Surface Area and Pore Structure Analysis 58
3.3.2 SEM-EDAX Analysis 58
3.3.3 XPS Analysis 58
3.3.4 Thermogravimetric Analysis 59
3.3.5 Temperature Programmed Desorption 59
3.3.6 Sulfur Analysis 60
3.3.7 Surface Functional Groups and pH Measurement 61
3.3.8 Ash and Metal Content Analysis 62
3.3.9 XAFS Analysis 62
4.0 RESULTS AND DISCUSSION 64
4.1 H_2S ADSORPTION ONTO ACFS 64
4.1.1 Characterization of Activated Carbon Fibers 64
4.1.2 Effect of Pore Structure and Surface Treatment on H_2S Uptake 67
4.1.3 Temperature Programmed Desorption 73
4.1.4 Summary 78
4.2 H_2S ADSORPTION ONTO ACTIVATED CARBONS 79
4.2.1 Characterization of Activated Carbons 79
4.2.2 Effect of Carbon Surface Chemistry on H_2S Uptake 81
4.2.3 Effect of Surface Treatment 86
4.2.4 Summary 90
4.3 SULFURIZATION OF ACFS AND BPL CARBON 91
4.3.1 Effect of Carbon Materials 91
4.3.2 Effect of Temperature 92
4.3.3 Effect of Sulfurization Protocol 99
4.3.4 Sulfur Distribution 100

4.3.5 Forms of Sulfurous Products --- XPS Results 101
4.3.6 Forms of Sulfurous Products on BPL --- XANES Results 103
4.3.7 Mercury Uptake Studies 105
4.3.8 Summary 113
4.4 OXIDATION OF H_2S ON ACFS FOR MERCURY UPTAKE 114
4.4.1 Structure of Raw ACFs 114
4.4.2 Sulfur Content and Distribution 114
4.4.3 Stability of Sulfur 120
4.4.4 Forms of Sulfur 124
4.4.5 Impact of Sulfur Content on Mercury Adsorption 127
4.4.6 Impact of Pore Volume and Surface Area on Mercury Adsorption 128
4.4.7 Summary 130
5.0 SUMMARY AND CONCLUSIONS 132
6.0 ENGINEERING SIGNIFICANCE OF THIS STUDY 136
6.1 DIRECT ENGINEERING APPLICATIONS 136
6.2 GENERAL IMPLICATIONS 138
7.0 RECOMMENDATIONS FOR FUTURE WORK 139
APPENDIX A. ADDITIONAL FIGURES 141
APPENDIX B. PHYSICAL PROPERTIES OF CHEMICALS 143
APPENDIX C. ELMENTAL SULFUR SUBLIMATION ENERGY CALCULATION 144
BIBLIOGRAPHY 145

LIST OF TABLES

Table 1. Flue gas from coal fired power plants and municipal waste incinerators [10] 4

Table 2. Differences between physical adsorption and chemical adsorption 11

Table 3. Properties of Kynol ACFs from literature and the manufacture 49

Table 4. Sources and chemical compositions of BPL and ACFs 50

Table 5. Micropore structure of ACFs before and after heat treatment 65

Table 6. Surface functionalities on raw ACFs determined by Boehm titration (mmol/g) 67

Table 7. Adsorbed, desorbed and retained amount (mg/g) of H_2S by ACFs before and after different surface treatments 70

Table 8. Precursor, surface area, and metal content of activated carbons 80

Table 9. Functionalities and pH of activated carbons 80

Table 10. Sulfur content in the bulk (sulfur analysis) and on the surface (EDAX) 97

Table 11. Summary of sorbent properties and mercury adsorption capacity 115

Table 12. Comparison of surface (EDAX) and average (QMS) sulfur content 118

Table 13. Comparison of the loss in pore volume and the volume of impregnated sulfur 119

Table 14. Effect of pore volume of raw ACFs on Hg uptake capacity 130

Table 15. Effect of surface area of raw ACFs on Hg uptake capacity 130

Table 16. Physical properties of chemicals * 143

Table 17. Elemental Sulfur sublimation energy calculation at 298 K* 144

LIST OF FIGURES

Figure 1. Structure of graphite [34] 15

Figure 2. Acidic and basic surface functionalities on a carbon basal plane [36] 17

Figure 3. Thermal decomposition of oxygen containing functionalities [38] 26

Figure 4. Experimental setup for H_2S adsorption/oxidation 53

Figure 5. H_2S breakthrough and desorption curves 54

Figure 6. Experimental protocols for the sulfurization process 56

Figure 7. Pore size distribution of ACFs before and after heat treatment 66

Figure 8. N_2 isotherms at 77K for raw ACFs 70

Figure 9. Adsorbed and retained amount of H_2S on ACFs per unit surface 72

Figure 10. Correlation of basic surface functionalities with H_2S retention (chemisorption) on raw ACFs 73

Figure 11. Gas species released during TPD of ACF10-raw: (a) sulfur containing species, (b) other species 75

Figure 12. Sulfur content of ACF-10 after desorption and TPD 76

Figure 13. Gas species released during TPD of ACF10-900C-4hrs: (a) sulfur containing species, (b) other species 77

Figure 14. Correlation of increased sufur content with surface area and metal contents 82

Figure 15. Effect of different carbon surface groups on irreversible H_2S adsorption without oxygen 84

Figure 16. Effect of basic surface functionalities on H_2S retention for all carbons 85

Figure 17. Change of carbon basicity after surface treatment 87

Figure 18. Effect of heat treatment on irreversible H_2S uptake without oxygen 88

Figure 19. Effect of ammonia treatment on irreversible H_2S uptake without oxygen 90

Figure 20. Effect of sorbent surface area on the increased sulfur content after sulfurization.....92

Figure 21. Effect of temperature on sulfurization of ACF25 and BPL in the presence of H_2S during stable temperatures only (S only) 93

Figure 22. CO_2 and CO evolution during temperature programmed desorption 94

Figure 23. Temperature programmed reaction between H_2S and BPL surface 96

Figure 24. Sulfur content and TGA results of BPL sorbents produced at different temperatures (H+S+C).....98

Figure 25. Sulfur content and TGA results of BPL sorbent produced by different sulfurization protocols at 600 °C 100

Figure 26. Pore size distribution of BPL before and after H_2S uptake at high temperatures.....101

Figure 27. XPS analysis of ACF25 before and after sulfurization.....102

Figure 28. Contents of different sulfur forms from XANES results 104

Figure 29. Effect of impregnation temperature on Hg uptake capacity of sorbents produced using the (H+S+C) protocol.....106

Figure 30. Effect of impregnation methods at 600 °C on Hg uptake capacity.....108

Figure 31. Effect of exposure to H_2S during heating and cooling on Hg uptake at different temperatures.....109

Figure 32. Correlation of Hg uptake capacity with total sulfur content for sorbent produced by sulfurization above 400 °C 111

Figure 33. Correlation of Hg uptake capacity with different sulfur species on sulfurized sorbents 112

Figure 34. Pore size distribution of ACFs before and after sulfur impregnation.....116

Figure 35. TGA analysis of ACF-10 before and after sulfur impregnation: (a) total weight loss, (b) derivative weight loss.....122

Figure 36. Estimation of the activation energy for desorption of impregnated sulfur on ACF10-150C-24hrs: (a) weight loss at different heating rates; (b) plot of –logB vs 1/T.....123

Figure 37. TPD of ACF10-150C.....125

Figure 38. XPS Spectrum of ACF25 before and after sulfur impregnation: (a) sulfur intensity and (b) oxygen intensity.....126

Figure 39. Correlation of sulfur content with Hg uptake capacity for sorbents produced through H_2S oxidation 128

Figure 40. Correlation of total functionalities with increased sulfur content: (a) with Centaur, (b) without Centaur 141

Figure 41. Hydrogen generation during temperature programmed reaction 142

Figure 42. Effect of sulfurization protocol at different temperatures 142

GLOSSARY

Sulfurization:

The incorporation of hydrogen sulfide onto carbon surface in an inert atmosphere at high temperatures is defined as sulfurization in this dissertation. The high temperature and strong interaction distinguish it from low temperature H_2S adsorption; and the absence of oxygen makes it different from H_2S oxidation.

Virgin (raw) carbon:

Carbon material that are as received, they are dried but without surface treatment of any type.

SEM: Scanning electron microscope

EDAX: Energy dispersive analysis, X-ray

XPS: X-ray photoelectron spectroscopy

FTIR: Fourier transform infrared spectroscopy

TGA: Thermogravimetric analysis

TPD: Temperature programmed desorption

XAFS: Sulfur K-edge X-ray adsorption fine structure analysis

XANES: Part of XAFS, X-ray adsorption near-edge structure (XANES)

ACKNOWLEDGEMENTS

I am deeply grateful to my research advisor, Dr. Radisav D. Vidic throughout my Ph.D. study. His extraordinary teaching skills and unparalleled creativity guided me through many difficult times. I especially appreciate his continuous support and endless help on my career development. I am also very grateful to my research co-advisor, Dr. Eric Borguet, for his help on developing a scientific mind and high quality research standards. His deep insight in surface science and dedication to science are very valuable to me and other students.

Appreciation is acknowledged to other members of the oral examination committee, Dr. Leonard W. Casson, Dr. J. Karl Johnson, and Dr. Robert Ries. I am thankful to Dr. Leonard W. Casson, Dr. Ronald Neufeld, Dr J. Karl Johnson, Dr. Jeen-Shang Lin, Dr. Robert Ries, Dr. David Waldeck, Dr. Christopher J. Earls, Dr. Jason Monell, Dr. Götz Veser, Dr. Jörg M. K. Wiezorek, and Dr. Shiao-Hung Jiang, who have shared their insights with me through enlightening discussions. Discussions with Even Granite, Christopher Matranga from DOE were also very rewarding.

I am especially grateful to Dr. Seok-Joon Kwon and Mr. Albert Stewart for their help in sample analysis, and Mr. Larry Herman for his assistance in instrument maintenance. I would like thank to Dr. Waldeck's group at the Department of Chemistry for providing assistance with XPS

analysis and Dr. Huggins at the University of Kentucky for the help in sulfur K-edge XAFS analysis. I also thank to Siama Toure for her assistance in metal content analysis.

I would like to express my thankfulness to my colleagues and friends, specifically Xue Feng, Yufan He, Dan Klein, Chantal Blake, Nicole You, John Stuart, Tao Ye, Siama Toure, Zhe Zhang, and many others, for their support and help on daily work and study.

This study is supported by the National Science Foundation. I also appreciate the support by the Department of Civil and Environmental Engineering, School of Engineering, and University of Pittsburgh.

This dissertation is dedicated to my wife, my parents, and my sisters. Without their support and encouragement, completion of this thesis is impossible.

1.0 INTRODUCTION

1.1 MERCURY

1.1.1 Toxicity and Regulations

Elemental mercury is a volatile metal. After being released from different sources, it can be transported to a great distance. It can be oxidized and deposited in water bodies and soils and it can also bioaccumulate in the food chain. Current air pollution control technologies can not effectively remove elemental mercury because of its volatility and low solubility in water.

Mercury can pose serious threat to public health in its various forms. If inhaled, mercury accumulates mainly in the brain and kidney. Interstitial pneumonitis and symptoms of respiratory disorders, including chest pain, cough and hemoptysis will occur upon acute exposure. Oxidized inorganic mercury compounds are a greater threat because of their water solubility [1]. However, organic mercury compounds, especially methyl mercury, are most toxic because they can be easily accumulated into the food chain [2-6]. Central nervous system defects, kidney damage and even some kinds of tumors have been associated with mercury exposure [3, 7].

Title III of the 1990 Clean Air Act Amendments (CAAA) identified 189 pollutants, including mercury, as potentially hazardous or toxic, and required EPA to evaluate their emissions by source, health and environmental implications, and the need to control these emissions. Two reports, namely the Mercury Study Report to Congress (1997) and the Study of Hazardous Air

Pollutant Emissions from Electric Utility Steam Generating Units -- Final Report to Congress (1998) were generated after systematic studies. It was concluded that mercury from combustion facilities was the hazardous air pollutant (HAP) of greatest potential concern to the environment and human health.

Based on the above work and subsequent collection of additional information, EPA confirmed the threat of mercury emission to human health and concluded further control of mercury emission from coal-fired and oil-fired power plants was deemed necessary. EPA started to regulate mercury emission in December 2000. Then EPA proposed that final control regulations be issued by December 15, 2004 and installation of mercury emission control technology would then be required no later than three years after finalized regulations go into effect on February 2008. On March 15, 2005, EPA issued the first-ever federal rule to permanently reduce mercury emissions from utility boilers. This Clean Air Mercury Rule will build on EPA's Clean Air Interstate Rule (CAIR) to significantly reduce emissions from coal-fired power plants through a two-phased "cap and trade" method. The first phase cap will be 38 tons/year (about 25% removal from current 52 tons/year) and emissions will be reduced by taking advantage of "co-benefit" reductions – that is, mercury reductions achieved by reducing sulfur dioxide (SO_2) and nitrogen oxides (NO_x) emissions under CAIR. In the second phase, due in 2018, a second cap of 15 tons/year (70% removal) will be fully implemented.

1.1.2 Sources and Discharge Conditions

Nriagu and Pacyna [8] estimated that about 1,000-6,000 tons of mercury is emitted from global anthropogenic sources. According to the Mercury Study Report to Congress (1997) [9],

approximately 87% of anthropogenic mercury emission is from combustion point sources, 10% is from manufacturing point sources, 3% is from other sources. Utility boilers, municipal waste combustors, commercial/industrial boilers, and medical waste incinerators contribute 33%, 19%, 18%, and 10% respectively to mercury emission from combustion sources.

Current emission estimates indicate that utility boilers are the single largest emission source (51.8 tons/yr), and about 80% of the utility boilers are fueled by coal [9]. Because the combustion zone in boilers operates at temperatures above 1000 °C (1800 °F), mercury in the coal is partly (about 42%) vaporized and emitted as a vapor. The rest of mercury bound to the fly ash is removed by particulate matter collectors. Oxidized mercury can be well collected by wet scrubbing system or via a sorbent injection method. Due to its high volatility and low solubility, Hg^0 is not well collected in the currently installed air pollution control systems, which are mainly designed for particulate matter and/or SO_2 control.

Besides utility boilers, municipal waste combustors (MWCs) and medical waste incinerators (MWIs) were also reported as major sources for the emission of mercury. The total mercury concentrations from these two streams are much higher. Because of the higher concentrations of HCl in these flue gases, mercury is mainly in its oxidized form. However, the final forms of mercury depend very much on the type of waste incinerated. Elemental mercury can still be a problem for MWCs and MWIs. Table 1 summarizes the conditions and compositions from coal fired power plants (CFPP) and municipal waste incinerators [10].

Table 1. Flue gas from coal fired power plants and municipal waste incinerators [10]

	Coal Fired Power Plants	Municipal Waste Incinerators
Temperature (°C)	121-177	177-299
Mercury Concentration ($\mu g/m^3$)	1-10	100-1000
Major Mercury Forms	Elemental or oxidized	Mainly oxidized
HCl Concentration (ppm)	5-100	100-1000
SO_2 Concentration (ppm)	100-3000	100-300
Excess Air (%)	15-25	50-110

1.2 HYDROGEN SULFIDE

1.2.1 Toxicity and Regulations

Hydrogen sulfide is an odorous pollutant commonly regarded as toxic. Hydrogen sulfide mainly attacks the neural system and important organs, such as the liver and the kidney [11-13]. Acute inhalation of high concentrations of hydrogen sulfide can be lethal [14, 15]. Although not clearly defined, adverse effects of exposure to low concentrations of hydrogen sulfide are suggested [12, 16].

Because of its acute and chronic toxicity, EPA has derived an oral reference dose (RfD) of 0.003 mg/kg/day and an inhalation reference concentration (RfC) of 0.001 mg/ m^3 for chronic exposure to hydrogen sulfide. OSHA has established an acceptable ceiling concentration of 20 ppm for hydrogen sulfide in the workplace, with a maximum level of 50 ppm allowed for a 10 minute maximum duration [17].

1.2.2 Sources and Discharge Conditions

Naturally occurring hydrogen sulfide originates mainly from bacterial anaerobic decomposition of sulfur-containing organic or inorganic compounds. A significant amount of hydrogen sulfide can be found in natural gas, volcanic gases, and petroleum. Human activities generate a significant amount of hydrogen sulfide through many processes including natural gas processing, petroleum refining, petrochemical manufacturing, paper production, coal gasification, and so on. H_2S concentrations in the gas streams from these processes vary from 0 to 60% by volume [18].

The Claus process is usually used to control gas streams with high concentrations of hydrogen sulfide. The feed gas into the Claus process is very concentrated hydrogen sulfide (concentrations from 5% to 60%). A single stage Claus reactor can only achieve conversion of hydrogen sulfide of about 70%. Current Claus processes are usually designed to achieve conversion of about 95-97.5% by using several stages. Typical tail gas from Claus plant still contains about 0.8% to 1.5% of H_2S with other gases such as COS, CS_2, and CO_2 at various concentrations. The discharging gas temperature is about 100-315 °C. The Claus process was previously considered as satisfying hydrogen sulfide reduction process. However, emissions from this process are now becoming an important source of H_2S pollution. For new sources, it is required to reduce H_2S emission from the Claus process tail gas.

Some processes generate gas streams containing hydrogen sulfide of relatively low concentrations. For example, for Integrated Gasifier Combined Cycle (IGCC) technology [19, 20] the main composition of the produced gas is carbon monoxide and hydrogen with hydrogen sulfide as an undesired component present at concentrations of about 0.5-1.1%. The gas temperature ranges

from 500 to 1000 °C, with the average of 550 °C. IGCC first converts coal into a combustible gas through a gasification process, during which the coal reacts with air or oxygen. Typical gas compositions are the following [21, 22]:

- Oxygen-blown gasifier (in vol %): 27.7% H_2, 39.4% CO, 13.1% CO_2, 18.4% H_2O, 1.1% H_2S, and 0.0% N_2
- Air-blown gasifier (in vol %): 14.2% H_2, 23.1% CO, 5.8% CO_2, 6.6% H_2O, 0.5% H_2S, and 49.8% N_2.

1.3 MERCURY CONTROL BY HYDROGEN SULFIDE ADSORPTION/OXIDATION

Removing low concentrations of vapor phase mercury from different flue gases, especially from coal fired power plants, is a very challenging task. Although sorbent injection method seems to be promising, the cost of injecting expensive sorbents is unacceptable to most plants.

Both mercury and hydrogen sulfide are toxic air pollutants, which require serious attention. In some cases, such as coke production and coal gasification, both mercury and hydrogen sulfide are generated in the same process. Common to both pollutants, adsorption is an effective method for their control. In addition, using sulfur compounds to control mercury is a well known method, which prompted the idea of controlling mercury pollution using hydrogen sulfide as the chemical regent.

Hg control by hydrogen sulfide adsorption/oxidation is a good example of the concept of industrial ecology. Similar to an ecological system, this concept uses a waste stream from one process to control the waste stream from another (or the same) processes, and is beneficial to the efficiency of industrial production as well as to the environment. This approach promises to be a low cost solution: it eliminates both wastes while no extra chemical agents are needed. The final products, sulfurized mercuric compounds, are stable and will no longer pose threat to the environment and public health.

1.4 OBJECTIVES AND SCOPE

The scope of this study is confined to the adsorption/oxidation of hydrogen sulfide on carbon surfaces and its application in vapor phase mercury control. The intent of this study was to investigate the interactions between hydrogen sulfide and carbonaceous surfaces and to understand the important factors and the mechanisms involved in these interactions. More specifically, the objectives of this study were:

- To investigate the nature and mechanisms of hydrogen sulfide adsorption process, both at low temperatures and high temperatures. The adsorption/incorporation of hydrogen sulfide into/onto carbon surfaces is defined as sulfurization.

- To study the effects of sorbent/operation parameters on the pore structure and surface chemistry of produced sorbents.

- To identify the most important sorbent characteristics (especially surface chemsitry) for effective removal of vapor phase mercury from the gas streams under consideration.

Focusing on a practical problem, this study is conducted to provide better understanding about both hydrogen sulfide removal and mercury removal, which will help in the design of more effective mercury control technologies. Connecting with adsorption, heterogeneous catalysis, surface chemistry, and air pollution control, the results of this study would also contribute to better understanding of surface phenomena in general.

2.0 LITERATURE REVIEW

2.1 ADSORPTION AND CATALYSIS

2.1.1 Physical and Chemical Adsorption

When a gas molecule approaches a surface, adsorption occurs at some short distance from actual contact due to the attractive and repulsive forces between them. Depending on the reactivities of surface and the gas molecule, as well as the interaction conditions, the bonding between the surface and the gas molecules can be either physisorption (physical adsorption) or chemisorption (chemical adsorption). Physisorption and chemisorption differ in the magnitude and origins of the interacting forces and the extent of perturbation of the respective electronic structures [23].

The attractive forces in physisorption are van der Waals forces, which originate from the difference in electron density and charge fluctuations of the adsorbate molecules and the adsorbent molecules. Physisorption is characterized by largely unperturbed electronic structures of both the adsorbate and the surface. In physisorption, the binding energy is usually below 0.25 eV, and the distance between the adsorbate and the surface is about 3–10Å [24, 25]. As a result, physical adsorption is reversible.

On the contrary, chemisorption occurs when there is an overlap between the electronic orbitals of the adsorbate and the surface molecules. There is an electron loss/gain or an electron sharing between the two groups of molecules after the rapture of the respective electronic structures. When there is a complete electron transfer, the bond is ionic; when the there is sharing of electrons, it is covalent. The equilibrium distance between the adsorbate and the surface is much shorter than that in physical adsorption, typically 1–3 Å. The bonding energy, about 1 eV [24], is much higher than that for physisorption,. Therefore, chemisorption is normally irreversible. Table 2 compares the difference between chemisorption and physisorption.

The nature of adsorption can be distinguished through the heat of adsorption analyses. Heat of adsorption can be measured by accurate microcalorimeter, by analysis of the adsorption isotherms at different temperatures [26], or by temperature programmed desorption (TPD) experiment. TPD applies to reversible adsorption processes and it is the easiest way to determine the heat of adsorption [27].

Table 2. Differences between physical adsorption and chemical adsorption

	Physisorption	Chemisorption
Bonding Nature	Weak interaction through van der Waals forces, electronic structure of the system is not disturbed	Strong Chemical bond, with loss/gain or share of electrons
Bonding Strength	Potential well 0.25 eV or less	Potential well greater than 0.25 eV
Reversibility	Reversible	Irreversible
Adsorption Sites	Random sites, normally at defects like vacancies, kinks *et al.*	At some specific sites where chemical bonding is possible
Number of Layers	Can be multi-layer	Normally monolayer
Heat	Exothermic	Exothermic or endothermic, depends on the reaction
Molecular integrity	Intact	Intact or dissociative

2.1.2 Surface Catalysis

Surface catalysis is the phenomena of accelerating the chemical reaction in the presence of a catalyst surface. A catalyst works by generating intermediates through strong interactions (chemical bonds), and these intermediates react more readily to give products than the reactants alone—and the catalyst is freed after the reaction is completed. It is well accepted that chemical bonding of one or two reactants with the catalyst surface is a necessary step for the catalysis to occur [27]. For a catalyst to be useful, it must bind the reactants quickly and effectively, stabilize the activated complex, and then quickly release the products of the reaction.

Chemisorption of molecules of at least one reactant is a necessary step for heterogeneous catalysis. The steps in heterogeneous catalysis include: (1) diffusion of reactant molecules to the surface; (2) adsorption on the catalyst surface; (3) surface reaction of the adsorbed species; (4) desorption of the products; and (5) diffusion of the products from the surface.

2.1.3 The Micropore Filling Theory and DR Equation

The Dubinin–Radushkevich (DR) equation is widely used to describe adsorption of vapors in microporous solids such as zeolites and carbon materials with low burn-offs [28]. DR Equation is based on the existence of a characteristic curve --- if the adsorption data at different temperatures are plotted as the logarithm of the amount adsorbed versus the square of desorption potential, all the data points should fall onto a smooth curve. The adsorption potential is expressed as

$$A = RT \ln (x) \quad (1)$$

Where $x=p/p_0$. Numerous studies by Dubinin and others [29-32] have already proven the validity of this equation. The basic form of the D-R equation can be written as:

$$W/W_0 = \exp[-(A/E)^2] \text{ or} \quad (2)$$

$$W/W_0=\exp [-(RT\ln(x)/E)^2] \quad (3)$$

With $x=p/p_0$. The characteristic energy, E, is unique for each adsorbent-adsorbate system. Activated carbon-benzene system with characteristic energy of E_0 was chosen as the reference, and the characteristic energies of other systems were obtained by multiplying E_0 with a scaling factor β, which is denoted as the similarity coefficient:

$$E= \beta E_0 \qquad (4)$$

The characteristic curve of a system is established by plotting the logarithm of the amount adsorbed W versus $\log^2(1/x)$. If the equation is applicable, the plot would be a straight line with a slope $-(RT/E)^2$ and an intercept $\log (W_0)$, from which the characteristic energy and the micropore volume can be obtained [30].

Mangun *et al.* [33] studied the effect of pore size on adsorption of hydrocarbons using activated carbon fibers. For the normal alkane series, the adsorbents with smaller pores demonstrated higher adsorption capacities for low boiling point alkanes as well as for adsorbing molecules at low concentrations. A formula was developed to predict the capacity of hydrocarbon uptake capacity based on the experimental data and the DR equation.

2.2 CARBON SURFACE CHEMISTRY

2.2.1 Structure of Carbonaceous Materials

Carbon is a versatile element, forming many allotropes through several ways of bonding. Graphite and amorphous carbons are formed through the sp^2 (trigonal) structures; Diamond is formed through the sp^3 (tetragonal) structures. Activated carbon and activated carbon fibers are graphitic materials composed of stacked layers of carbon atoms. Each layer is composed of continuous hexagons of carbon atoms and each carbon atom is in contact with three neighboring atoms. The C-C bond is covalent, with bond length of 1.42 Å and bond strength of 524 kJ/mole [34]. The adjacent layers are bonded with weak π bonds (7kJ/mole), and the spacing is 3.35 Å [34]. The structure of the graphite crystal can be illustrated in Figure 1 [34]. Graphite has a density of 2.26 g/cm^3, with an extremely high boiling point of over 3700 °C. Upon heating, the graphite structure expands, especially at the interplane direction.

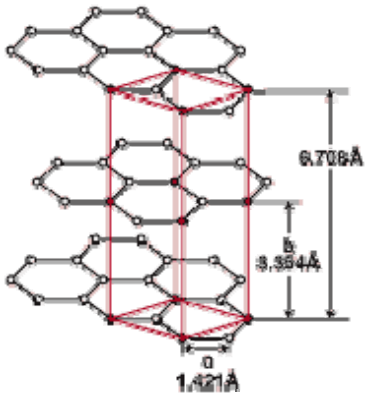

Figure 1. Structure of graphite [34]

In reality, the graphite structure is not as ideal as described above. Activated carbons or carbon fibers are formed by crystallites of considerably different sizes with many defects in the crystallites, including edges, dislocations, vacancies and steps. As a result, pores with different shapes and high surface area are formed. In addition, oxygen, sulfur, hydrogen, halogens, and metals can be incorporated into the carbon structure, forming various surface functionalities or impurities.

These defects and impurities are the possible "active sites" with chemical reactivity, in contrast to perfect graphite, which is one of the most chemical inert materials. The chemical reactivity of graphite increases with the increase in temperature. Graphite carbons can react with acids, alkalis, and gases under different conditions. Activated carbons and activated carbon fibers are actually "activated" through these reactions after carbonization of the precursor materials (usually organic carbon containing materials). The morphology of carbon materials is important

to physisorption of gases or vapors. However, the carbon surface chemistry is critical for chemisorption of gas species [35]. Carbonaceous materials are a combination of the bulk graphite structure and the "active sites" on the carbon surface. Both the graphite structure and the "active sites" are affected by many factors, including the elemental composition, carbonization and activation method and storage environment [34].

2.2.2 Oxygen Containing Functionalities

Among the various functionalities present on the activated carbon surface, the oxygen-containing surface groups are significant because of their ubiquitous presence and vital influence on the adsorption properties of activated carbons. Much of the current understanding of oxygen containing functionalities relies on established knowledge of oxygen containing surface functionalities in organic chemistry. Functionalities detected on the carbon surface include the following: carboxylic, lactonic, phenolic, carbonyl, pyrone, chromene, quinine, and ether groups. Carboxylic groups can also exist in the form of carboxylic anhydride.

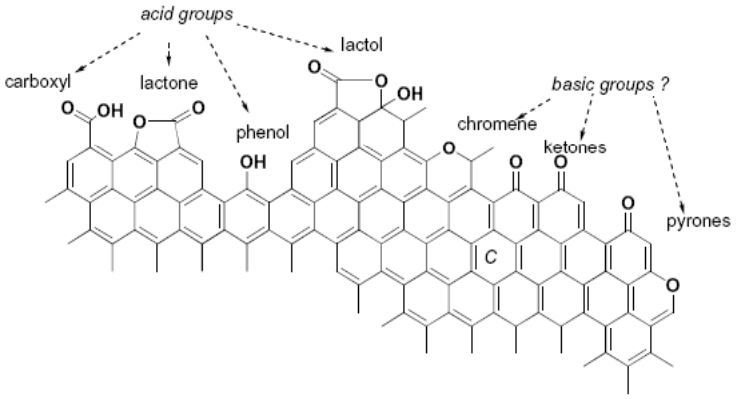

Figure 2. Acidic and basic surface functionalities on a carbon basal plane [36]

2.2.3 Characterization

Characterization of the oxygen-containing surface functionalities on activated carbons is complicated, partly because of the complexity of functionalities on the carbon surface, and partly because of the incomplete understanding of their behavior. The most common method is titration, which was first proposed by Boehm [37]. The basic principle of Boehm titration is that different acidic/basic functionalities can be neutralized using bases/acids of different strength. Currently, the total basic surface functionalities are measured as a single value because the nature of basic functionalities is not well known. The Boehm titration method has limited application with small samples [38]. Generally, normal infrared spectroscopy application is hindered by the high absorbance of carbon materials. Currently, the most successful technique

for small quantities of oxygen containing surface functionalities is X-ray photoelectron spectroscopy (XPS). However, even with XPS, the preparation of samples and interpretation of the spectrum still need further development.

Besides the above techniques, other commonly used methods include thermal desorption spectroscopy and electrokinetic measurements [39]. Recently, Inverse gas chromatography has emerged as a new method for detecting oxygen surface functionalities [40]. Surface imaging techniques, such as SEM and STM, are also starting to be used in probing the activated carbon surface functionalities [41].

2.2.4 Oxidation of Carbon Surface

Oxygen containing functionalities are created when the carbon surface is oxidized. Several oxidation methods can be used to introduce oxygen containing surface functionalities. These methods include oxidation by gases (air, carbon dioxide, steam, and so on), oxidation by aqueous oxidants (such as nitric acid, hypochlorite, permanganate, bichromate, and other strong acid/base), electrochemical oxidation, oxidation with oxygen plasma, and microwave treatment in the presence of oxygen. The most common activation processes used to produce activated carbons are oxidation by gases and aqueous chemical solutions.

HNO_3 is believed to be more effective than H_2O_2 and $(NH_4)_2S_2O_8$ in introducing a large amount of oxygen containing surface functionalities [42, 43]. With the increase in oxidation time, the surface functionalities will shift from carboxylic groups to other oxygen containing functionalities [44]. Pore volume increase and pore size distribution changes were observed after HNO_3 oxidation [45]. Activated carbons were modified with HCl and HNO_3 optionally followed by

NaOH [46]. NaOH causes an increase in the amount of hydroxyl groups, while the HCl treatment results in an increase in the amount of oxygen functional groups such as phenols, ethers, and lactones. Ozone and NaOH treatment increased hydroxyl and carboxyl groups on the carbon surface [47]. Figueiredo *et al.* [38] has shown that oxidation of activated carbons by oxygen increases mainly the concentration of hydroxyl and carbonyl surface groups, while oxidation in the liquid phase increases the concentration of carboxylic acids on the carbon surface.

Reactions in oxygen plasma yield a low surface acidity, mostly due to carboxylic groups, with minimal modification of the initial sample porosity [48]. Oxygen plasma treatment of an isotropic carbon fiber introduced stable oxygen functionalities after short exposure. However, prolonged treatment will eliminate some of the grafted groups [49].

Electrochemical method combines electrical oxidation and chemical oxidation [50, 51]. Increases in carboxyl or ester groups were observed after HNO_3 and electrical oxidation. Electrochemical oxidation increased surface activity by introducing polar oxygen-containing groups over extended ultramicropore surface [52].

Oxygen containing functionalities can be removed in an inert environment or in vacuum at elevated temperatures. However, once it is exposed to air, oxygen is chemisorbed and oxygen containing surface functionalities will be reintroduced onto the carbon surface.

2.2.5 Adsorption Properties

The presence of oxygen containing functionalities has different effects on different gas adsorbates. Graphite planes were considered to be nonpolar with strong potential toward organic

molecules. Addition of oxygen containing functionalities is believed to increase the polarity of the carbon surface. As a result, the adsorption capacity for polar adsorbates usually increases. This is supported by computer simulation conducted by Muller *et al.* [53]. In their study of the adsorption of methane/water vapor mixtures on porous activated carbons, they found the selectivity for methane adsorption dramatically decreased with the increase in the density of surface oxygen containing functionalities. This indicates that these functionalities were the primary sites for water vapor adsorption.

The effect of carbon surface chemistry on adsorption of water vapor adsorption has been well studied. Microcalorimetric techniques [54] revealed the importance of carbon surface chemistry on water adsorption and three possible mechanisms were proposed: (i) chemical adsorption with H_{ads} > 12 kcal/mol, (ii) condensation with H_{ads} of approximately 10 kcal/mol, and (iii) physical adsorption with H_{ads} bellow 10 kcal/mol. The primary adsorption sites for chemisorption and micropore filling were created by N_2 treatment at 950 ˚C and drying at 175 ˚C respectively. Hydrophobic carbon surfaces subsequently oxygenated at 150 ˚C showed significant increases in the amount of water adsorbed through physical adsorption. Analyses revealed that acidic surface groups might be the primary adsorption sites for water vapor [55]. By comparing the enthalpy of immersion of carbon into water, it was found that the interaction between acidic sites (surface oxygen) and water was higher than the interaction between basic sites and water vapor [56]. Both computer simulation and experimental data showed that an increase in site density (caused by oxidation of the carbon surface) led to an increase in adsorption prior to micropore filling [57].

For nonpolar gas molecules, it was reported [58] that the higher the total number of oxygen surface groups (through HNO_3 and H_2O_2 oxidation), the lower the adsorption capacity. This is

especially true in humid conditions when competitive adsorption with water vapor is involved. It was proposed that addition of surface functionalities on the pore walls can also cause steric hindrance for big molecules [59].

Similar explanations were proposed in the liquid phase since the basal plane of the graphite material is considered hydrophobic, while introduction of oxygen containing surface functionalities makes the carbon surface more hydrophilic. Oxidized fibers displayed increased wettability compared to the raw fibers[44]. Quinlivan *et al.* [60] proposed that the best activated carbon for drinking water treatment should exhibit an elemental (O+N):C ratio below 0.05 to assure sufficient hydrophobicity. The adsorption of dyes from wastewater also reflects the importance of negatively charge surface, which has showed higher capacity for cation dyes [61]. It is suggested [62] that the irreversible adsorption of phenol from aqueous solution is caused by the complex formation between phenol and surface functionalities, as well as through polymerization. However, the decrease of phenol adsorption with the increase in oxygen containing functionalities was also reported [63].

2.2.6 Nitrogen Containing Functionalities and Other Functionalities

Nitrogen containing surface functionalities can be introduced through either reaction with nitrogen containing reagents (such as NH_3 and amines) or activation with nitrogen containing precursors. Activated carbon fibers were grafted with a high concentration of amine groups by nitric acid oxidation followed by reaction with excess tetraethylenepentamine (TEPA). The grafting process was believed to occur through the acidic oxygen containing functionatlities

except hydroxyl groups [64]. Possible structures of the nitrogen containing surface functionalities include the following: amide group, imide group, lactame group, pyrrolic group, and pyridinic group [35].

Nitrogen containing surface functionalities incorporated into the activated carbon fiber surface are usually basic in nature and these functionalities probably account for the increase in adsorption of SO_2 from simulated flue gas [65]. Enhancement of CH_3SH adsorption by nitrogen containing functionalities was also reported [66]. Nitrogen containing surface functionalities are very stable. Heat treatment studies show that the order of stability of the functional groups is quaternary nitrogen > pyridinic > pyrrolic > pyridine N-oxide. Pyridine N-oxide surface groups desorb NO and form N_2 via surface reactions at low temperature. Pyrrolic and pyridinic functional groups decompose and react with other surface species to give NH_3, HCN, and N_2 as desorption products, but most pyrrolic groups are preferentially converted to pyridinic and quaternary nitrogen. Approximately 15-40 wt % of the original nitrogen was retained on the carbon mainly as quaternary nitrogen after heat treatment to 1400 °C [67].

Halogen containing surface functionalities can also be prepared through carbon surface reaction with halogen containing reagents [45]. It was postulated that chlorination of activated carbon increases its Lewis acidity but decreases it Bronsted acidity, which can be explained by the resonance effect introduced into the aromatic rings of graphene layers by the chlorine atoms covalently bound to their edges [68].

It was reported [69] that hydrogenation increased the carbon basicity and effectively protected the carbon surface from air oxidation through the following changes of the carbon surface: removal of surface oxygen, stabilization of some of the active sites by forming C-H bonds, and gasification of the most reactive unsaturated carbon atoms [70].

Sulfur can form very stable surface functionalities with carbon [71, 72] (see Section 2.5 for additional information). In addition, metals embedded into the activated carbon structures also have significant effect on the carbon surface chemistry [37].

2.2.7 Carbon Acidity and Basicity

Different basal planes and/or different surface functionalities yield carbon surface that show different acidic and basic properties. Boehm [37] reported that carbons with acidic surface groups have cation exchange properties. Carbons with low oxygen content exhibit basic surface properties and an anion exchange behavior. Most functionalities, including carboxylic, lactonic, phenolic, and carbonyl groups, are grouped as acidic surface functionalities [37] and their acidity decreases in the given order, which is the basis of Boehm titration for quantifying different surface functionalities.

On the other hand, the origin of the carbon's basicity is still not well understood. It was proposed that certain oxygen containing surface functionalities can contribute to the carbon basicity. These functionalities include chromene, ketone, and pyrone [36] as shown in Figure 2. Theoretical analysis [73] and quantum mechanic calculation [36] proved that pyrone like groups can

indeed exhibit basicity in a wide range of pK(a) values. The basicity of pyrone-like structures is explained by the electronic π-conjugation throughout the sp^2 skeleton. Through the insertion of an additional carbon ring, the basicity of the resulted compound significantly increases with the highest possible pK(a) value of 14.2 [36]. Without the inserted carbon ring, the pK(a)s of these pyrone groups were lower than 6.0. Other effects, such as the modification of the etheric position and the relative position of oxygen atoms were also studied. The reaction energies of these pyrone-type structures with H_3O^+ support the importance of pyrone-type structures to carbon basicity [74].

Some researchers [75, 76] attributed the basicity of carbon surface to nitrogen containing functionalities because the basicity of the carbon materials increased markedly after the introducing nitrogen containing functionalities. H_2 treatments at high temperatures (> 800 °C) also created basic (hydrophobic) surfaces, which are stable after prolonged air exposure. [70]

The contribution of basal planes of the graphitic crystals to the carbon basicity is very important. It was pointed out that the π-electrons of these layers could act as Lewis bases [68]. Ab initio calculations on various cluster models were carried out to study the contribution of basal planes to the carbon basicity [77]. Calculations indicate that the size of the basal plane slightly affects the strength of the interaction between the plane and H_3O^+, whereas the presence of the π−π contacts strongly reinforces this electrostatic interaction. These results support the contribution of carbon basal planes to the carbon bascity. They also revealed that the π-cation interactions may play an important role in the acidity and basicity of carbon materials. XPS revealed that the highest concentration of basic sites were found for the samples with the narrowest graphite peaks [78]. The correlation between the concentration of basic sites and the full width at half maximum (FWHM, related to the heterogeneity of carbon surface) of the graphite

peak is very good, which suggests that the basic sites on carbon blacks are associated with the basal planes of the graphene layers. Studies of solid base catalysts found that the basic catalytic properties appear only upon the removal of water and carbon dioxide from the surfaces [79]. It is believed that surface and bulk atoms rearrange with increasing temperature, indicating the importance of the bulk structure to the basicity of the catalysts. For the most extensively oxidized sample, the number of basic sites is approximately zero, while for a heat treated carbon the number of acidic sites is very small [80]. This again indicates that acid surface sites are oxygen based while basic sites are associated with the carbon surface itself [36].

It seems that both the π-electrons of graphite structure and oxygen containing surface functionalities can contribute to carbon basicity. For example, the basicity of pyrone groups is actually a combination of the basal plane and the adjacent rings containing ketone and etheric groups [81]. However, the issue of whether the carbon basicity is mainly due to basic-oxygen-containing groups or the delocalized π-electrons is still under debate.

2.2.8 Decomposition of Oxygen Containing Functionalities

Oxygen containing surface functionalities decompose upon heating by releasing CO_2 at lower temperatures and CO at higher temperatures. Although the actual temperature of decomposing specific oxygen containing surface functionalities depends on several factors, including the heating rate, carbon materials, and experimental system, the assignment of these decompositional peaks to specific oxygen containing functionalities and specific temperatures can be summarized as shown in Figure 3 [38]. Carboxylic groups decompose at 100-400 °C to release CO_2; lactonic groups decompose at relatively higher temperatures to produce CO_2;

anhydride groups decompose at about the same temperature range as lactonic groups (350-630 °C) generating both CO and CO_2; phenol, carbonyl, ether, and quinine groups decompose at 600-1000 °C to release CO. Oxygen containing surface functionalities can be estimated by deconvoluting the CO and CO_2 peaks observed during the heating process [38]. IR studies have shown the same trend of decomposition of oxygen containing surface functionalities [82].

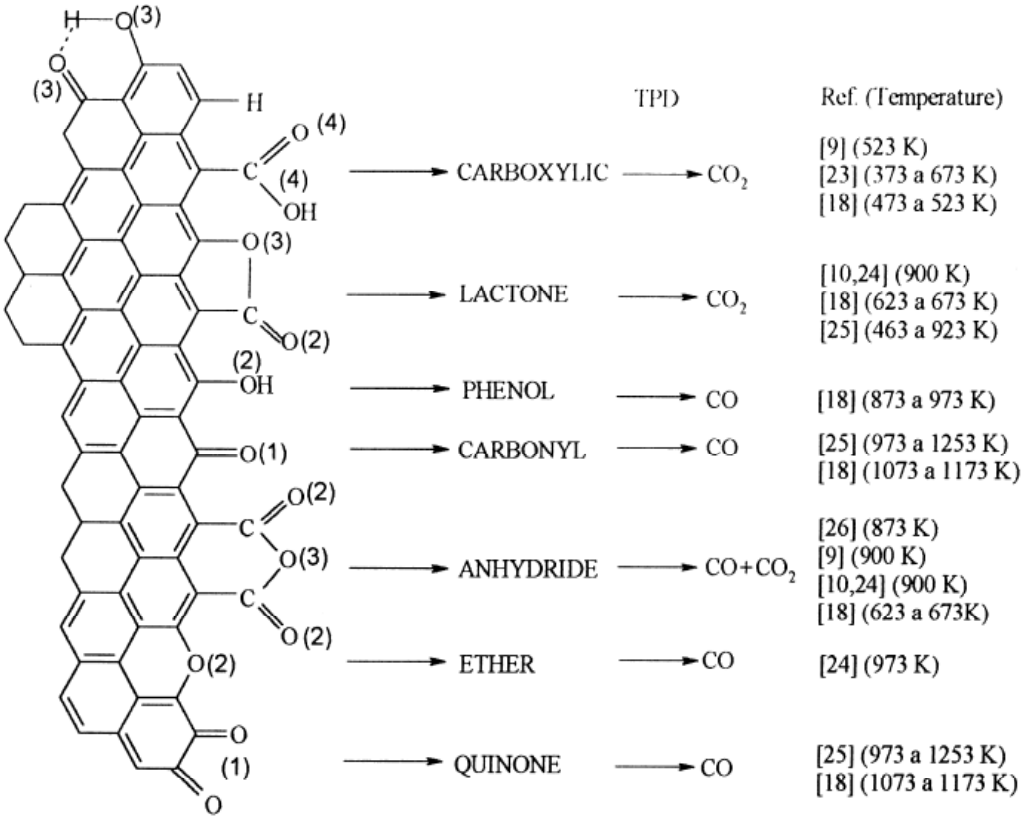

Figure 3. Thermal decomposition of oxygen containing functionalities [38]

Many reports have confirmed that the decomposition of oxygen containing surface functionalities at elevated temperatures increases basicity of the carbon surface [78, 83]. This is due to the fact that strongly acidic functionalities decompose at lower temperatures, while the weakly acidic groups decompose at higher temperatures. Carbon materials after complete removal of oxygen containing functionalities show strong basicity. This is an indication that the π-electrons of the graphite crystals plays an important role in the carbon basicity.

The concept of "active surface area", or the density of active sites on the carbon surface, was proposed by Laine *et al.* in 1963 [84]. Highly graphitized carbon black was oxidized at different levels to create different amount of "active sites". The amount of "active sites" was measured by the coverage of the surface by oxygen containing surface functionalities, which were formed after oxidation of the sample by air at 300 °C for 24 hours. Decomposition of these functionalities will create a constant amount of unoccupied "active sites" again.

It was found that gradual annealing in vacuum removed mainly acidic surface groups that are located in macropores or on the outer surface of the carbon, and at the same time, rearranged weak acidic functionalities [59]. Darmstadt [85] proposed that the increase in the surface energy on the carbon surface might be related to the formation of active sites that are formed upon removal of non-carbon elements during the carbon black formation. Detailed scheme on the formation of active sites was proposed by Phillips [83].

Compared to traditional electrical heating, microwave treatment in an inert environment promises to be an efficient and attractive way of removing oxygenated functionalities from

carbon surfaces, as well as increasing the hydrophobicity and basicity of carbons [86]. Microwave treatment is a very effective method for modifying the surface chemistry of the ACFs with the production of pyrone groups. As a result very basic carbons are readily obtained.[87]

Daley *et al.* [88] found that oxidation of the ACFs by aqueous oxidant decreased the adsorption capacity for SO_2. However, the subsequent heat treatment increased SO_2 adsorption after decomposition of the surface oxygen containing functionalities. This increase in adsorption capacity was directly correlated to the amount of CO_2 evolved during heat-treatment of the oxidized ACFs. These results indicated that the new active sites were formed during oxidation, but they were occupied by CO_2 evolving functionalities. After decomposition of these surface functionalities, these new sites were ready for SO_2 adsorption. "Oxidation followed by heat treatment" was proposed as an effective way of producing sorbents for acidic gases.

Fundamental interpretation of the acidity and basicity involves proton or electron transfer, corresponding to the definition of Bronsted and Lewis acidity/basicity respectively. Leon y Leon and Radovic [89] reviewed the carbon surface chemistry from different perspectives, suggesting that both the pyrone groups and the basal planes with π electrons account for the basicity of the carbon surface [89, 90].

2.2.9 Summary

Graphite materials are composed of carbon basal planes with different kinds of defects and impurities. While the surface area and pore structure are important to physisorption through van der Waal's forces, defects and imputrities are important for chemisorption of gaseous species,

especially oxygen. Oxygen containing surface functionalities have similar structure to organic chemical functional groups, and different surface functionalities have different thermal stability. Addition of surface oxygen containing functionalities can be achieved using different oxidants under various conditions. The presence of these functionalities increased the carbon surface acidity, polarity, and hydrophobicity, affecting the adsorption properties toward many adsorbates. Decomposition of oxygen containing surface functionalities increased the carbon basicity. The carbon basicity originates from certain oxygen containing functionalities (i. e. pyrone groups) and from the π electrons of basal planes.

2.3 MERCURY REMOVAL BY ADSORPTION

2.3.1 Mercury Control Technologies

Currently, only a few technologies are considered effective for vapor phase mercury removal. These technologies include wet scrubber, sodium sulfide injection, spray dryer adsorption (SDA), and activated carbon injection. Wet scrubbers are currently installed in many power plants. In general, wet scrubber is ineffective in removing elemental mercury. Wet scrubber can only achieve 25-50% removal of elemental mercury [91], with the highest removal efficiency of 70% reported. [92] In addition, wet scrubbing has the potential problem of secondary pollution: treatment of mercury in the water phase is another complex task. Sodium sulfide has been used for mercury control in municipal waste combustors in many countries. Similar technology is also proposed for Hg removal from power plants [93]. However, the fine particles from the reaction of Na_2S with mercury are very difficult to remove and hydrogen sulfide formation is an additional problem with this method. SDA method is very effective in removing most air contaminants. However, its mercury removal efficiency is only about 3-50% [94] because it can not remove mercury in elemental form.

2.3.2 Mercury Removal by Activated Carbon Injection

Compared with above mentioned technologies, activated carbon injection is currently considered to be the most promising technology in terms of Hg removal efficiency and reliability. Raw activated carbon can be effective in removing mercury at high sorbent to mercury ratios [9, 10, 95]. Although very effective, the high cost involved hinders the practical application of this technology in mercury control. It is estimated that cost for mercury emission control by activated carbon injection method ranges from $14,200 to $70,000 per pound [96, 97]. In order to lower the cost, improvements on the sorbent (either to decrease the cost or to increase the adsorption capacity) must be made to facilitate the application of this technology.

The factors affecting the performance of this method include: sorbent properties (carbon type, particle size, pore structure, surface chemistry, moisture content, and so on), sorbent/mercury ratio, temperature, and flue gas composition [98]. Modification on the surface chemistry of activated carbon may be the most effective way of improving mercury adsorption capacity. Although introducing oxygen containing functionalities [99, 100] and halogens [101, 102] can improve Hg uptake capacity, the more promising method is to introduce sulfur onto the carbon surface [103]. The latter method improves Hg uptake capacity more significantly and produces more stable products [104], thus eliminating long-term liabilities of the adsorption technology.

2.3.3 Sulfur Impregnated Activated Carbons

Sinha and Walker [105] tested mercury adsorption capacity of sulfur impregnated activated carbon, which was produced through H_2S oxidation at 140 ºC. Breakthrough of mercury from a fixed-bed reactor at room temperature decreased with an increase in sulfur content. Such

behavior was explained by the narrowing of micropores in the virgin sorbent through sulfur deposition. However, at 150 ^{o}C, the sulfurized carbon had much higher capacity than the original carbon. Otani *et al.* [106] added sulfur onto activated carbon surface by soaking in CS_2 solution. Mercury adsorption capacity was found to increase with an increase in sulfur content up to 13% and no decrease in mercury adsorption capacity was observed even for very high sulfur content on the sorbent. The authors suggested that a decrease in activated carbon surface area in their method of sulfur impregnation was less pronounced than that in the method used by Sinha and Walker [105].

Impregnation of sulfur onto activated carbon through the reaction between elemental sulfur and the carbon surface at elevated temperatures was studied by Vidic and co-workers [101, 103, 104, 107-109]. Their studies suggested that the following factors are important for mercury uptake by sulfur impregnated sorbents: sulfur content, sulfur forms, sulfur distribution, and pore structure/surface area of the sorbent. Sulfur impregnated carbons produced at higher impregnation temperatures (400-600 ºC) performed better than those produced at lower temperatures (25-150 ºC). The authors suggested that higher temperature produced short chain sulfur allotropes and more uniform sulfur distribution on the sorbent's surface. Liu [103, 104] argued that the short-chained elemental sulfur such as S_2 is the most important sulfur form for vapor phase mercury removal. This short-chained sulfur interacts strongly with the carbon surface. However, he did not explore the nature of this interaction. Liu and Vidic [103] tested the impact of temperature and the initial sulfur to carbon ratio (SCR) on developing better sorbent for mercury removal. The impregnation temperature was found to be more important than SCR. This was attributed to the fact that sorbents generated under higher temperature still retained their high surface area and mesopore structure. Kwon *et al.* [109] compared mercury adsorption capacity of

BPL carbon impregnated with sulfur through two different methods: reaction with elemental sulfur at 600 ºC and oxidation of H_2S at 150 ºC. They found the former method to be much more effective in producing high capacity sorbents than the latter. Sorbents impregnated through H_2S oxidation exhibited highly non-linear correlation between sulfur content and mercury uptake capacity, with optimal sulfur content around 5 wt% [109]. However, the stability of sulfur deposited on carbon surface through H_2S oxidation at 150 ºC is not adequate for full scale applications. Sulfur impregnation through H_2S oxidation can be justified by the industrial ecology approach for producing effective sorbents where waste stream from one process serves as a raw material for another process. Also, the low temperature during H_2S oxidation means lower cost.

Similar results were found by Hsi *et al.* [110, 111] using sulfur impregnated activated carbon fibers (ACFs). ACF impregnated with elemental sulfur at 400 ºC was found to be the most effective mercury sorbent [111]. Although this sulfur impregnated sorbent had a surface area of only 94 m^2/g, 86% of the surface area was attributed to micropores ($d < 2$ nm). It should be mentioned that this study used simulated flue gas to test the mercury uptake capacity. Sulfur deposited on activated carbon fiber existed in three forms, namely elemental sulfur, organic sulfur, and sulfate, with only the first two forms acting as mercury adsorption sites [110]. Hsi *et al.* [112] also observed that the significant effect of organic sulfur remaining in the coal derived activated carbon was very effective in removing vapor phase mercury. The authors suggested that both sulfur content and micropore structure are important for the uptake of vapor phase mercury.

Lee and Park [113] reported that the adsorption performance of sulfur-impregnated activated carbon depended on the pore characteristics of virgin activated carbon used as raw material and the types of sulfur, rather than on the amount of sulfur impregnated. The authors observed two

types of sulfur impregnated through interaction between elemental sulfur and activated carbon surface: one desorbed around 250 °C and the other desorbed around 400 °C. Higher content of the latter form of sulfur significantly improved Hg uptake. They suggested that the raw activated carbon for sulfur impregnation should have an average pore diameter above 2 nm.

Other researchers also looked into the effect of sulfur forms and pore structure on vapor phase mercury uptake. Daza *et al.* [114] applied various techniques to characterize Palygorskite (a fibrous mineral with hydrated magnesium silicate, $Mg_3Si_4O_{10}(OH)_2$) impregnated with sulfur through catalytic oxidation of hydrogen sulfide. The impregnation was achieved in a fixed bed reactor operated at 140 °C with O_2:H_2S = 1:1. They found that the π form of sulfur and a pore diameter larger than about 7.5 nm yielded the best sorbents. In addition, the authors proposed that monolayer coverage of sulfur molecules on the internal surface will produce the most efficient sorbent for Hg removal. They also suggested that pore structure that creates no steric hindrance for HgS formation is a general requirement for good mercury sorbent [115], with a minimum pore size per monolayer of deposited sulfur of around 8 nm. Recently, Guijarro *et al.* [116] tested the mercury uptake capacity of sulfurized sepiolite. They suggested that macropores above 400 nm are of utmost important for mercury uptake because high surface area sorbents impregnated with high sulfur content would result in quick blockage of the pore entrance by HgS.

In summary, sulfur forms, sulfur content/distribution, and sorbent pore structure affect the mercury uptake capacity of sulfur impregnated sorbents. Using elemental sulfur as the sulfurizing agent, higher temperature (up to 600 °C) generates better sorbents. Elemental sulfur

and organic sulfur are probably the key species for Hg removal. A good balance between sulfur content, sulfur distribution, and sorbent pore structure produces sorbents with maximum capacity.

2.4 HYDROGEN SULFIDE ADSORPTION ON CARBON SURFACE

H_2S adsorption/oxidation onto carbon surfaces was widely studied. However, some basic questions are still not clear in the literature. Whether the adsorption of H_2S is physical or chemical in nature? What are the roles of oxygen containing functionalities on the carbon surface?

Some researchers reported that physical adsorption is the dominant mechanism for H_2S uptake by carbon materials under certain conditions. If the adsorption is occurring under vacuum and without the disturbance of surface functionalities, the micropore filling theory[117, 118] can explain the adsorption isotherms very well. This means physisorption is the dominant mechanism for adsorption of H_2S. Boki and Tanada [119] studied the adsorption of H_2S onto activated carbon surface using a vacuum system at three different temperatures. The Dubinion-Astakhov equation can be applied to describe the adsorption isotherm. The isosteric heat of adsorption of two carbon samples were less than twice the value of the heat of condensation, while the heat of adsorption of one carbon sample was more than twice the value of heat of condensation. By comparing the pore size distribution of the three carbon samples, the authors

believe that the higher heat of adsorption of the third carbon sample was due to the small pore size. The adsorption of H_2S on activated carbon is mainly physical in nature. At the same time, the authors observed that a small amount of H_2S was chemisorbed onto carbon surfaces, and the lower the temperature, the smaller this amount.

Other studies also showed that the adsorption of H_2S onto microporous sorbents is physical in nature. In studying the adsorption isotherms of different sorbates onto microporous adsorbents, Aranovich and Donohue [120] compared the predicted results using Dubinin-Radushkevich (DR) equation and experimental results. The authors found that the adsorption of all the adsorbates including H_2S follows the micropore filling mechanism. Lee et al [121-123] used a gravimetric adsorption apparatus equipped with electrobalance and also reported that adsorption of hydrogen sulfide can be explained by the micropore filling theory.

Bagreev et al [124] studied the sorption of hydrogen sulfide on activated carbons by inverse gas chromatography (IGC) at infinite dilution under dry and anaerobic conditions. Surface modifications were conducted for some carbons by HNO_3 and ammonium persulfate oxidation. The structures of carbons were evaluated based on the adsorption of nitrogen. Heats of adsorption were calculated from the IGC experiments at various temperatures. There was a good correlation between the heat of H_2S adsorption and the characteristic energy of nitrogen adsorption calculated from the Dubinin–Raduskevich (DR) equation. These results indicate that under dry and anaerobic conditions, the adsorption of H_2S is mainly physical, and surface functionalities have no contribution. The authors also pointed out that this result may indicate that during H_2S oxidation on carbon surfaces, oxygen from the air, rather than from the carbon surfaces is the major oxidant. In another paper, Bagreev and Bandosz [125] studied the adsorption of H_2S on fifteen samples of activated carbon using inverse gas chromatography (IGC) at infinite

dilution in Helium. The results showed that the lower the average pore size, the stronger the interaction between H_2S and the carbon surface, which is due to the increase in adsorption potential.

The above claims of physical adsorption of H_2S are all based on studies at ideal conditions (at low temperature, anaerobic, or in vacuum). Studies conducted under real conditions (higher temperature, with the presence of other gases like oxygen, and uncleaned surface) revealed that chemical adsorption was unavoidable and important.

Bandosz and co-workers[126-128] studied the importance of carbon surface chemistry by comparing the H_2S breakthrough capacities of activated carbons with significantly different surface properties. While the effect of pore of pore structure is not clear, surface treatment using ammonia or nitric acid can result in significant change in H_2S removal capacities due to the modification on carbon surface chemisty. They reported that a good performance of carbons as hydrogen sulfide adsorbents was the result of a proper combination of surface chemistry and carbon porosity; more acidic environment promotes the formation of high-valent sulfur compounds and decrease the H_2S removal capacities; a basic environment favors the formation of elemental sulfur (sulfur radicals) and increases sulfur removal capacity. A critical acidity, estimated at pH≈5, should not be exceeded for a good catalyst. Otherwise, the carbon will have negligible H_2S breakthrough capacity.

Mikhalovsky [129] showed that H_2S adsorption from an inert atmosphere on activated carbons resulted in the formation of surface oxygen-containing complexes and elemental sulfur. This result indicated that the adsorption of hydrogen sulfide on carbon surface was dissociative and chemical in nature. Pieplu et al [130] reported that H_2S adsorption on catalyst surface is a

possible step for H_2S oxidation. There are two modes of H_2S adsorption onto these surfaces: dissociative and non-dissociative. TPD studies showed that the two desorption peaks associated with H_2S adsorbed by the two adsorption modes were around 105-130 ºC and 290-315 ºC. The dissociative adsorption may be due to the interaction between H_2S and -OH group or cations, such as Na^+, Al^{3+} and Ti^{4+}.

Since modification of surface chemistry is likely to be more effective for improving H_2S removal capacity by activated carbons, different kinds of impregnates were introduced. Bagreev *et al.* [131] studied the effect of NaOH on adsorption of H_2S, using four different kinds of carbons, with different amounts of impregnated NaOH. They found that impregnation of NaOH significantly improved H_2S removal capacity. However, when more than 10% of NaOH was introduced, it likely resulted in pore blocking. Again, they found the H_2S removal capacities were dominated by the presence of NaOH, and were not sensitive to surface areas and pore structures of these activated carbons. Other reports on NaOH [132, 133] or K_2CO_3 [134, 135] impregnation also showed significant improvement of the H_2S removal capacity. It is believed that presence of alkaline chemicals facilitates the dissociation of H_2S on carbon surfaces.

There are numerous reports on the decomposition of hydrogen sulfide on metal, metal oxides and other surfaces [136-139]. These studies indicate that chemical adsorption, even the decomposition of H_2S, can occur on the carbon surface because of the presence of metal and metal oxides in many carbon materials.

In summary, both surface chemistry and pore structure are important for H_2S adsorption/removal. The relative contribution of the two parameters, whether obvious or not to the investigators, is very much depend on the experimental conditions. Only when the

functionalities are significantly removed or reaction conditions are ideal, the effect of pore structure is obvious and physical adsorption is dominant. For physical adsorption, smaller pore size can exert stronger interaction between H_2S and carbon according to the micropore filling theory. However, under real conditions, surface functionalities are almost unavoidable. As a result, the effect of surface chemistry is more prominent. The interaction between surface functionalities and H_2S is much stronger than forces exerted during physical adsorption (van der Waals forces) and H_2S dissociation might occur. It seems that alkaline impregnates are very effective to improve H_2S removal capacity.

2.5 SULFURIZATION OF CARBON SURFACES

The interaction between active gases and the carbon surfaces under high temperatures is quite different from that under low temperatures. The fundamental difference is that high temperature provides enough energy to initiate chemical reactions between the gas molecules and carbon substance. Under these circumstances, physical adsorption is normally negligible and the interactions are mainly chemical in nature. The species retained on the carbon surface are either the dissociated adsorbates or the product of adsorbate-carbon reaction. The term sulfurization is used to describe the process of incorporation of sulfur onto the carbon surface.

Puri systematically summarized the research work on carbon-sulfur solid complexes [71]. It was found that formation of C-S complex was reported at the temperature range of 100-1000°C with sulfur containing gases like H_2S, CS_2, SO_2, and sulfur vapor. Decomposition of H_2S on

surfaces of charcoals was reported at temperatures as low as 100 °C [140]. The amount of combined sulfur decreased with the decrease in hydrogen or oxygen content of the carbon. The fixation of sulfur was believed to take place through addition to unsaturated sites as well as substitution of hydrogen or oxygen or hydroxyl groups initially presented on the charcoals. All these results support the idea that hydrogen sulfide can react chemically with carbon surfaces even at relatively low temperatures.

Blayden and Patrick [141] studied the formation and behavior of sulfur carbons by heating the polymer carbon in the presence of sulfur vapor and elemental sulfur. The experimental work indicated that the unpaired spin centers and hydrogen content might play important roles in the sulfurization of the carbon surface. The authors suggested that the bonding of C-S complexes was akin to that of thioethers or disulfides. Formation of peripheral heterocyclic structures or bridging of neighboring carbon atom layers might also take place. Valenzuela Calahorro *et al.* [142] reported that about 9.9% of sulfur was incorporated into carbon surface by heating activated carbon in high concentrations of hydrogen sulfide.

All carbon-sulfur complexes formed were found to be very stable [71]. It was not possible to recover any bonded sulfur by boiling in 2.5N NaOH solution; hydrogen sulfide and carbon sulfide were found in the effluent gas when the product was heated to 500 °C and the amount of emitted gases increased with the increase in temperature. An appreciable amount of sulfur was retained even after heating the samples to 1200 °C. The sulfur could only be completely removed by heating the product in hydrogen at 900°C.

The mechanism of sulfurization on the carbon surface is still not clear although many studies proposed the possible pathways. Puri and Hazra [72] observed that the amount of sulfur fixed on the

carbon surface correlates well with the oxygen content present as "CO-Complex" (the oxygen containing complex that releases CO upon heat treatment). The authors believe that oxygen and hydrogen content, extent of surface instauration, and pore structure were more important parameters than surface area. It was found that the strongly bonded amount of sulfur on H_2S treated charcoals was close to the surface instauration of the charcoals. It was postulated that H_2S interacts with quinonic and phenolic hydroxyl groups and then produce thioquinone and thiophenol groups [143]. The rest of the loosely bonded sulfur was added to the unsaturated sites that are not very reactive. The produced C-S complexes can catalyze the sodium azide-iodine reaction, which indicated the formation of sulfide and hydrosulfide groups.

To evaluate the possibility of using activated carbon as the sorbent for removing hydrogen sulfide from coal gasification environment (simulated coal gas containing 0.5% H_2S, 49.5% N_2, 13% H_2, 8.5% H_2O, 21% CO, and 7.5% CO_2), Cal *et al.* [19, 20] conducted systematic experimental studies. Activated carbons after various kinds of surface modification were used to remove H_2S at 550 °C. The results showed that both HNO_3 oxidation and Zn impregnation improved the H_2S adsorption capacity. They also found that temperatures between 400-600 °C had no significant impact on the process. H_2 regeneration was found to be the most effective method with all the sulfur being removed from the carbon surface. Based on literature review and the above observations, Cal *et al.* proposed that the following three mechanisms may possibly explain the adsorption of hydrogen sulfide on activated carbon surface:

- Addition to carbon active sites:

$$C+H_2S = C\text{-}S + H_2O \qquad (5)$$

- Substitution of oxygen:

$$C\text{-}O + H_2S = C\text{-}S + H_2O \quad (6)$$

- Reaction with metals:

$$C\text{-}M + H_2S = C\text{-}M\text{-}S + H_2 \quad (7)$$

Sugawara *et al.* [144] studied the effect of hydrogen sulfide on the behavior of organic sulfur in coal and char during heat treatment up to 800 °C. They concluded that a considerable amount of hydrogen sulfide was absorbed during heat treatment, forming organic sulfur forms, such as thiophenes and sulfides. Sulfur forms in the samples were determined using Sulfur K-edge X-ray adsorption near-edge structure spectroscopy. These forms of sulfur tend to concentrate as the gasification proceeds.

Recently, Ozaki *et al.* [145] reported the decomposition of H_2S on the thermally stable turbostratic carbons, which is derived from furan resin. Iron was added to the surface of the carbon. 0.5 vol% H_2S passed through a fixed bed reactor and decomposition of H_2S was observed. The surface iron species were believed to be responsible for the decomposition of H_2S around 350 °C, while decomposition of H_2S above 600 °C might be due to the Lewis acidic site.

Besides the sulfurization of carbon surfaces, sulfur can be easily incorporated into hydrocarbons and other compounds. There are several reports about sulfurization of organic matter by sulfides in aqueous phase under low temperature (around 50 °C) [146, 147]. Van Dongen *et al.* [147] proposed that the reaction most likely starts with sulfurization of the carbonyl functionality. Studies [148, 149] also showed that sulfur can be incorporated into the surface of polymers and result in

significant increase in the surface sulfur content. Thiophenes and polysulfides were believed to be the possible products. CH_4 and H_2S were found to react in a plasma reactor to produce a thin film containing about 27% of sulfur [150, 151]. The produced film was believed to have a structure of polymeric $(CS_2)_x$. Many metal/metal oxide surfaces can be easily sulfided by hydrogen sulfide. Saleh observed the chemisorption of H_2S on Pd at 80 °C, and the reaction with Pd to be dissociative [152].

In summary, significant amount of sulfur was incorporated into the carbon surface at in the absence of oxygen high temperatures higher than 100 °C. Higher hydrogen/oxygen content and greater extent of insaturation seem to lead to higher sulfur content. Sulfurization is probably achieved through the following mechanisms: addition to carbon active sites, substitution of hydrogen/oxygen or other non-carbon elements, and combination with metals. The sulfurization products seem to be organic sulfur and/or sulfides, with possible organic sulfur structure as thiophene or thioquinone. Sulfurization by hydrogen sulfide may be a possible way of producing mercury removal sorbents since the sulfur produced is low-valent.

2.6 OXIDATION OF HYDROGEN SULFIDE ON ACTIVATED CARBON

The direct oxidation of H_2S by oxygen is a catalytic exothermic reaction [130]:

$$H_2S + ½\ O_2 = H_2O + 1/n\ S_n \qquad \Delta H=-222\ kJ/mol \qquad (8)$$

The oxidation process based on this overall reaction (the actual process is comprised of several steps) is patented as the Claus reaction in 1890 and widely used for sulfur recovery from many industrial processes. The reaction needs catalyst to proceed because the kinetics without catalysts is extremely low. Various materials showed catalytic effect for this reaction, with alumina-based catalyst as the most common one. Activated carbon is also a very effective catalyst, but it is limited by its thermal stability in the presence of oxygen. The reaction can take place even at room temperature with catalysts. However, in real sulfur-recovering processes, the reaction temperature is normally much higher (usually above 200 °C). Depending on many reaction parameters, but mainly on temperature and O_2/H_2S ratio and gas composition, other side reactions can occur. The following are a few examples:

$$H_2S + 1½\ O_2 = SO_2 + H_2O \quad (9)$$

$$1/n\ S_n + O_2 = SO_2 \quad (10)$$

$$SO_2 + ½\ O_2 = SO_3 \quad (11)$$

$$CO_2 + H_2S = CO + 1/n\ S_n + H_2O \quad (12)$$

$$CO + S = COS \quad (13)$$

$$SO_3 + H_2O = H_2SO_4 \quad (14)$$

Higher temperature results in higher reaction rate. However, for activated carbon in the presence of oxygen, high temperature can burn the carbon and destroy the porous structure. The

carbon activity was maximized between 150 °C and 200 °C [153, 154]. Stejins *et al.* [155] reported that the only product formed below 200 °C are water and elemental sulfur. However, for temperatures above 300 °C, formation of SO_2 becomes significant.

In terms of sulfur retention, Blayden and Patrick [141] found that lower sulfurization temperature resulted in higher sulfur retention, while the sulfur retained on activated carbon rarely exceeded 5% at temperature at 300-500 °C. Coskun and Tollefson [156] showed that sulfur loading increased with the increase in reaction temperature from 24 °C to 152 °C.

Klein and Henning [157] proposed that depending on the reaction conditions reaction orders for oxygen and hydrogen sulfide were 0-1 and 0.5-1, respectively depending on the reaction conditions. Mikhalovsky and Zaitsev [158] compared the sulfur loading with and without the presence of oxygen. Under inert environment, sulfur content of only 6% was achieved, while sulfur content as high as 95% was found for the same carbon in the presence of air.

Catalytic reactions should involve the chemisorption of at least one of the reactants. For the oxidation of H_2S, chemisorption of oxygen is obvious and there are strong indications that H_2S may also be chemisorbed before the oxidation reaction.

Pieplu et al [130] reviewed the Claus catalysis and H_2S selective oxidation. The second step of the Claus reaction (the reaction between SO_2 and H_2S) was believed to take place between chemisorbed SO_2 and gaseous or adsorbed H_2S. The intermediate state of chemically adsorbed SO_2 is most likely to be HSO_3^-, which is produced from SO_2 linked to -OH surface groups.

Studies on the oxidation of H_2S at room temperature by Bandosz and co-workers [124, 126, 127, 131, 159, 160] revealed that a more acidic environment promotes the formation of sulfur oxides and sulfuric acid while a basic environment favors the formation of elemental sulfur (sulfur radicals).

The proposed reaction mechanism involved reaction of adsorbed hydrogen sulfide ion with dissociatively adsorbed oxygen as the limiting step [126]. Bagreev and Bandosz [131] found the catalytic effect of the impregnated NaOH. It was believed that NaOH neutralizes H_2S and shifts the dissociation reaction of hydrogen sulfide forward, thus increasing the content of HS^- ions, which facilities the oxidation process.

Mikhalovsky [158] suggested that carbon surface functionalities and transition metals affected the catalytic activity and selectivity to different products. It was proposed that surface functionalities contribute significantly to the formation of SO_x during H_2S oxidation. By varying different impregnation procedures, a vanadium-grafted catalyst with high selectivity towards elemental sulfur (over sulfur oxides) was developed, which worked effectively at the temperature exceeding the melting point of sulfur [158].

Yan *et al.* [161, 162] suggested that elemental sulfur and oxidized sulfur species were major products of H_2S oxidation on activated carbon surface at low temperature and in the presence of water vapor. The authors discussed the effect of surface pH at three ranges: pH > 7.0, 7.0 > pH > 4.5, and pH < 4.5. The first range favors the formation of elemental sulfur; the second range favors the formation of sulfur oxides and sulfuric acid in the presence of water, while physical adsorption dominates in the last range.

In summary, literature review on H_2S oxidation suggests that important parameters affecting the oxidation of hydrogen sulfide include: temperature, O_2/H_2S ratio, and carbon surface chemistry. Lower temperature and basic surface functionalities favor the formation of

elemental sulfur and activated carbon exhibits maximum activity between 125-200 °C. High temperature and functionalities of lower pH increase the selectivity to sulfur oxides and decrease the catalytic activity.

3.0 MATERIALS AND METHODS

3.1 CARBON MATERIALS

3.1.1 Activated Carbon Fibers

One of the carbonaceous sorbents selected for this study is activated carbon fiber (ACF). ACFs obtained from American Kynol, Inc. (Pleasantville, NY) have carbon content of over 95%. ACFs are produced from the novolac resin that is manufactured by polymerization of phenol and formaldehyde. Detailed information about the surface properties and structure of this sorbent is available in the literature [163]. These ACFs have uniform pore size distribution comparing to other carbon materials. Slit shaped micropores below 2 nm in diameter are predominant, with very few pores in the mesopore range (2 nm < d < 50 nm) and no pores in the macropore range (> 50 nm). ACFs were dried at 120 °C for 2 hours and ground into powder before H_2S adsorption and oxidation.

ACF10, ACF15, ACF20, and ACF25 were produced using increasing activation time that leads to higher surface area and larger pores. The properties of ACF10 to ACF 25 reported by literature [164] and the manufacturer were summarized in Table 3. ACF-10, ACF15, ACF20, and ACF-25 are expected to have estimated surface areas of 1000, 1500, 2000, and 2500 m^2/g, respectively. However, the BET surface area values reported in the literature [164] are not always

the same as the estimated values. The average pore width increases from ACF-10 to ACF-25. ACFs are good materials for studying the effect of pore size because they have relatively narrow pore size distribution. The pore size distribution of raw ACFs was also investigated in this study and the results are shown in Figure 7 (Chapter 4). ACFs have negligible ash content (about 0.01 wt%), which is probably from the manufacturing process and impurities of the raw materials. The major elements are carbon and oxygen with very limited amount of hydrogen and nitrogen. Previous studies indicated that with the increase in serial number, the oxygen content decreased [65, 165, 166].

Table 3. Properties of Kynol ACFs from literature and the manufacture

ACF Properties	ACF-10	ACF-15	ACF-20	ACF-25
Average Pore Width*	7.1	7.8	7.8	9.7
BET Surface Area (m^2/g)**	1000	1500	2000	2500
BET Surface Area (m^2/g)*	877	1518	1615	1918
Micropore Volume (cm^3/g)*	0.307	0.631	0.686	0.884
Total Pore Volume (cm^3/g)*	0.307	0.686	0.686	0.893
Fractional Microporosity (%)*	100	100	99	69.3
Benzene Adsorption (wt%)**	23.7	40.1	50	66
Iodine Adsorption (mg/g)**	1110	1630	1670	2290

* Reference [164] ** American Kynol, Inc, shipping invoice

Table 4. Sources and chemical compositions of BPL and ACFs

Carbon	Base Material	Ash Content	Elemental Composition (wt%)			
		(wt%)	O	C	H	N
BPL	Bituminous Coal	6.6	5.40[#]	---	---	---
ACF-10	Resin	0.01	8.11*	91.4*	0.33*	0.16*
ACF-20	Resin	0.01	---	---	---	---
ACF-25	Resin	0.01	4.50*	95.2*	0.06*	0.24*

*Mangun *et al.* 2001 [65, 165]; similar data were also reported by Foster *et al.*[166]
[#]Zhu *et al.* [167].

3.1.2 Activated Carbons

Five virgin activated carbons, namely BPL, F400, PCB, BD, and Centaur, were obtained from Calgon Carbon Corporation (Pittsburgh, PA). As received carbons were grounded and sieved, only particles of 10×16 U.S. mesh size were used for H_2S uptake test and further surface modification. All the virgin carbon samples were thoroughly washed and dried in an oven at 120 °C. Dried carbons were stored in a dessicator until use. The basic information about these five virgin carbons can be found in Table 8 (Chapter 4). BPL carbon is derived from bituminous coal and it was chosen as a typical activated carbon for experimental study.

3.2 EXPERIMENTAL SETUP AND PROCEDURE

3.2.1 Sample Preparation

Surface Treatment on ACFs

For H_2S adsorption test, the ACFs were mechanically ground into powder and dried at 120°C for 2 hours before any further treatment. 1g of powder ACF was fed to the fixed bed reactor for each run. "Dried" virgin samples were dried in nitrogen at 140°C for 2 hrs; "Heat treated" samples were heated to 900 °C for 4 to 6 hours. "Oxidized" samples were first dried, then heated up to 200°C for 2 hrs in a pure O_2 stream. After surface treatment, the samples were cooled down to room temperature for H_2S adsorption.

Surface Treatment on Activated Carbons

Heat treatment: Three carbon samples (BPL, PCB, and F400) were heated in a ultra high purity (UHP) nitrogen or argon stream at 10 °C/min up to 300 °C, 600 °C, and 900 °C separately for 3 hours, then the samples were cooled down to 23 °C at 10 °C/min for H_2S uptake test.

Ammonia Treatment: 2 g of each carbon sample was soaked in 25 ml of 29 wt% ammonia solution in a sealed bottle. The carbon-solution mixture was kept for 24 hours with shaking. Then the carbon sample was separated by filtration and dried at 110 °C for 5 hours.

3.2.2 H_2S Adsorption, Sulfurization, and Oxidation

H_2S Adsorption

Figure 4 shows the fixed bed reactor system for H_2S adsorption/oxidation. The gases were supplied by pressurized tanks. For H_2S adsorption, standard H_2S gas of 200 ppm (Praxair, in nitrogen, certified) was used for adsorption test. Higher concentrations of H_2S were generated by diluting 5% H_2S standard gas (Praxair, diluted in nitrogen, certified) with nitrogen (Praxair, UHP). Mixed gas with a total flow rate of 150 ml/min was fed through a quartz reactor (38cm long with 1cm OD), which was positioned vertically in the middle of a tubular furnace (Lindberg Heavi-Duty, Watertown, WI) with a temperature controller. The effluent gases were analyzed continuously by a QMS 300 (Stanford Research Systems, Sunnyvale, CA).

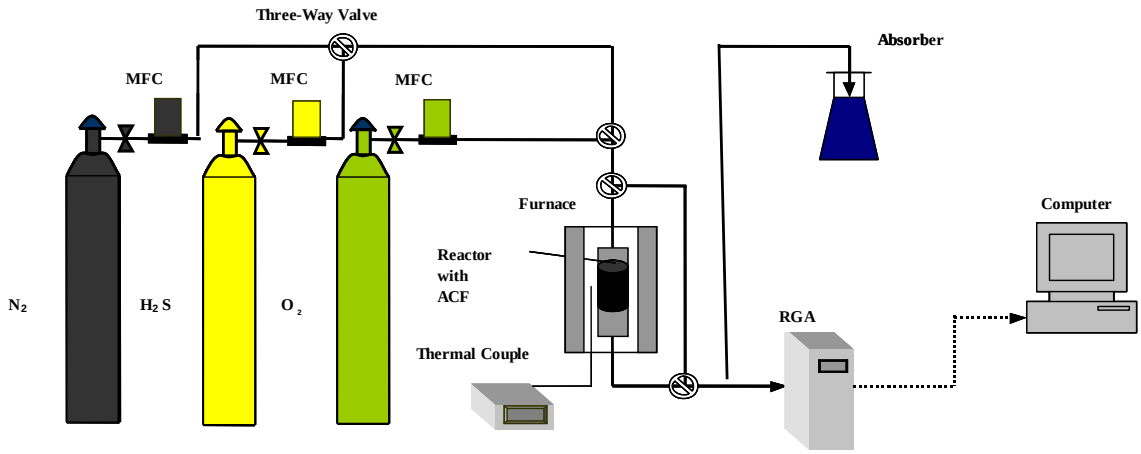

Figure 4. Experimental setup for H_2S adsorption/oxidation

The fixed-bed reactor was first flushed with pure N_2 for 30 min then the inlet gas was switched to gas mixture with desired H_2S concentration and the data collection was initiated. The H_2S concentration was continuously monitored by QMS until saturation was reached. After saturation the inlet gas was switched back to pure N_2 and the H_2S concentration desorbed from the carbon surface was recorded continuously. As a result, a breakthrough curve and a desorption curve were generated. Figure 5 illustrates the experimental procedure to obtain adsorbed amount and desorbed amount. The "adsorbed amount" can be obtained by integrating the area above the breakthrough curve. The desorbed amount can be obtained by integrating the area below the desorption curve. This is defined as the "desorbed amount". The difference between adsorbed

amount and desorbed amount is defined as the "retained amount" on the ACFs' surface. The adsorption of H_2S onto activated carbons was studied in the same way as the adsorption onto ACFs except that the "retained amount" was determined using a sulfur analyzer (SC-132, Leco Sulfur Analyzer, St. Joseph, MI).

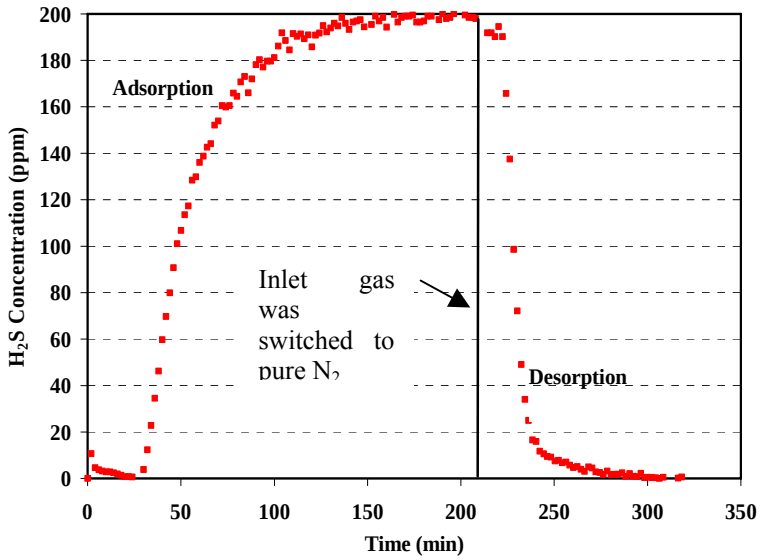

Figure 5. H_2S breakthrough and desorption curves

Sulfurization of Carbon Surface

The same fixed bed reactor system was used for H_2S uptake test with similar procedures. Sulfurization was conducted at the temperature range of 200-800 °C. 3000 ppm H_2S was generated by diluting 5% H_2S standard gas (Praxair, diluted in nitrogen, certified) with nitrogen (Praxair, UHP). 500 mg of carbon sample was loaded in the quartz reactor. After drying at 120 °C for 2 hours with nitrogen flowing through the reactor, sulfurization of carbon surfaces was

carried out using different sulfurization protocols at different temperatures. While all samples were subjected to the same temperature programmed process, different sulfurization protocols expose the carbon surface to H_2S at different stages. As shown in Figure 6, the following samples were prepared at maximum temperature of 600 °C and H_2S concentration of 3000 ppm: for **600C-S**, H_2S was present during stable temperature only; for **600C-H+S**, H_2S was present during heating and stable temperature; for **600C-H+S+C**, H_2S was present during heating, stable temperature, and cooling; for **600C-S+C**, H_2S was present during stable temperature and cooling; and for **600C-C**, H_2S was present during the cooling process only. Using QMS to monitor the exit gas, it was determined that 6 hours of exposure to H_2S was sufficient to reach complete breakthrough of H_2S. Sulfur analysis also confirmed that no increase in the sulfur content was observed even if the impregnation time was increased to 14 hours. For all the runs, the stable temperature period lasted for 6 hours.

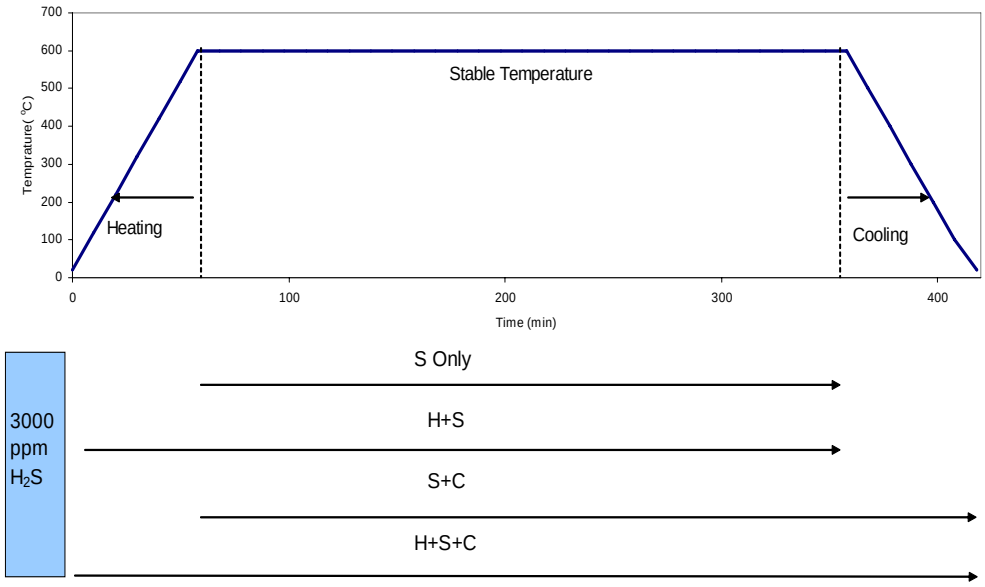

Figure 6. Experimental protocols for the sulfurization process

H_2S Oxidation

For H_2S oxidation, the same fixed reactor system was employed with an additional oxygen tank. 5% H_2S (Praxair, 5% in nitrogen, certified) and O_2 (Praxair, Pure) were diluted by N_2 (Praxair, UHP) to a desired concentration (3000 ppm H_2S and 12,000 ppm O_2) by controlling the flow rate of each gas with mass flow controllers. The total gas flow rate to a quartz reactor was maintained at 150 ml/min. Other conditions were the same for H_2S adsorption.

ACF10 was impregnated with sulfur at 80 ^oC and 150 ^oC until the effluent H_2S concentration reached the influent level after 24 hours. These samples were labeled as ACF10-80C-24hrs and ACF10-150C-24hrs. ACF25 was impregnated with sulfur at 150 ºC for 2, 6, and 24 hours.

Designation for these sorbents includes temperature and duration of the impregnation process, i.e. ACF25-150C-2hrs means the ACF-25 was impregnated with H_2S at 150 ºC for 2 hours. The amount of sulfur deposited on the sorbent was determined from the breakthrough curve.

Temperature Programmed Reaction on H_2S-Carbon Interaction

1 g of carbon materials was first loaded into the fixed bed reactor, then at room temperature 12,000 ppm H_2S (generated by diluting 5% H_2S by argon) was introduced into the reactor. After adsorption for 40 min, the reactor was heated up at 10 °C/min up to 900 °C. In this process, atomic mass units (AMUs) 1 to 100 were monitored, and only the active AMUs were selected and analyzed.

3.2.3 Hg Uptake Test

All the mercury uptake tests followed the same procedure. Raw and sulfur-impregnated carbon materials (ACFs and BPL carbon) were tested for vapor phase elemental mercury uptake at 140 °C in a fixed-bed reactor. Industrial grade nitrogen (99.5%) was used as the carrier gas with a flow rate of 550 ml/min, which is controlled by a mass flow controller (Tylan General, Torrance, CA). The inlet mercury concentration was maintained at 350 $\mu g/m^3$ by controlling the temperature of the permeation tube (VICI Metrons Inc. Santa Clara, CA) filled with liquid mercury. Mercury concentration was analyzed continuously using an atomic absorption spectrophotometer (Model 403, Perkin-Elmer, Norwalk, CT) equipped with 18-cm hollow quartz cell (Varian Australis Pty, Ltd., Mulgrave, Victoria, Australia) and the mercury adsorption capacity was calculated by integrating the area above the breakthrough curve. For each sample, the mercury uptake test was conducated at least twice. Repeated measurements showed that the mercury uptake capacities can be determined with a relative standard deviation less than 12%.

3.3 SORBENT CHARACTERIZATION

3.3.1 Surface Area and Pore Structure Analysis

The surface area and pore size distribution of virgin and impregnated ACFs were analyzed using nitrogen adsorption at 77 K in a Quantachrome Autosorb Automated Gas Sorption System (Quantachrome Corporation, Boynton Beach, FL).

3.3.2 SEM-EDAX Analysis

SEM (Scanning Electron Microscope) – EDAX (Energy Dispersive Analysis, X-ray) analysis was conducted using a Philips XL30 SEM equipped with an EDAX detector. Besides observing the image of ACFs, the EDAX detector was used to measure the surface elemental composition of the ACF samples that were pasted as a thick layer onto a tape before insertion into the vacuum chamber.

3.3.3 XPS Analysis

XPS (X-ray photoelectron spectroscopy) analysis was performed using a Physical Electronics Model 550 equipped with a cylindrical, double-pass energy analyzer. The ACF samples were attached to a tantalum surface by conductive silver paste (LADD Research Industries) before insertion into the vacuum chamber.

3.3.4 Thermogravimetric Analysis

Thermogravimetric analysis (TGA) was conducted using TGA7 (Perkin-Elmer, Norwalk, CT) where the sample was maintained at 120 ºC for 2 hours and then heated to 850 ºC with a heating rate of 10 ºC/min in a high purity nitrogen atmosphere. For some analysis, the QMS 300 was attached to the exiting tube of the TGA gas line to enable simultaneous detection of the weight loss and gas species evolved from the sample.

For the ACFs samples impregnated with sulfur through H_2S oxidation, TGA data can also be used to estimate the activation energy for the desorption of impregnated sulfur from the carbon surface. TGA analysis of a sample (ACF10-150C-24hrs) at different heating rates (2, 6, 10, and 14 ^{o}C/min) yields different rates of weight loss versus temperature. The activation energy can be estimated according to the following equation [168]:

$$E_a = -18.18\, d(\log B) / d(1/T) \qquad (15)$$

where, E_a is the activation energy for desorption in J/mol; B is the heating rate in K/sec; and T is the temperature corresponding to a given weight loss at a given heating rate in K.

3.3.5 Temperature Programmed Desorption

Two kinds of temperature programmed desorption tests were carried out. A typical temperature programmed desorption was conducted inside the fixed bed reactor after H_2S

adsorption/desorption or sulfurization. Starting from room temperature, the temperature of the tubular furnace was raised at 10°C/min (or 3.3°C/min in some cases) up to 900°C in a nitrogen or argon gas stream and effluent gas was monitored with the QMS 300. AMUs of interest and the desorption temperatures were recorded continuously.

A special temperature programmed desorption (TPD) was conducted for H_2S oxidation samples using a TGA coupled to the QMS 300 to sample the effluent gas from the TGA. This method enabled simultaneous detection of the weight loss and gas species released from ACF10-Raw and ACF10-150C. However, elemental sulfur released during heating was observed to quickly condense as yellow solid at the outlet of the TGA chamber, and could not be detected by the QMS. The nitrogen or argon gas flow rate was 12 ml/min and heating rate was 10 ºC/min if not specified.

3.3.6 Sulfur Analysis

Sulfur analysis was conducted using a Leco Model SC-132 Sulfur Determinator (Leco Co., St. Joseph, MI). The basic principle of the instrument is to completely oxidize the sample in a pure oxygen stream under extremely high temperatures to produce SO_2 that is quantitatively analyzed by an IR cell. The sulfur content can be determined based on the weight of the sample and amount of sulfur detected.

To analyze the sulfur content of each sample, the furnace temperature was first preheated to 1200 °C and a ceramic boat containing about 100 mg of sample was placed inside the furnace. Sulfur content is displayed based on calibration. For each set of analyses, calibration was

conducted using the standard sample (Leco Co., St. Joseph, MI) of known sulfur content (3.11 wt% ±0.06%). Repeated anyses on one sample showed that the relative standard deviation of sulfur analysis is within 8%.

3.3.7 Surface Functional Groups and pH Measurement

The Boehm titration was conducted according to the methods decribed by Bohem[169, 170]. Titration followed the ASTM Method 2310B and 2320B. The basic principle is explained by Boehm [37]. The procedure is briefly described as follows:

1. Prepare standard acidic and basic solutions: 0.25N and 0.05N NaOH, 0.05N $NaHCO_3$, 0.05N Na_2CO_3, and 0.05N HCl.
2. Weigh 2 g of each carbon sample and put it into five 160 ml vials, with each vial containing 100 ml of the above prepared solutions.
3. Completely seal the vials and put them into a shaker for 24 hours.
4. Remove the carbon samples by filtration and titrate the basic solutions using HCl and titrate the HCl solution using 0.05 N NaOH to pH=7 as the endpoint.
5. The amount of acidic sites for a specific group were calculated under the assumption that 0.25N NaOH neutralizes total acidity; 0.05N NaOH neutralizes carboxyl, phenolic, and lactonic groups; Na_2CO_3 neutralizes carboxylic and lactonic groups; and $NaHCO_3$ only reacts with carboxylic groups.

Repeated anayses on one sample showed that the deviation of Boehm titration is less than 0.05 mmol/g (50 μmol/g).

The pH of the carbon sample was measured by placing 2 g of carbon in 100 ml deionized water. After the sample was shaked for 24 hours, the filtrate pH was measured using a pH meter (Accument pH meter 25, Fisher Scientific, Pittsburgh, PA).

3.3.8 Ash and Metal Content Analysis

Ash content was determined by heating 1 g of carbon sample at 500°C for 24 hours in a Type F62730 muffle furnace (Barnstead/Thermolyne, Dubuque, IA). The residuals were weighed and calculated as percent ash content. The residue ash was dissolved in 25 ml of 12 N HCl, then filtered through an acid-resistant cellulose acetate filter (Millipore, Bedford, MA). The filtrate was analyzed using atomic adsorption spectrophotometer (AAS, Perkin Elmer, 1100B) equipped with flame and graphite furnace. Contents of six different metals were analyzed: iron, copper, aluminum, magnesium, manganese, and calcium.

3.3.9 XAFS Analysis

The sulfur K-edge X-ray adsorption fine structure analysis (XAFS) spectra were recorded at beam-line X-19A at the National Synchrotron Light Source (NSLS) at Brookhaven National Laboratory, NY. Before analysis, the sulfur impregnated carbon samples were grounded into powders. The X-ray adsorption near-edge structure (XANES) region of the spectra were

analyzed by the means of least-squares to obtain peaks associated with electronic transition from 1s to 3p levels within the sulfur atoms. Further information about the sulfur K-edge XAFS measurement are reported by Huggins *et al.* [171-173].

4.0 RESULTS AND DISCUSSION

4.1 H_2S ADSORPTION ONTO ACFS

4.1.1 Characterization of Activated Carbon Fibers

Table 5 summarizes the surface area and pore volume of ACFs before and after heat treatment, while Figure 7 shows the pore size distribution of selected samples. Based on these results, the pores of raw ACFs were divided into three ranges corresponding to three peaks consistently shown in the pore size distribution figures. The pore volume of each region was obtained from the BET analysis and is listed in Table 5.

With the increase in serial number of raw ACFs (from ACF10 to ACF25), both surface area and pore volume increased, which is consistent with the manufacturer's specifications. After heat treatment at 900 °C for 4 hours (sample ACF10-900C-4hrs), the pore volume and surface area of ACFs increased slightly, which may be due to the release of adsorbed species, or the expansion of pores because of additional volatilization of ACFs. Another explanation is the reaction between active gases with the ACFs to form higher surface area and bigger pore volume. Although present in very limited amount (<3 ppm), oxygen from the ultra high purity (UHP) nitrogen gas stream

may contribute to the surface area and pore volume increase. Similar results were also reported by Daley *et al.* [88], although they concluded that heat treatment has almost no effect on the pore structure of ACFs.

Analysis of the pore volume change in different ranges shows that higher serial number of ACF has higher portion of bigger pores. From ACF10 to ACF20, there is a significant increase in both medium and big micropores as a result of longer activation, but the small micropore volumes did not change significantly. From ACF20 to ACF25, the pore volume increase is mainly due to the increase in big micropores. Figure 7 (a) also shows that with the increase in serial number, the pore size distribution becomes less uniform in all ranges. The same behavior was obtained after heat treatment in this study (as shown in Figure 7 (b) and (c)) because the heat treatment increased mainly the medium and big micropores for ACF10 and only big micropores for ACF25.

Table 5. Micropore structure of ACFs before and after heat treatment

Samples	Pore Volume (cm^3/g)				Surface Area
	Small Pores	Medium Pores	Big Pores	Total	(m^2/g)
	(4.0-7.2 Å)	(7.2-9.0 Å)	(>9.0 Å)	(>4.0 Å)	
ACF10-Raw	0.274	0.039	0.065	0.378	920
ACF20-Raw	0.258	0.104	0.329	0.691	1453
ACF25-Raw	0.263	0.101	0.489	0.853	1920
ACF10-900C-4hrs	0.291	0.069	0.112	0.472	965
ACF25-900C-6hrs	0.276	0.095	0.554	0.925	1964

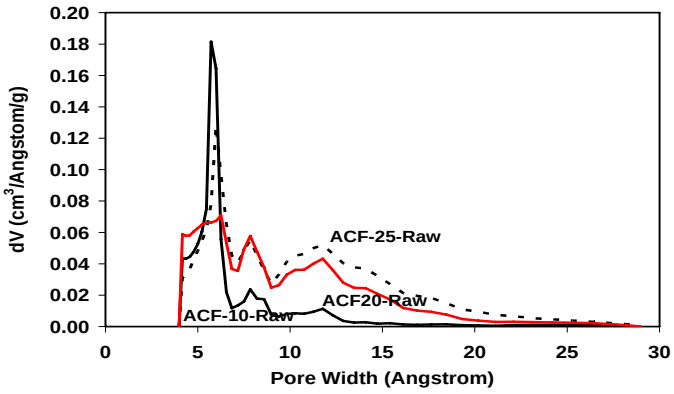

(a) raw ACFs

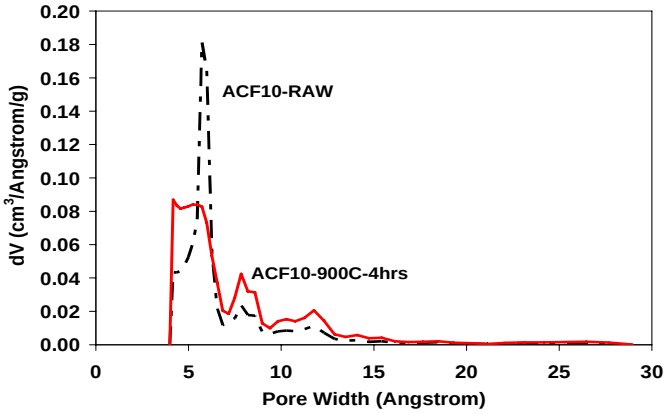

(b). ACF10 before and after heat treatment in N_2

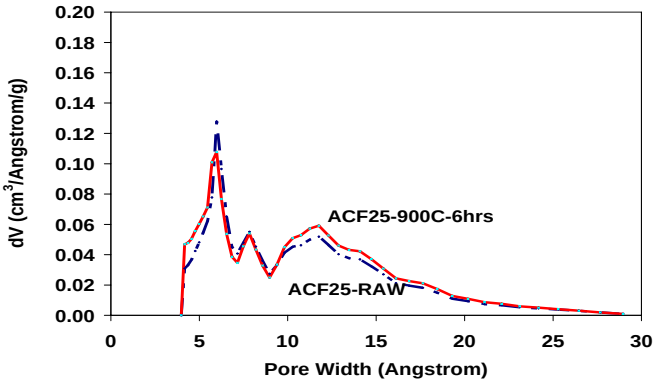

(c). ACF25 before and after heat treatment in N_2

Figure 7. Pore size distribution of ACFs before and after heat treatment

Table 6 summarizes the surface functionalities obtained through Boehm titration. The total acidic surface functionalities decreased with an increase in serial number. However, the total amount of basic functionalities increased with the increase in serial number. The basicity on carbon surfaces is reported to be associated with, such as pyrone, chromene, or quinone groups [36]. Also, the increase in the density of graphitic platelets carrying π electrons during extended activation might contribute to the increase in basicity [36].

Table 6. Surface functionalities on raw ACFs determined by Boehm titration (mmol/g)

ACF #	Total Acidic	Carbonyl	Carboxyl	Lactonic	Phenolic	Total basic
ACF10	3.11	2.42	0.348	0.037	0.309	0.439
ACF20	2.70	2.04	0.326	0.068	0.270	0.670
ACF25	2.09	1.43	0.309	0.079	0.273	0.790

4.1.2 Effect of Pore Structure and Surface Treatment on H_2S Uptake

Raw ACFs before and after surface treatment (oxidation at 200 ºC and heat treatment in nitrogen at 900 ºC) were subjected to H_2S adsorption/desorption tests. The H_2S adsorption experiments were carried out at room temperature, with 200 ppm H_2S in pure nitrogen. Table 7 summarizes test results. As mentioned above, the adsorbed amount is divided into retained amount and desorbed amount. The latter one is the amount desorbed in nitrogen. The desorbed amount can be viewed as physically adsorbed, while the retained amount can be viewed as chemisorbed.

Table 7 shows that regardless of the surface treatment, with the increase in serial number of the ACFs, the adsorbed and retained amount of H_2S increased. According to the sorbent characterization shown in the previous section, the surface area, pore volume, average pore size, and total basic functionalities increased with the increase in serial number of ACFs. Considering the fact that retained amount could not be easily removed from the carbon surface, it is believed that the increase in the retained amount is mainly due to the change in the amount of active sites that may be related to surface area.

The desorbed amount decreased with the increase in serial number. However, the decrease in desorbed amount (about 1 mg/g for all cases) is not significant compared with the increase in retained amount. A slight decrease in desorbed amount with the increase in serial number can be qualitatively explained by the micropore filling theory [117, 118], which predicts that pores of smaller size will adsorb more adsorbates at lower concentrations due to the higher adsorption potential exerted by their walls. Figure 8 shows the N_2 adsorption isotherms of raw ACFs at 77K. Indeed, at a relative pressure (p/p_0) of 1.2E-5, there is a crossing point, below which ACF10 has higher adsorption capacity than ACF25. Although the average pore size increased with the increase in serial number, the micropore volume did not change significantly, leading to relatively small changes in desorbed amount (Table 5).

Table 7 consistently shows that both oxidized and heat treated ACFs have higher adsorbed and retained amount than the raw ACFs (dried), with oxidized ACFs achieving the highest retention of hydrogen sulfide. Oxidation at low temperature (200 ºC) is not likely to change the pore structure. It can, therefore, be concluded that surface chemistry contributed more to this phenomenon. Oxidation obviously increases the surface oxygen containing functionalities, which may be one form of the active sites for H_2S uptake. The amount of H_2S retained on the ACF

surface was likely oxidized by, or strongly bonded to these surface functionalities. Bouzaza *et al.* [174] observed that oxidation of H_2S occurred even if the gaseous oxygen was not present in a dry atmosphere. They concluded that the oxidation is due to the oxygen-containing surface functionalities of the carbon fibers. Therefore, oxidized carbon surface probably enhanced H_2S retention through oxidation.

The increased H_2S uptake by heat treated ACFs can also be explained by the change in surface chemistry but through a different mechanism. It is commonly believed that heat treatment under inert environment will decrease and even totally eliminate the surface oxygen containing functionalities, especially acidic oxygen containing surface functionalities, without significantly changing the pore structure. Decomposition of acidic surface functionalities increased the basicity of ACF surface [36], which is helpful for retaining the acidic H_2S. It is reported [70] that the removal of oxygen during high-temperature N_2 treatment leaves unsaturated carbon atoms at crystallite edges, which lead to very high heat of adsorption during adsorption of oxygen. Since the retained amount increased after heat treatment, these unsaturated sites are likely responsible for H_2S uptake.

Table 7. Adsorbed, desorbed and retained amount (mg/g) of H_2S by ACFs before and after different surface treatments

Surface Treatment		ACF10	ACF20	ACF25
Raw(Dried)	Adsorbed	1.43	2.18	2.65
	Retained	0.37	1.29	1.77
	Desorbed	1.06	0.89	0.88
Oxidized	Adsorbed	1.96	3.62	4.57
	Retained	0.86	2.71	3.77
	Desorbed	1.1	0.91	0.8
Heat Treated	Adsorbed	1.61	2.74	3.86
	Retained	0.57	2.14	3.34
	Desorbed	1.04	0.6	0.52

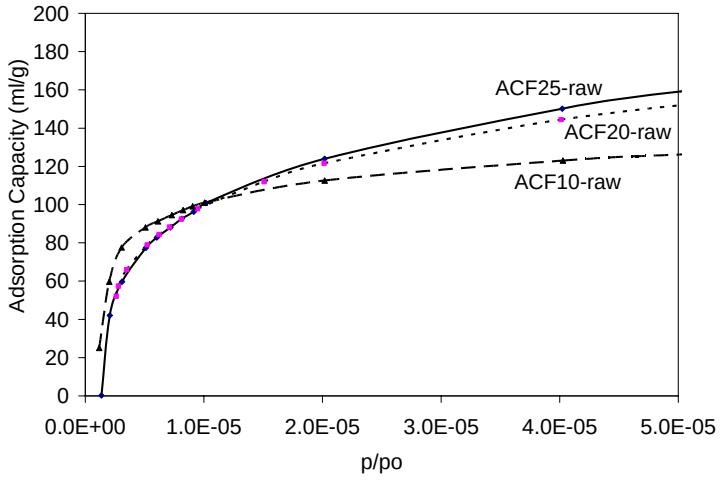

Figure 8. N_2 isotherms at 77K for raw ACFs

The adsorbed and retained amounts per unit pore volume or per unit surface area can be calculated using the data shown in Table 5 and Table 7. All the data were obtained at 23 °C. The results in terms of surface area depicted in Figure 9 clearly show that the retained amount per unit surface area of raw (virgin) ACF increased with the increase in surface area. ACFs with higher serial numbers were produced after longer activation time, leading to an increase in both surface area and oxygen containing active sites per unit surface area. If the surface area alone were responsible for increased retention of H_2S, the retained amount per unit surface area should remain constants for all ACFs. However, Figure 9 clearly shows that the retained amount per unit surface area changed from one ACF to another. It can therefore, be concluded that the surface chemistry is more important for H_2S chemisorption. The retained amount of H_2S per unit surface area increased after heat treatment (ACF10-Raw vs. ACF10-900C-4hr and ACF25-Raw vs. ACF25-900C-6hr), which can be explained by the increase in the amount of active sites. The desorbed amount, which is the difference between adsorbed and retained amount, decreased with the increase in pore volume and pore size, which can be explained in terms of micropore filling theory.

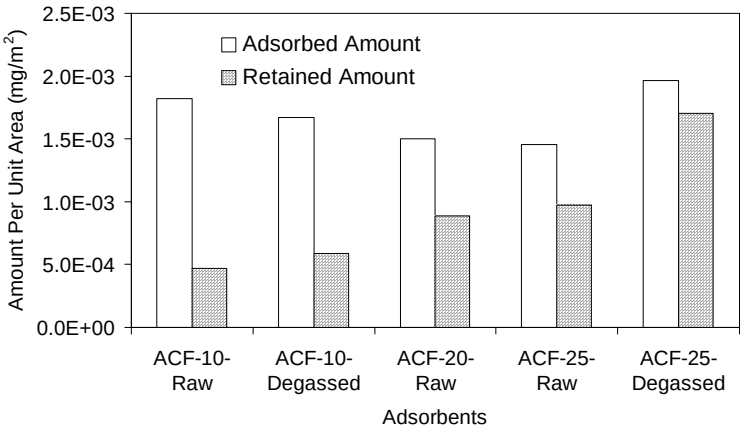

Figure 9. Adsorbed and retained amount of H_2S on ACFs per unit surface

Surface basic functionalities represent possible active sites that are responsible for H_2S retention through acid/base interactions. The amount of basic functionalities detected by Boehm titration was correlated with the retained amount on raw ACFs in Figure 10. Strong linear correlation between the basic surface functionalities and the amount of H_2S retained by raw ACF is not unexpected because H_2S is an acidic gas. Bashkova *et al.* [175] reported a strong correlation between basic functionalities and adsorption of methyl mercaptan, which also revealed the importance of acid-base interactions in acidic gas adsorption.

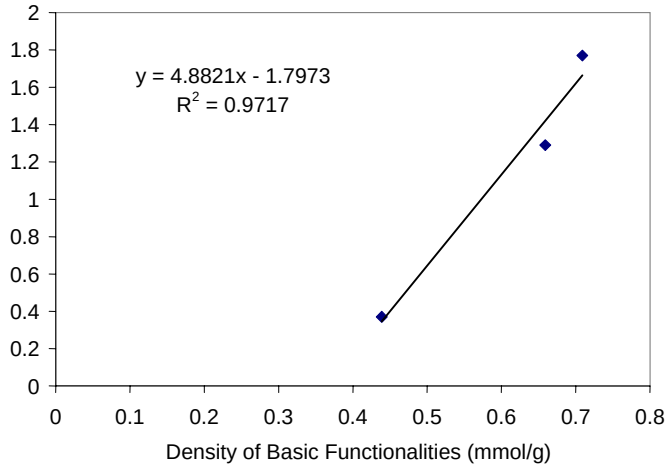

Figure 10. Correlation of basic surface functionalities with H_2S retention (chemisorption) on raw ACFs

4.1.3 Temperature Programmed Desorption

Temperature programmed desorption (TPD) reveals possible interactions between adsorbed H_2S and carbon surface because higher desorption temperature reflects stronger bonding. The effluent during TPD experiments was monitored at specific AMUs, namely 16 (O), 28 (CO or N_2), 32 (S or O_2), 34 (H_2S), 44 (CO_2), 64 (S_2 or SO_2) and 76 (CS_2).

Figure 11(a) shows the TPD profiles for raw ACF10 after adsorption of 3000 ppm H_2S followed by desorption in nitrogen. The desorption in nitrogen was carried out for 24 hours to ensure that all reversibly adsorbed sulfur species were removed. Figure 11(a) shows that most sulfur species were released between 260-450 °C. TGA test also shows that most of the weight loss occurred between 220-420 °C for raw ACF10 after adsorption and desorption at 23 ºC. According to Pieplu *et al.* [130], the dissociatively adsorbed H_2S desorbed at 290-315 ºC. Among the sulfur

containing species, SO_2 was released first, while COS was released at slightly higher temperatures. Figure 11 (b) shows that a trace amount of O_2 was released around 160 °C. Raw sorbent has oxygen content around 5%, which is the most probable source of O_2 because ultra high purity of N_2 was used as the carrier gas. The results in Figure 11 indicate that H_2S was strongly bonded to the carbon surface and that most of the H_2S was probably oxidized by oxygen (at the carbon surface) during the adsorption process or during the TPD run. Figure 11 (b) shows that there was sufficient amount of oxygen on the ACFs surface for complete H_2S oxidation because CO_2 desorption was still observed at temperatures above 200 °C [59, 176]. These results revealed that the oxygen containing surface functionalities are important active sites for retaining H_2S onto the raw ACF surface.

Sulfur analysis shows that indeed there is a significant amount of sulfur retained on the carbon surface after nitrogen desorption and that some sulfur remained on the carbon surface even after exposure to 850 °C (Figure 12). The sulfur that remained after TPD run may have been imbedded deeply into the carbon structure during the heating process.

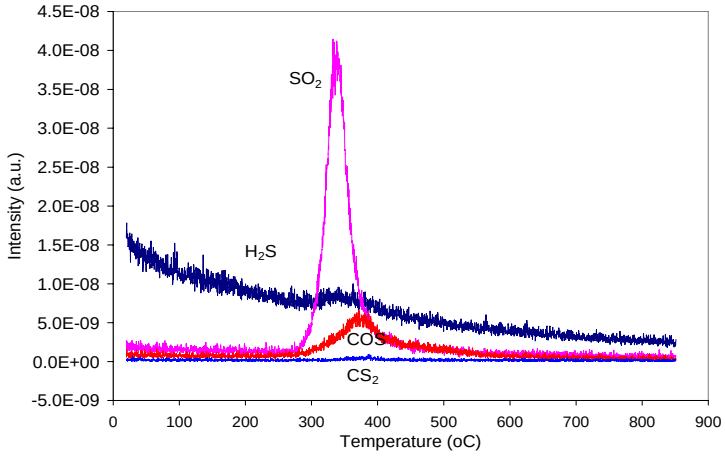

(a)

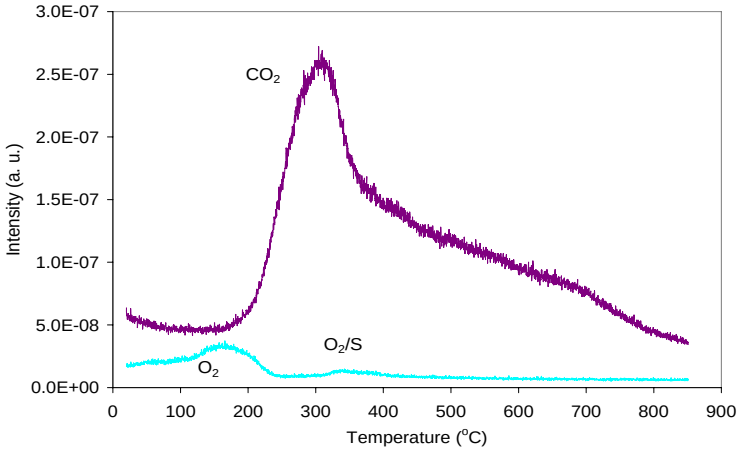

(b)

Figure 11. Gas species released during TPD of ACF10-raw: (a) sulfur containing species, (b) other species

(16 (O), 32 (S or O_2), 34 (H_2S), 44 (CO_2), 64 (S_2 or SO_2) and 76 (CS_2))

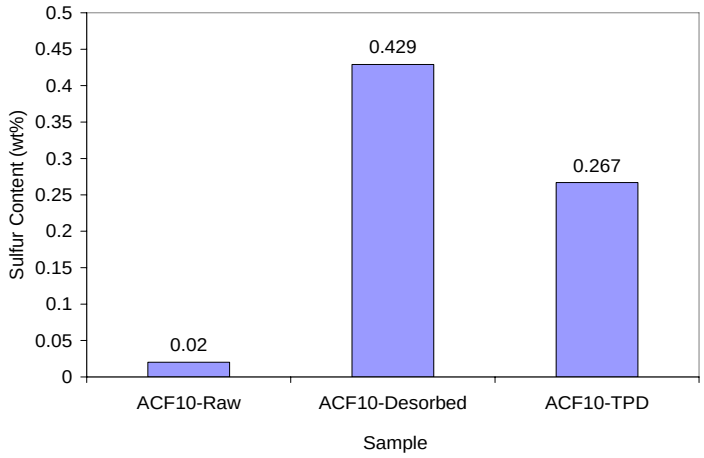

Figure 12. Sulfur content of ACF-10 after desorption and TPD

Figure 13 shows TPD profiles for heated treated ACF10 (ACF10-900C-4hr) after adsorption of 3000 ppm H_2S and desorption in nitrogen. In contrast to the results obtained for raw ACF10 (Figure 11), the major sulfur species desorbed in the effluent was H_2S, while small amount of SO_2 was released at lower temperatures (Figure 13(a)). Another major difference is that there was no significant amount of CO_2 evolving from heat treated ACF10 (Figure 13 (b)). Such behavior was expected because most of the surface oxygen was removed during sample pretreatment. These results show that the sulfur species can be strongly bonded to the carbon surface even when most of the oxygen was removed from the surface. In that case, the majority of the sulfur species were present on the carbon surface in the reduced form. These results on Figure 11 and Figure 13 show different pathways responsible for the increase in the retained amount of H_2S for raw and heat treated samples (Table 7). For raw ACF10, the presence of oxygen promotes the oxidation of H_2S,

as reported by previous researchers [158, 174]. For heat treated ACF10, the decomposition of oxygen containing functionalities creates unsaturated basic sites [70] or liberated π-electrons associated with basal planes, thereby promoting the retention of H_2S mainly through acid-base interactions.

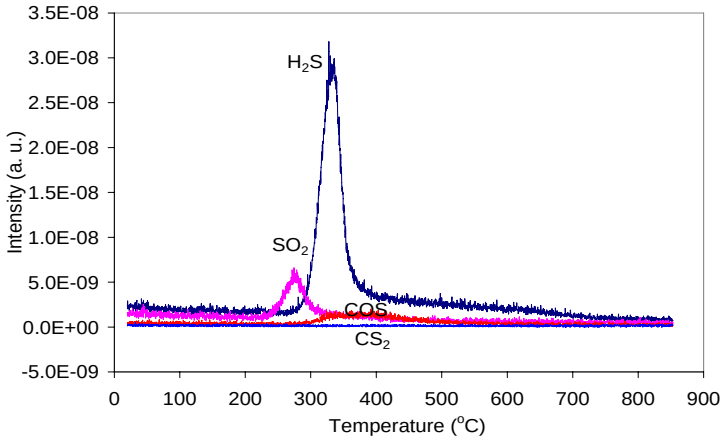

(a)

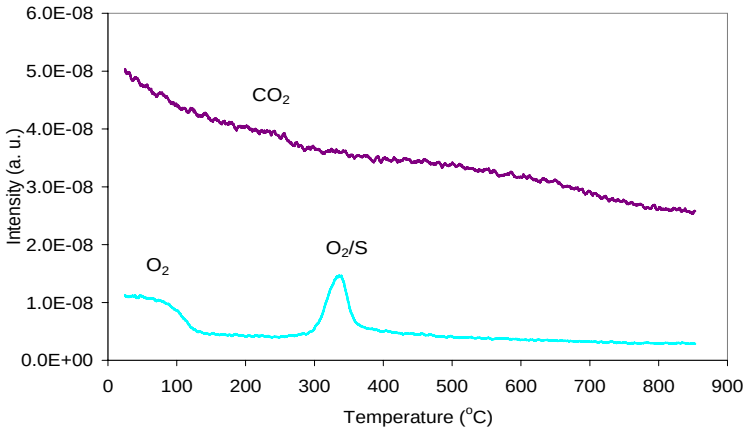

(b)

Figure 13. Gas species released during TPD of ACF10-900C-4hrs: (a) sulfur containing species, (b) other species

(16 (O), 32 (S or O_2), 34 (H_2S), 44 (CO_2), 64 (S_2 or SO_2) and 76 (CS_2))

4.1.4 Summary

To understand the nature of H_2S adsorption onto carbon surfaces under dry and anoxic conditions, effect of carbon pore structure and surface chemistry were studied using activated carbon fibers (ACFs) with different pore structures and surface areas. Surface pretreatment including oxidation and heat treatment were also conducted before adsorption/desorption test in a fixed bed reactor. Raw ACFs with higher surface area showed greater adsorption and retention of sulfur and heat treatment in nitrogen further enhanced adsorption and retention of sulfur. The retained amount of hydrogen sulfide correlated well with the amount of basic functionalities on the carbon surface, while the desorbed amount reflected the effect of pore structure. TPD and TGA anayses showed that the retained sulfurous compounds were strongly bonded to the carbon surface. In addition, surface chemistry of the sorbent might determine the predominant form of adsorbate on the surface.

4.2 H_2S ADSORPTION ONTO ACTIVATED CARBONS

4.2.1 Characterization of Activated Carbons

Table 8 lists the origin, surface area, and metal content of virgin activated carbons used in this study. BD and PCB were derived from wood and coconut shells, respectively; Centaur, BPL, and F400 were derived from bituminous coal. Because of the difference in origin, the latter carbons have much higher ash contents, especially the Fe and Al contents, while PCB has the lowest ash content. The BET surface areas were obtained from the literature [125, 177, 178].

Table 9 lists the density of different surface functionalities on virgin activated carbons as determined by Boehm titration. The carbonyl group seems to be the major acidic functional group although it is the weakest acidic group [89]. The density of total acidic functionalities is higher than total basic groups for all carbons. The pH values of different carbons are consistent with the ratio of acidic and basic surface groups on the carbon surface (i.e. more basic groups and less acidic groups resulted in higher pH of the carbon sample) except Centaur. Centaur is produced through special chemical treatment at high temperatures. It is patented and specifically designed for catalytic applications [179, 180].

Table 8. Precursor, surface area, and metal content of activated carbons

Carbons	Base Material	BET Surface Area	Ash Content	Metal Content (mg/kg)					
		(m^2/g)	(wt%)	Al	Ca	Cu	Mg	Mn	Fe
BD	Wood	510	2.7	48	378	53	313	603	140
Centaur	Bituminous Coal	632	4.1	1290	350	108	139	41	1040
BPL	Bituminous Coal	1067	6.6	1292	841	251	198	21	2868
PCB	Extruded Coconut	1124	0.8	6	105	13	365	9	182
F400	Bituminous Coal	1224	7.3	86	325	21	101	5	2984

Table 9. Functionalities and pH of activated carbons

Activated Carbons	Carboxyl	Lactonic	Phenolic	Carbonyl	Total Acidity	Total Basicity	Total Groups	Acidity/ Basicity	pH
BD	0.300	0.112	0.608	0.138	1.158	0.215	1.373	5.39	4.72
Centaur	0.042	0.012	0.074	0.410	0.538	0.390	0.928	1.38	5.26
BPL	0.070	0.130	0.130	0.408	0.738	0.313	1.050	2.36	5.45
PCB	0.150	0.000	0.123	0.568	0.840	0.535	1.375	1.43	7.80
F400	0.025	0.030	0.195	0.760	1.010	0.588	1.598	1.89	5.88

Unit: mmol/g

4.2.2 Effect of Carbon Surface Chemistry on H_2S Uptake

Figure 14 depicts the correlation between irreversibly adsorbed (retained) H_2S and surface area, ash content, and specific metal contents for the five sobents evaluated in this study. It is clear that ash and specific metal content had no significant effect on H_2S retention at 23 °C under dry and anoxic conditions. Such behavior is expected because metals as active sites for H_2S uptake usually require much higher temperature [20]. With the increase in the BET surface area of the carbon samples, there is a trend of increase in the H_2S uptake capacity, which is consistent with the adsorption results with ACFs. This indicates that the density of active sites for H_2S uptake increases with the increase in BET surface area of the carbons. During the formation of higher surface area, more defects and higher heterogeneity must be created at the same time. This explains why the "active surface area" sometimes has good correlation with the BET surface area of carbon materials [84].

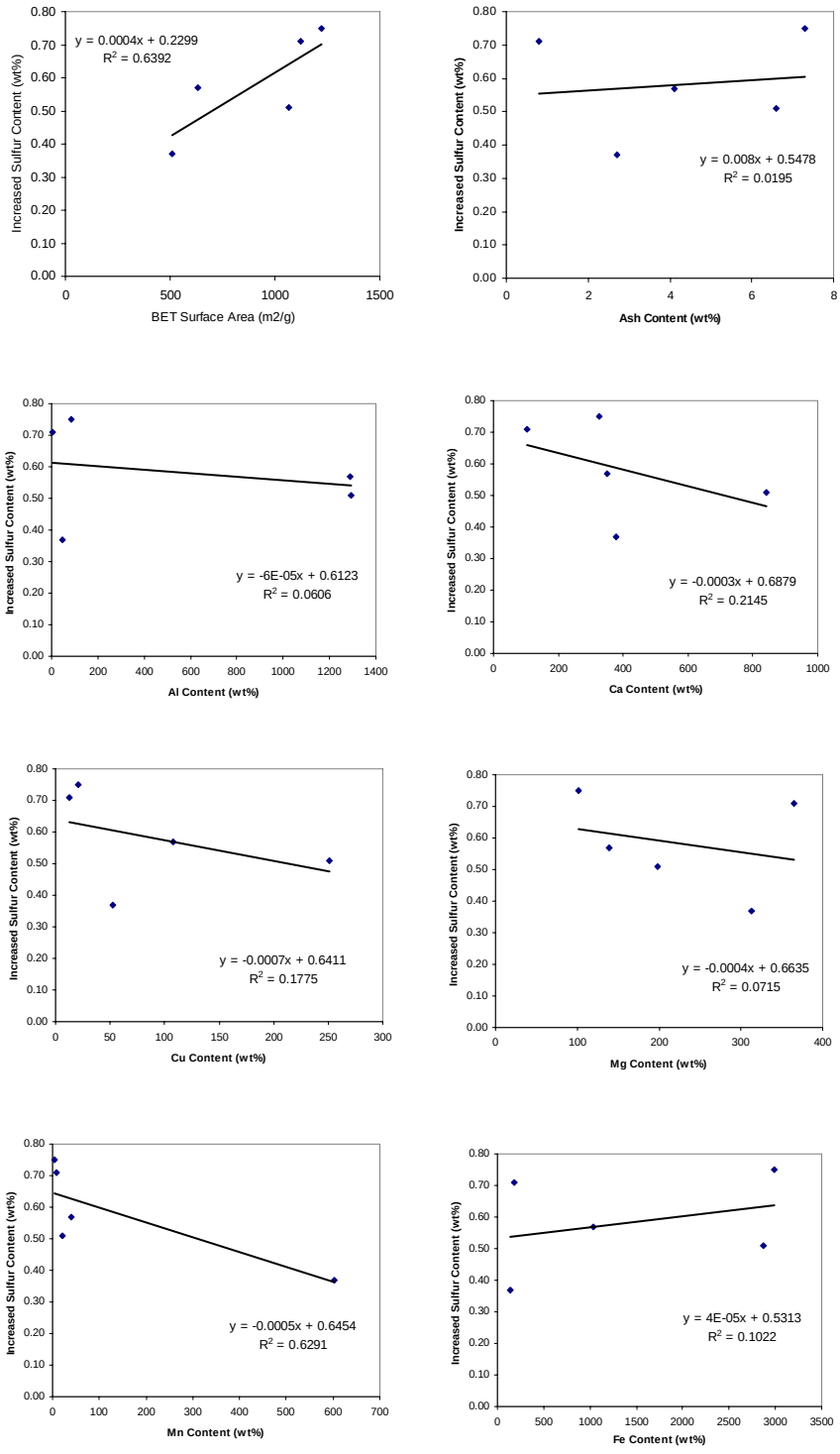

Figure 14. Correlation of increased sufur content with surface area and metal contents

Figure 15 depicts the correlation between irreversibly adsorbed H_2S and different surface functional groups, including total acidic and total basic surface functionalities. Generally, there is a weak inverse correlation between the density of strong acidic functionalities (carboxylic, lactonic, and phenolic) and H_2S retention. There appears to be no correlation between total acidic functionalities and H_2S retention. These results suggest that strong acidic functionalities have adverse effects on irreversible H_2S uptake. The higher density of acidic surface groups suggests that more "active sites" created during activation of these carbons had already been occupied by oxygen, leaving less sites for hydrogen sulfide bonding. In addition, these acidic oxygen containing surface groups do not seem to bond hydrogen sulfide under dry and anoxic conditions.

At the same time, the density of total basic surface groups showed good correlation with the H_2S uptake capacity (Figure 15). Basic surface groups are believed to be associated with the pyrone groups and the π electrons of the carbon basal planes [73, 89]. The high electron density makes these functionalities strong Lewis basic sites, which is beneficial for fixing the hydrogen sulfide molecule through interaction with hydrogen. In this case, carbon basicity seems to be a measurement of the surface insaturation toward acidic molecules. Previous studies also support that basic environment enhance the adsorption of H_2S onto carbonaceous surfaces [126,181]. High CO_2 uptake by activated carbon was also attributed to the presence of more basic functionalities [182]. Similar results were obtained for tests with ACFs (section 4.1). For this set of experiment, the uptake of H_2S showed good correlation with the density of carbonyl group too. Carbonyl groups are the weakest acidic functionalities, and some of the carbonyl groups could show basic properties if surrounded by other neighboring functional groups [73].

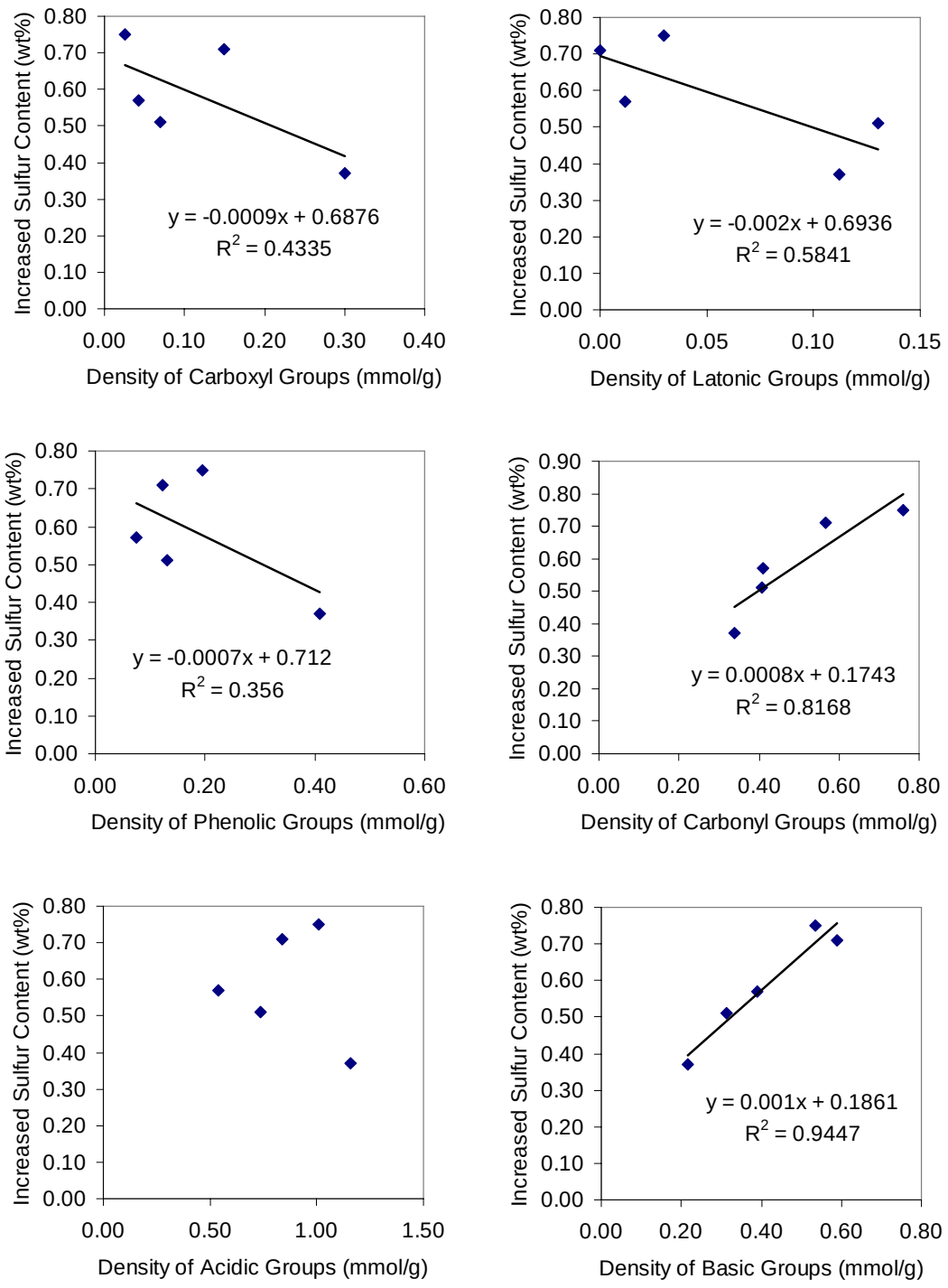

Figure 15. Effect of different carbon surface groups on irreversible H_2S adsorption without oxygen

The correlation between H_2S retention and the density of basic surface functionalities on both ACFs and activated carbons is summarized in Figure 16, which reveals the importance of acid-base interactions for H_2S adsorption onto carbonaceous surfaces. However, the contribution of carbonyl group to the uptake of H_2S by ACF surface is not obvious, which may be because that ACF is a different carbon material from activated carbons.

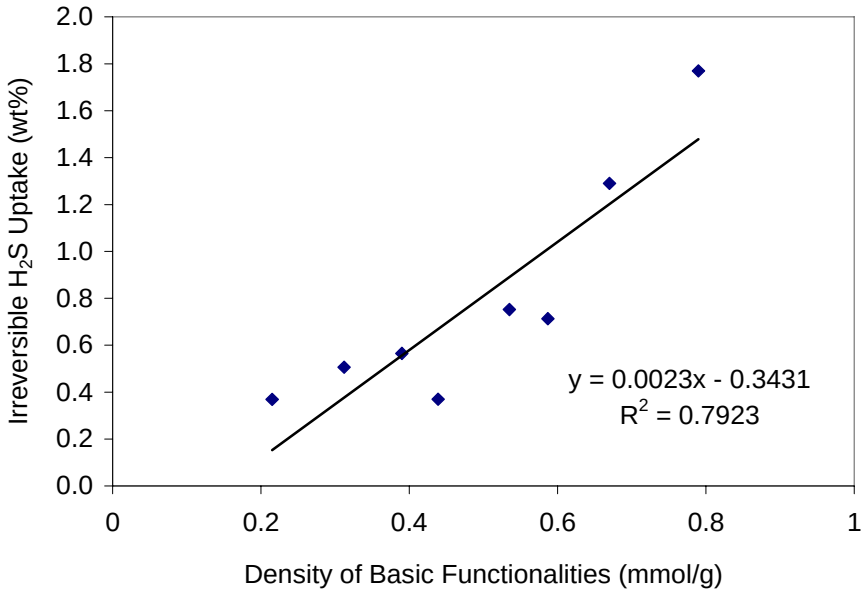

Figure 16. Effect of basic surface functionalities on H_2S retention for all carbons

The effect of surface functionalities on the retention of H_2S in the presence of oxygen is not obvious. The retained amount of H_2S in the presence of oxygen increased significantly when compared to the uptake in the absence of oxygen but neither the basic surface functionalities nor the total surface groups showed good correlations with the retention of H_2S. The oxidation of H_2S in the presence of oxygen can be catalyzed by the carbon surface and this difference in

mechanism can explain the high H_2S retention and weak correlation with the surface functionalities. However, it seems that Centaur carbon has exceptionally high H_2S uptake capacity, as shown in Figure 40(a). Such behavior is clearly due to the special treatment used for the production of this carbon [179, 180]. If this carbon was not included in the analysis, the H_2S retention increased with the increase in total surface groups and basic surface groups. As shown in Figure 40(b), the total surface groups seem to have better correlation with the H_2S uptake capacity.

4.2.3 Effect of Surface Treatment

The effect of heat treatment temperature on carbon basicity is shown in Figure 17. The increase in heat treatment temperature led to higher basicity of the resulted carbon material. This can be understood because most acidic functionalities decompose at lower temperatures while weak acidic groups decompose at higher temperatures. Many reports have confirmed that the decomposition of oxygen containing surface functionalities at elevated temperatures increases carbon basicity [85]. Phillips [83] further postulated that the evolution of the oxygen containing gases during heating always take away carbon atoms from the carbon basal plane, forming unsaturated "active sites".

As shown in Figure 18, heat treatment (outgassing) in argon increased the retained amount of H_2S for all three activated carbons used in these epxeriments. However, maximum H_2S retention was observed after 300 °C heat treatment and higher surface treatment temperature resulted in lower H_2S uptake capacity under dry and anoxic conditions. It was reported that different oxygen containing surface groups decompose at different temperatures to release CO_2

at lower temperatures and CO at higher temperatures [38]. Carboxylic groups decompose at 100-400 °C to release CO_2 ; lactonic groups decompose at somewhat higher temperatures to produce CO_2; anhydride groups decompose in the same temperature range as lactonic groups to release both CO and CO_2; phenol, carbonyl, ether, and quinine groups decompose at 600-1000 °C to release CO. IR study also showed the same trend of decomposition of oxygen containing surface functionalities [82]. These results indicate that functionalities that are stable at higher temperatures, i.e. carbonyl groups, pyrone groups, are important sites for chemisorption of H_2S onto the carbon surface because their removal decreases H_2S retention.

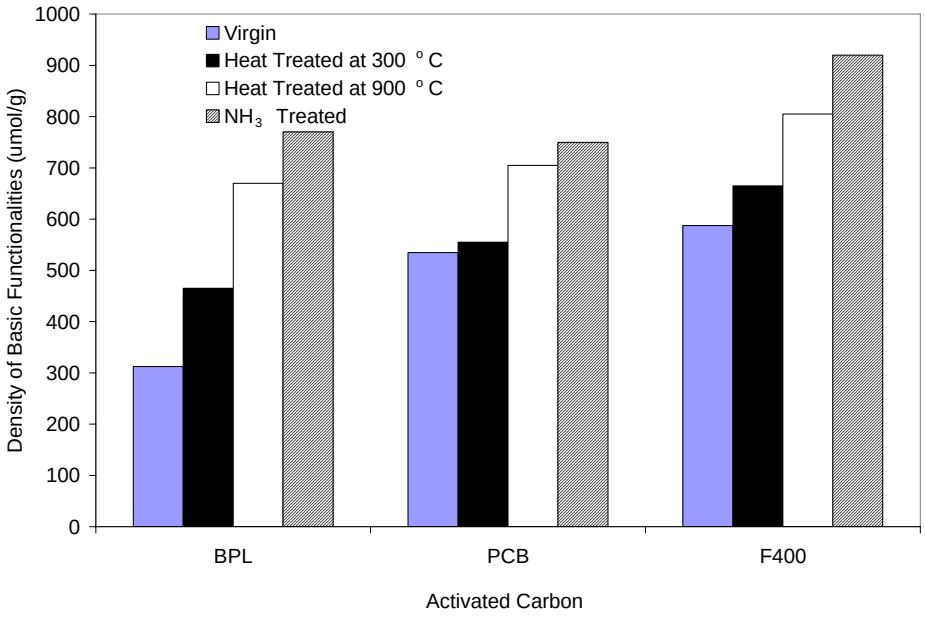

Figure 17. Change of carbon basicity after surface treatment

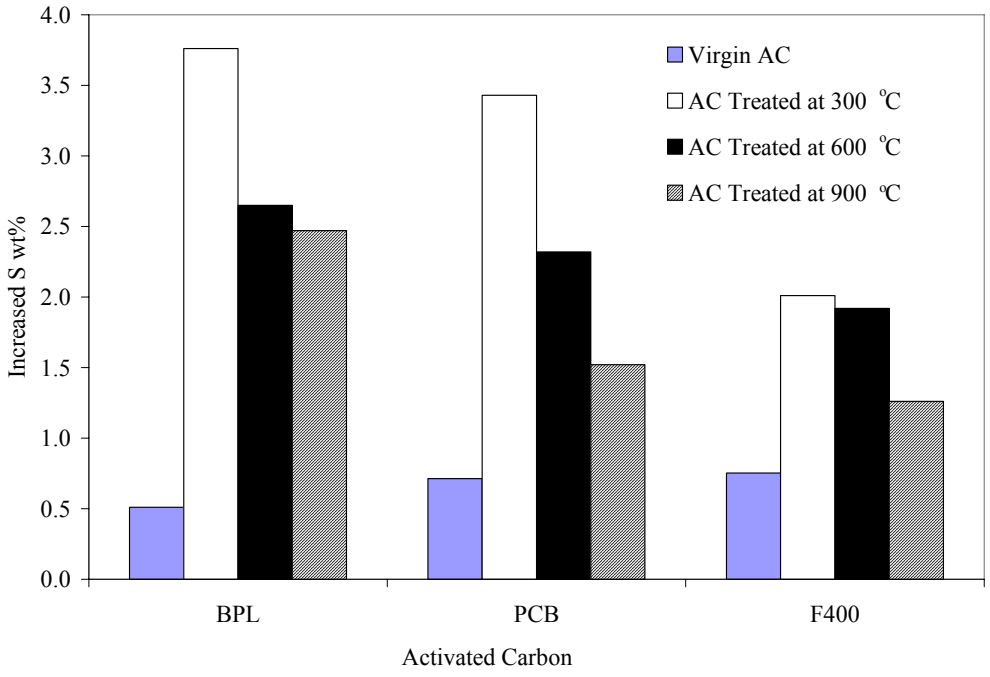

Figure 18. Effect of heat treatment on irreversible H_2S uptake without oxygen

In contrast to the results with virgin activated carbons, samples obtained after heat treatment did not show linear relationship between the density of basic surface functionalities and H_2S uptake capacity. The higher basicity after heat treatment is attributed to π-electrons of the graphite structure as well as the more stable oxygen containing surface groups. With more oxygen containing surface functionalities decomposed at higher temperatures, the impact of the π-electrons of the graphite structure becomes more important. Since the H_2S uptake capacities of the three activated carbons after 900 °C treatment was still higher than that of the virgin carbons, carbon basicity due to the carbon basal planes did enhance H_2S uptake. The enhanced uptake of H_2S is possibly through the formation of more active sites as proposed Phillips [83]. However, the maximum H_2S uptake occured after exposure to 300 °C when strong acidic functionalities have

decomposed. The results with virgin and heat treated samples support the hypothesis that the surface functionalities responsible to carbon basicity (i. e. pyrone and chromene groups) are extremely important for the uptake of H_2S on the carbon surface. However, the contribution of weak acidic groups (i. e. carbonyl groups) to H_2S uptake could not be ruled out.

H_2S retention was possibly through addition to Lewis basic sites as a first step. These Lewis basic sites include strong basic functionalities such as chromene group or weak acidic groups such as carbonyl group. At the same time, Lewis basic sites can also be produced after the decomposition of acidic functionalities during heat treatment. After the chemisorption of H_2S, scission of H-S bond can produce $^{\cdot}SH$ radical, which is a very important intermediate for the formation of other sulfur species [183]. Similar to the effect of carbon surface chemistry on H_2S uptake, the catalytic activity of carbon surface toward specific chemical reactions can be optimized at medium basicity, when some of the CO_2 yielding functionalities are removed [73, 89]. This enhanced catalytic activity is probably due to the improved retention and dissociation reactions after the elimination of strong acidic functionalities.

As shown in Figure 19, carbon surfaces treated with ammonia showed a dramatically increased retention of H_2S. This can possibly be attributed to the increase in nitrogen containing surface functionalities. Nitrogen containing surface groups can also increase the carbon basicity, as shown in Figure 17. Activated carbons after ammonia treatment were found to be grafted with nitrogen containing surface functionalities, which are responsible for the high basicity of the resulted carbon materials [67]. The nitrogen containing surface groups are likely to be the active sites accounting for the increase in irreversible H_2S uptake, probably by mechanisms similar to those for untreated carbons. Enhancement of CH_3SH adsorption by nitrogen containing functionalities was also reported [66].

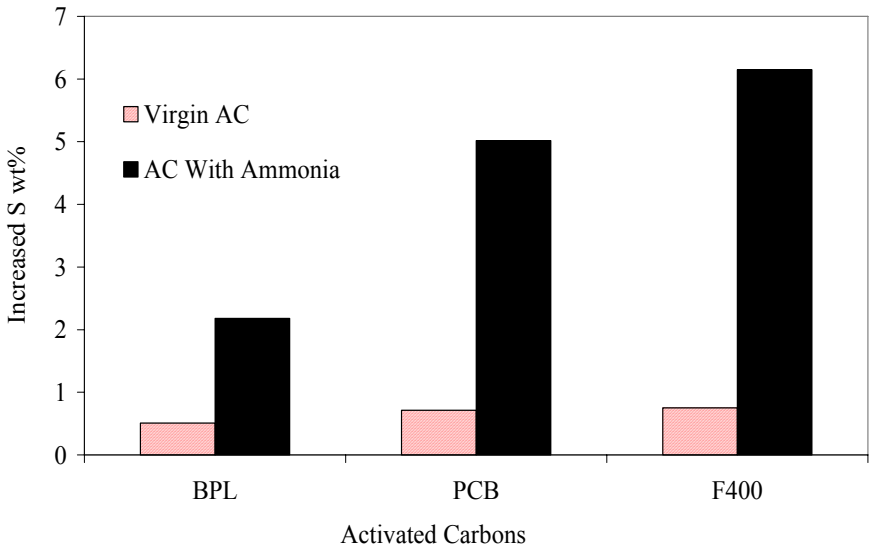

Figure 19. Effect of ammonia treatment on irreversible H_2S uptake without oxygen

4.2.4 Summary

Five activated carbons were evaluated for H_2S retention (irreversible adsorption) in a fixed bed reactor system. H_2S retention was tested under dry and anoxic conditions at room temperature. Before retention test, the metal contents and oxygen containing surface functionalities were characterized by atomic adsorption spectrophotometer (AAS) and Boehm titration. Metal contents did not show significant effect on the H_2S uptake capacity. There was a good correlation between the retained amount of H_2S and the density of total basic functionalities, indicating the importance of acid-base interaction for H_2S uptake under dry and anoxic conditions. The removal of strongly acidic surface functionalities by heat treatment enhanced H_2S retention but further heat treatment did not lead to higher H_2S retention although

carbon basicity increased. Ammonia treatment increased H_2S retention probably through the formation of nitrogen containing surface functionalities. With the presence of oxygen, the retained amount of H_2S increased dramatically; there seem to be a better correlation between the H_2S retention and total surface groups.

4.3 SULFURIZATION OF ACFS AND BPL CARBON

4.3.1 Effect of Carbon Materials

Four carbon materials (i.e., three ACFs and BPL carbon) were tested for H_2S uptake at 600 °C (600C-S Only). The results in Figure 20 clearly show that for all the carbon materials tested, the increased sulfur content (the ultimate sulfur content minus the sulfur content of the virgin carbons) showed good correlation with the surface area of virgin carbon material. Surprisingly, significantly higher metal content on BPL carbon did not promote the hydrogen sulfide uptake, indicating that metals are not effective sites for hydrogen sulfide uptake. As shown in Table 4, with the increase in ACF serial number, the oxygen content decreases. This suggests that the oxygen containing functionalities are not the major factor for H_2S uptake either. These results support the hypothesis that the active sites for H_2S uptake at high temperature are closely related to the pore structure, indicating that they are derived from the carbon structure itself. As discussed by Mangun *et al.* [165], the active sites on ACFs for SO_2 uptake are probably the defect sites, which can be created by oxidation and then degassing.

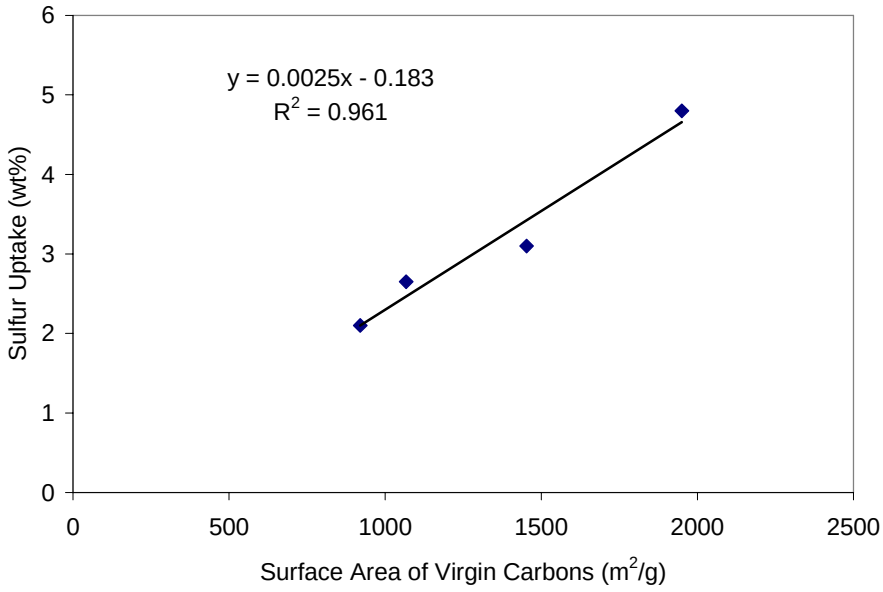

Figure 20. Effect of sorbent surface area on the increased sulfur content after sulfurization

4.3.2 Effect of Temperature

Figure 21 shows the effect of temperature in the range of 400-800 °C on ultimate sulfur content of ACF-25 and BPL carbon with H_2S fed to the reactor during the stable temperature only (S Only). Sulfur loading on these carbonaceous sorbents increased with an increase in temperature. These samples have much higher sulfur content than those produced at low temperatures (section 4.1). Such behavior is reasonable since the higher temperature can provide more energy to facilitate greater interaction between H_2S and carbon surface and promote formation of more active sites for H_2S uptake.

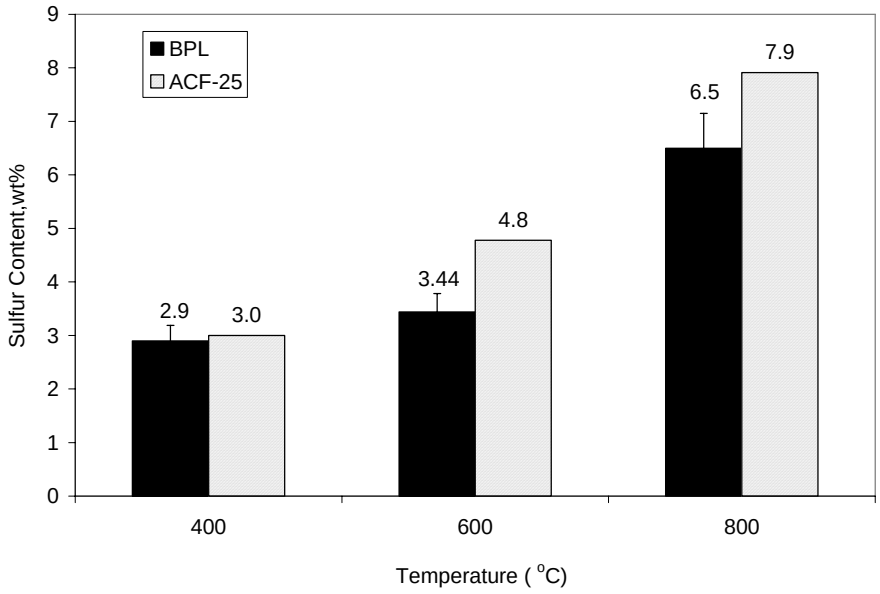

Figure 21. Effect of temperature on sulfurization of ACF25 and BPL in the presence of H_2S during stable temperatures only (S only)

Figure 22 depicts temperature programmed desorption (TPD) profile of virgin BPL. The major decomposition products of the surface functionalities are CO_2 at lower temperatures and CO at higher temperatures. The maximum release of the two gases occurred at 370 °C (643K) and 790 °C (1063K), respectively. Similar results were also reported by Li *et al.* [100]. The increase in temperature leads to the decomposition of more surface functionalities, thereby, creating more active sites for sulfur bonding, leading to higher sulfur content at higher temperatures. These observations agree with the mechanism proposed by Mangun *et al.* [165] for SO_2 uptake. Since the temperature ranges for the decomposing of the surface functionalities are different, the reactivity of these active sites towards H_2S may not be the same.

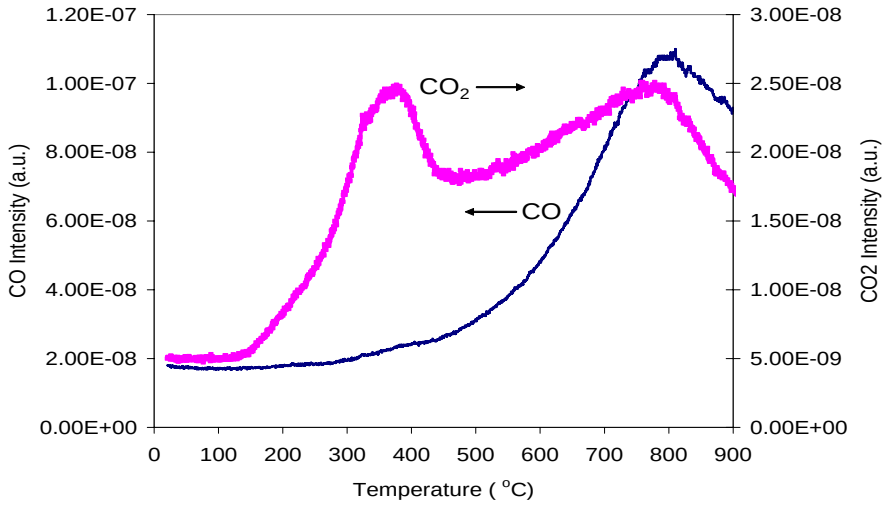

Figure 22. CO_2 and CO evolution during temperature programmed desorption

The temperature programmed reaction results shown in Figure 23 can provide further insight into the reaction mechanism. Complete breakthrough of H_2S at room temperature occurred after about 25 minutes. Once the reactor heating commenced, two H_2S peaks representing the desorption of weakly and strongly adsorbed H_2S were observed at 50 and 450 ^oC, respectively. Similar results were reported in previous studies of H_2S adsorption onto carbon surfaces at low temperatures (section 4.1). At reactor temperatures between 150 °C to 600 °C, there was no significant decrease in H_2S concentration and no other sulfur containing gas species were observed in the gas stream. This indicates adsorption of H_2S in this temperature range could be attributed to addition to unsaturated active sites created by the decomposition of CO_2 yielding

functionalities or addition to "CO-Complex" as proposed by Puri and Hazra [72]. Above 600 °C, the concentration of H_2S started to decrease dramatically. At the same time, the formation of H_2 was observed (Figure 41 in APPENDIX), indicating the decomposition of H_2S to H_2 and S that is catalyzed by the carbon surface. This hypothesis is supported by the observation of yellow elemental sulfur at the exit of the reactor. Above 800 °C, another species, CS_2, started to evolve. This suggests the direct chemical reaction between carbon and H_2S, and incorporation of sulfur into the graphite structure.

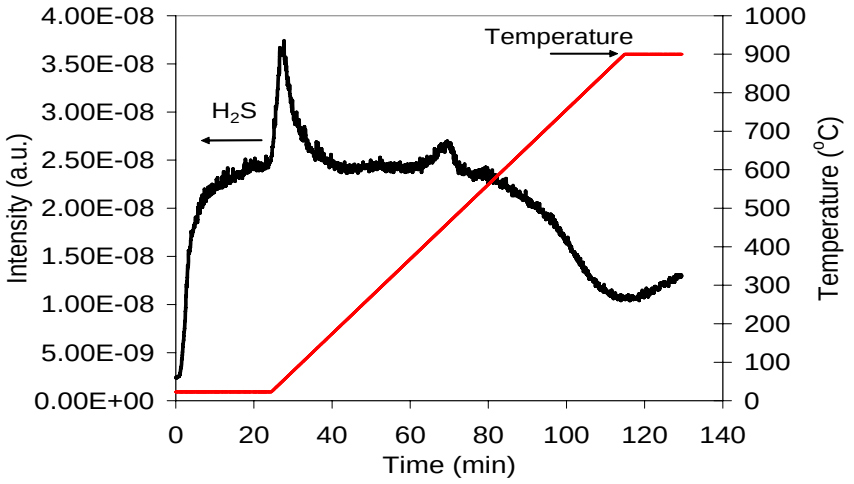

(a)

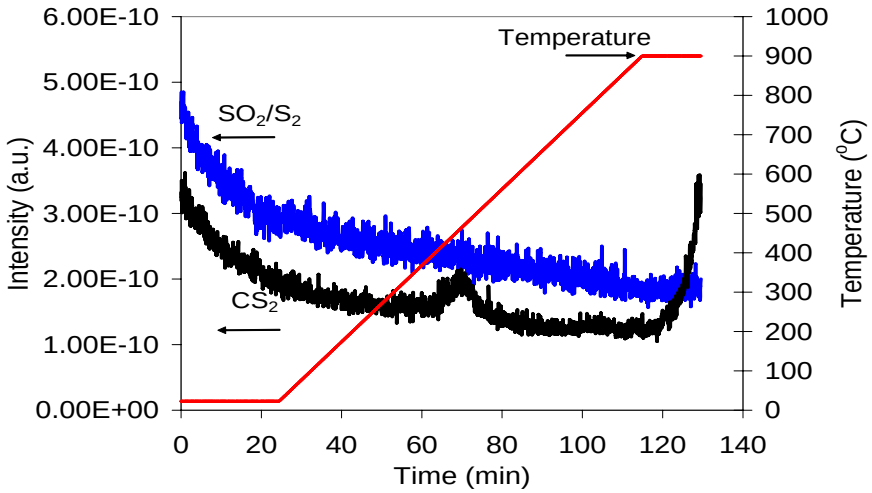

(b)

Figure 23. Temperature programmed reaction between H_2S and BPL surface

EDAX was used to determine elemental composition of the surface of ACF-25. The S, O, and C contents on the surface were determined after sulfurization at different temperatures and the surface sulfur content is compared with that obtained from the bulk sulfur analysis by the Leco Sulfur Analyzer in Table 10. The increase in temperature led to a decrease in oxygen/carbon content and increase in the sulfur content. Such behavior suggest that uptake of H_2S is associated with the decomposition of carbon surface functionalities and loss of active carbon atoms. The loss of active carbon atoms, forming volatile carbon disulfide, was observed at temperatures above 500 °C (Figure 23b). Sulfur content on the surface is higher than that in the bulk because the gas-solid reaction between H_2S and carbon occurs mainly on the surface.

Table 10. Sulfur content in the bulk (sulfur analysis) and on the surface (EDAX)

Sample	Bulk Sulfur Content [wt.%]	Surface Content [wt.%]		
		S	O	C
ACF25-Virgin	0.2	0.2	4.38	95.41
ACF25-400C-S Only	3.0	6.04	2.13	91.83
ACF25-600C-S Only	4.8	6.95	1.61	91.44
ACF25-800C-S Only	7.9	11.52	1.31	87.17

Figure 24 shows the effect of temperature on ultimate sulfur content of BPL carbon exposed to H_2S throughout the entire process and associated TGA results. Figure 24 shows that the sulfur content increases with the increase in temperature, which can be explained by the

creation of more active sites for sulfur binding. The peak in sulfur content around 300 °C may be associated with the peak in decomposition of functionalities yielding CO_2. This result seems to support the hypothesis of Puri and Hazra [184] that "CO-Complex" enhances H_2S adsorption.

TGA test results in Figure 24 indicate that the dominant weight loss occurred in the temperature range from 300 °C to 500 °C. It is also evident that activated carbons impregnated with sulfur at temperatures below 400 °C lost most of the deposited sulfur during the TGA test. On the other hand, the sulfur content of carbons impregnated at 600 °C and 800 °C was much higher than the total weight loss, which means that sulfur was more strongly bonded to the carbon surface, which may be due to the formation of strongly bonded sulfur forms (e. g. organic sulfur). Formation of very stable sulfur species at 800 °C were also reported by Sugawara *et al.* [144].

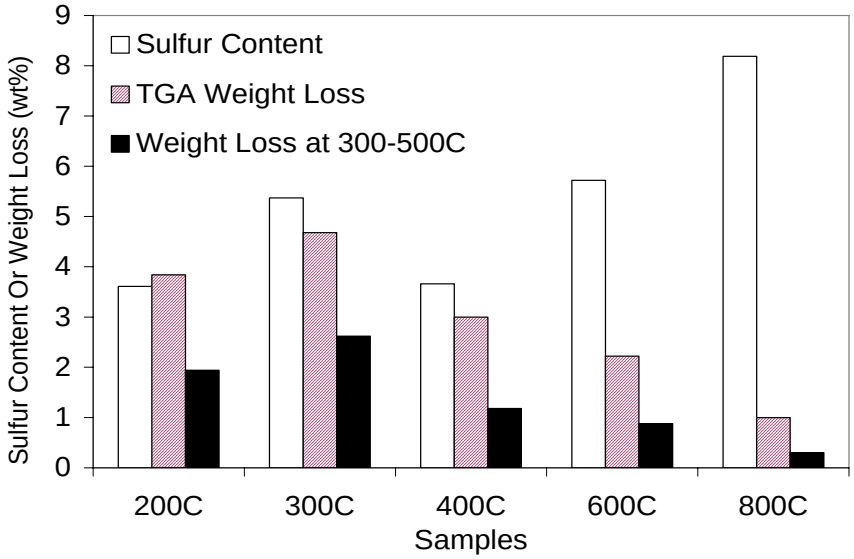

Figure 24. Sulfur content and TGA results of BPL sorbents produced at different temperatures (H+S+C)

4.3.3 Effect of Sulfurization Protocol

It can be seen from Figure 25 that the presence of H_2S during the heating and cooling process can increase the total sulfur content of BPL at 600 °C. Similar behavior was observed at other impregnation temperatures (Figure 42 in APPENDIX). The difference in the ultimate sulfur content of samples produced at different temperatures is clearly due to the presence of H_2S during heating and cooling process. For BPL-600C-C only, the sulfur content is lower than the other samples. However, considering the short duration of the cooling process (about 60 minutes), the uptake of sulfur is significant. Two factors may contribute to the increased uptake of sulfur during the cooling process. Firstly, the hydrogen sulfide molecules could not escape from the carbon surface once they are attached to the active sites (created at higher temperatures) because of the decreasing temperature; secondly, the carbon structure itself experiences an annealing process, which may also help to capture more sulfur species due the structural changes.

TGA test depicted in Figure 25 showed that the three samples (600C-C Only, 600C-H+S+C and 600C-S+C) with the presence of H_2S during the cooling process have much higher weight loss than 600C-H+S only and that 600C-H+S+C has the highest weight loss. Weight loss mainly occurred at the temperature range of 300-500 °C. Again this indicates that the sulfur added during the cooling process was not very strongly bonded to the carbon surface, but most probably trapped as free elemental sulfur.

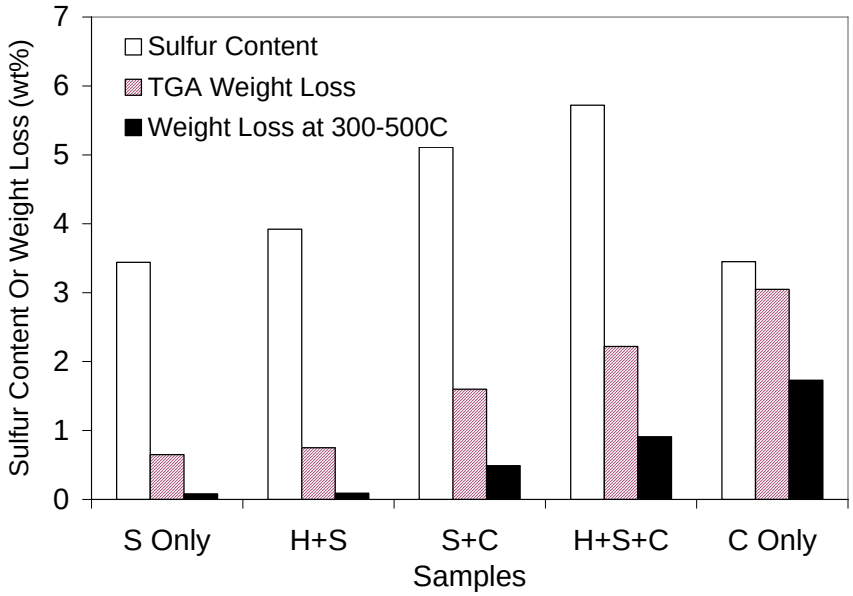

Figure 25. Sulfur content and TGA results of BPL sorbent produced by different sulfurization protocols at 600 °C

4.3.4 Sulfur Distribution

Pore size distribution for BPL before and after hydrogen sulfide uptake shown in Figure 26 suggests a slight change in pore volume in the 10-20 Å range after sulfurization. The presence of H_2S during the cooling process further decreased the pore volume at smaller pore size range. However, the change in pore size distribution after hydrogen sulfide uptake is not significant. Such observation leads to the conclusion that the sulfurous compounds produced are extremely

well distributed on the surface of the sorbent. Furthermore, it is more likely that the organic sulfur or chemically fixed elemental sulfur is the dominant sulfur form since the free elemental sulfur would tend to agglomerate into isolated islands on the carbon surface and significantly alter the pore size distribution of the sorbent.

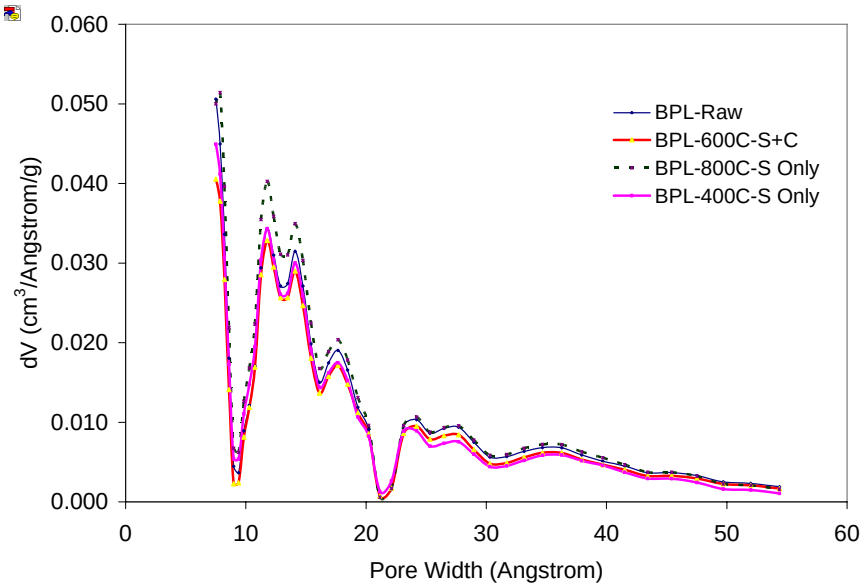

Figure 26. Pore size distribution of BPL before and after H_2S uptake at high temperatures

4.3.5 Forms of Sulfurous Products --- XPS Results

XPS analysis was conducted to identify the produced sulfur species on ACFs and the typical spectra are shown in Figure 27. Standard library spectra provide the following information about the peaks related to sulfur species: free elemental sulfur has a peak around

164.05 eV; chemisorbed sulfur has a peak at 161.8-162.6 eV; organic sulfur has a peak between 163-164.1 eV; and oxidized sulfur shows a peak above 167 eV. Unfortunately, there is an overlap between the region of elemental sulfur and that of organic sulfur. The results depicted in Figure 27 suggest that either organic sulfur or elemental sulfur were the dominant sulfur forms on ACF surface. According to Sugawara *et al.*[144], thiophene may be the possible structure of organic sulfur products deposited on the carbon surface at high temperatures.

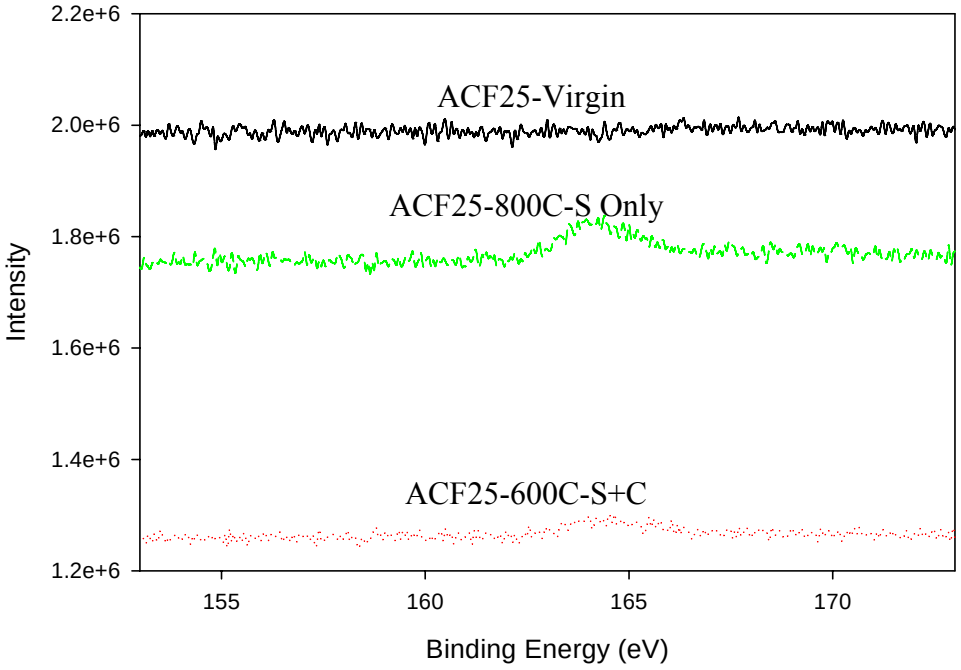

Figure 27. XPS analysis of ACF25 before and after sulfurization

4.3.6 Forms of Sulfurous Products on BPL --- XANES Results

Figure 28 shows the sulfur K-edge XAFS spectra and the summary of different sulfur forms. By applying the least-squares technique, the relative ratio of different sulfur species can be obtained from the spectra. The total sulfur content was obtained from sulfur analysis and the sulfur content of each species is shown in Figure 28 (b). Sulfur was deposited on the carbon surface in three major forms, namely elemental sulfur, organic sulfur, and sulfate. This is consistent with the previous results reported by Hsi *et al.* [110]. It is interesting to point out that sulfate was not detected on ACFs by XPS, which may be due to the extremely low metal content of this carbonaceous material (Table 4).

The major difference among samples is in the elemental sulfur and thiophene content. For those samples prepared without the presence of H_2S during the cooling process, i.e. BPL-400C-S only, BPL-600C-S only, and BPL-800C-S Only, thiophene content increased with the increase in temperature, with an abrupt increase in metal sulfide content from 600 °C to 800 °C.

For samples produced at 600 °C, the presence of H_2S during the cooling process (BPL-600C-S+C versus BPL-600C-S only) increased both the elemental sulfur content and thiophene content. When elemental sulfur was used as the sulfurizing agent (BPL-600C-El. Sulfur), the majority of the sulfur content was mainly in elemental and organic sulfur form. These observations suggest that exposure to H_2S during cooling process facilitate the formation of low valent sulfur forms. The sulfur species may be formed through the interaction between carbon and sulfur atoms after the decomposition of H_2S (Figure 23).

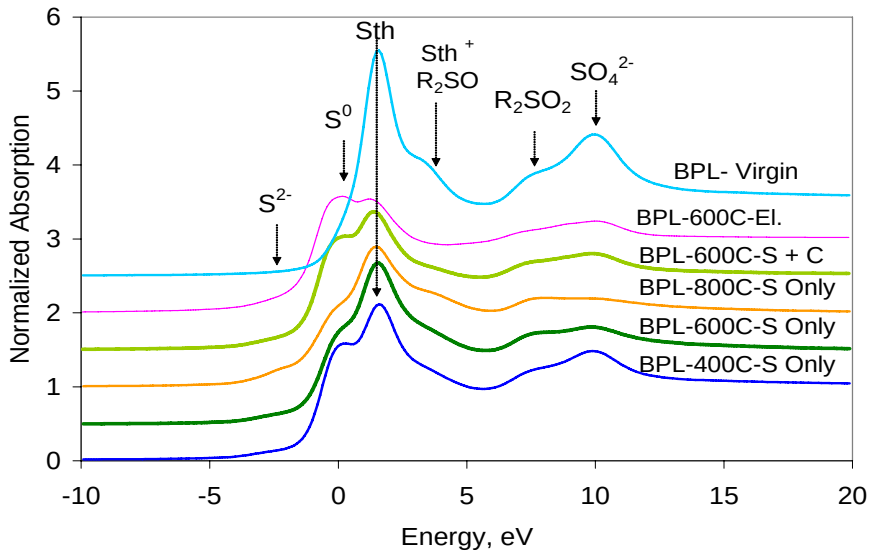

(a) Summary of XANES spectra of prepared samples

(S^{2-}: metal sulfide; S^{0}: Elemental sulfide; R_2SO: Sulfoxide; R_2SO_2: Sulfone; SO_4^{2-}:Sulfate)

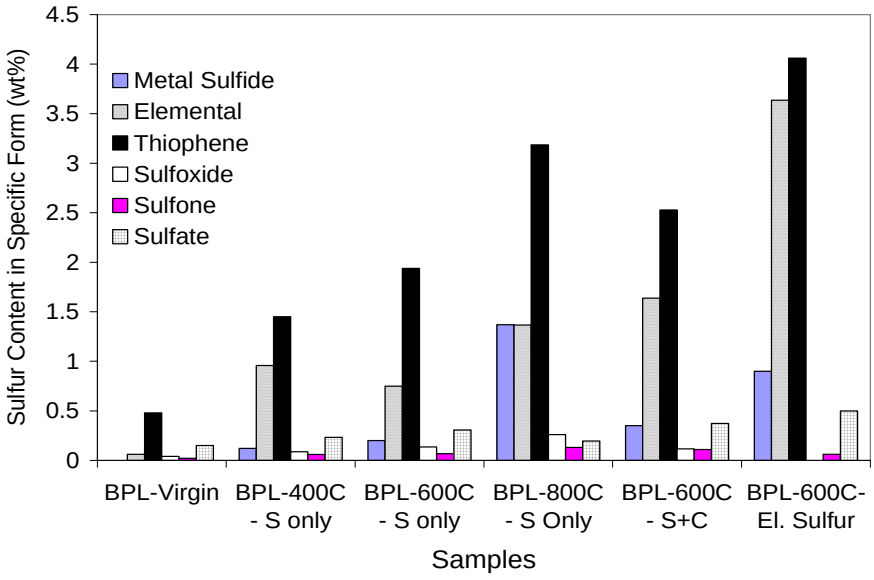

(b) Different Sulfur forms in prepared samples

Figure 28. Contents of different sulfur forms from XANES results

4.3.7 Mercury Uptake Studies

Effect of impregnation temperature

As shown in Figure 29, the H+S+C sulfurization protocol at 400-600 °C produced effective mercury sorbents, with 600 °C being the best impregnation temperature for the production of effective mercury sorbents. This is consistent with previous studies using elemental sulfur for sulfur impregnation onto activated carbons [103, 104, 111]. Considering that neither the pore structure nor the sobent surface area was significantly changed during the impregnation process (Figure 26), it can be concluded that the forms of sulfur species played a key role in the very high capacity of the sorbent produced at 600 °C. Because elemental sulfur and thiophene are the two major species produced at higher temperatures, it is reasonable to assume that either one or both of the two species function as the key mercury uptake sites.

It is important to note that BPL-800C-H+S+C had significantly lower mercury uptake capacity than BPL-600C-H+S+C despite much higher total sulfur content. As shown in Figure 28, this sorbent also had the highest metal sulfide contents. It can therefore, be concluded that sorbents prepared at very high temperatures contain sulfur species already combined with metals or other compounds, which are no longer effective for mercury uptake. The sulfur species formed at very high temperatures may be imbedded into the graphite structure (Figure 23), affecting their mercury uptake capacity.

Sulfurization probably occurred after the decomposition of certain oxygen containing surface functionalities. Temperature programmed desorption studies with virgin BPL carbon found that different oxygen containing surface functionalities decompose at different temperatures [38]. For example, acidic functionalities will decompose to CO_2 at temperatures

below 600 °C. Phenolic and carbonyl groups will decompose at higher temperatures, yielding CO as the main product [185]. The results of this study suggest that the decomposition of CO_2 evolving groups is helpful for the formation of sulfur forms active in mercury uptake since effective mercury sorbents were produced at temperatures lower than or at 600 °C.

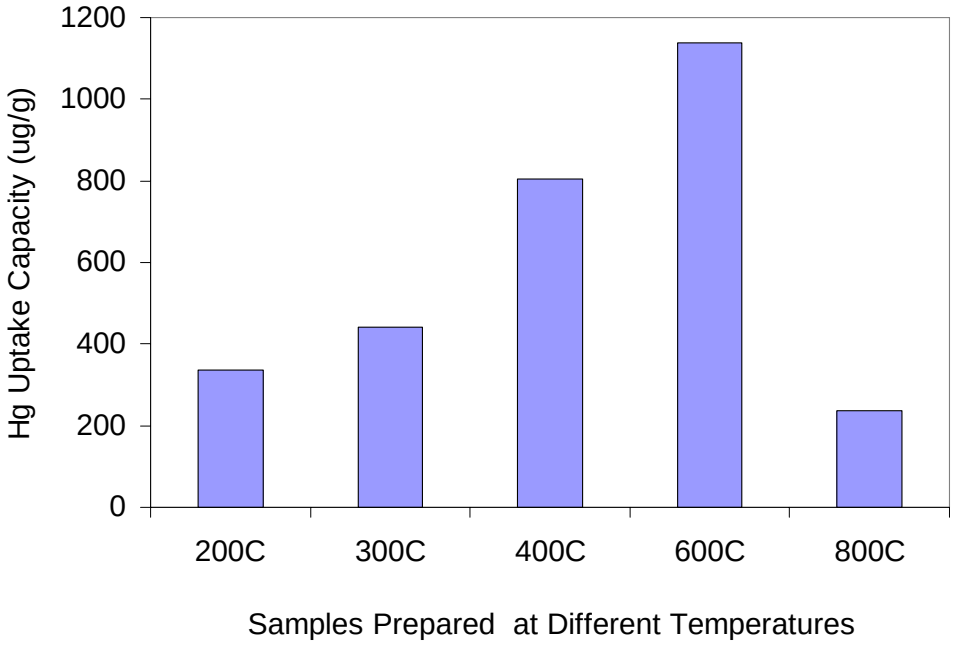

Figure 29. Effect of impregnation temperature on Hg uptake capacity of sorbents produced using the (H+S+C) protocol

Effect of impregnation protocol

Besides temperature, the impregnation protocol was found to be important for producing effective mercury sorbents. As shown in Figure 30, the production of sorbents at 600 °C by exposure to H_2S during the stable phase (600C-S only) and during both heating and stable phase (600C-H+S) did not produce effective mercury sorbents. The presence of H_2S during the cooling process has a unique impact as can be seen from the performance of 600C-S+C, 600C-H+S+C, and 600C-C only. The effectiveness of 600C-C only indicates that the formation of sulfur species effective in mercury capture actually occurs between 400°C to 600 °C. However, heating up to around 600 °C might have created the active sites necessary for the formation of such species during the cooling process. These active sites may be created by decomposing CO_2-yielding oxygen containing functionalities, most probably lactone group [185]. The performance of 600C-S only and 600C-H+S also indicates that the effective sulfur species are not thermally stable because they are easily removed if H_2S is not present in the gas stream during the cooling process.

Figure 30 also shows that adding H_2S during the heating process can improve the performance of the Hg sorbent created by exposure to H_2S during the stable process and the cooling process. It has been reported that metal sulfides can catalyze the decomposition of hydrogen sulfide into hydrogen and elemental sulfur [138, 186]. The difference in the performance of 600C-H+S+C and 600C-S+C suggests that the species (probably elemental sulfur) formed during the heating process are also effective in mercury capture.

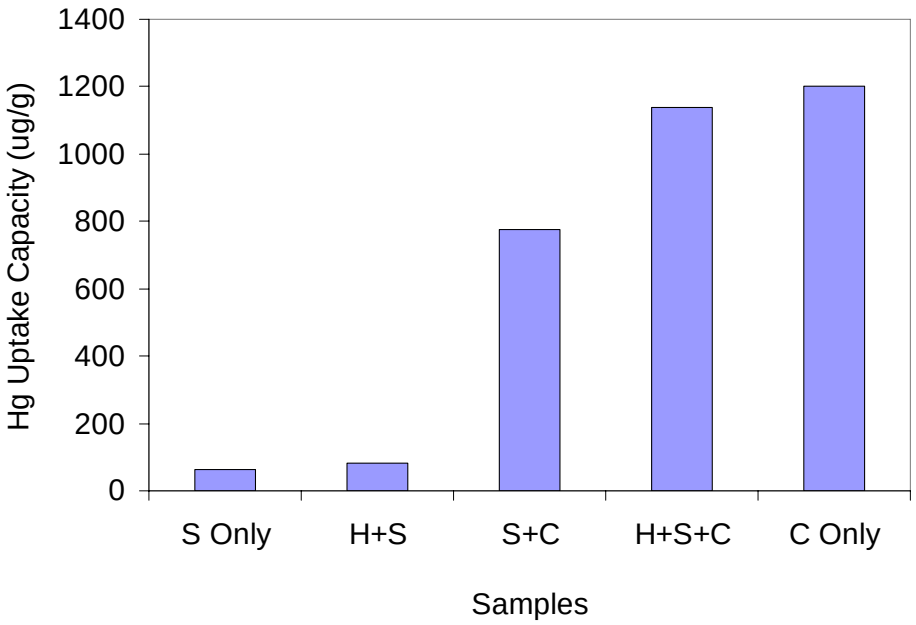

Figure 30. Effect of impregnation methods at 600 °C on Hg uptake capacity

The results depicted in Figure 31 show that the presence of H_2S during the cooling process also significantly increased Hg uptake capacity at 400 °C. However, the 400C-H+S+C was not as effective as 600C-H+S+C. This again indicates the creation of active sites for producing effective sulfur species requires temperature as high as 600 °C. Increasing the temperature to 800 °C resulted in higher sulfur content, but sulfur species created under such conditions are not effective for mercury removal. As mentioned above, this may be related to the formation of other metal sulfides or the removal of certain surface functionalities that were formed at lower temperatures.

The results above indicate that the most effective sulfur species were formed during the cooling process after high temperature (400-600 °C) treatment. Temperatures as high as 800 °C will eliminate or block the active sites for the formation of these sulfur species. Liu *et al.* [103, 104] has

reported that very effective mercury sorbents were produced using elemental sulfur as the sulfurizing agent at 600 °C. The same temperature was found to be effective in this study using H_2S as the sulfuring agent. However, besides the importance of temperature, the exposure to H_2S during the cooling process is also found to be an important factor in producing effective mercury sorbents.

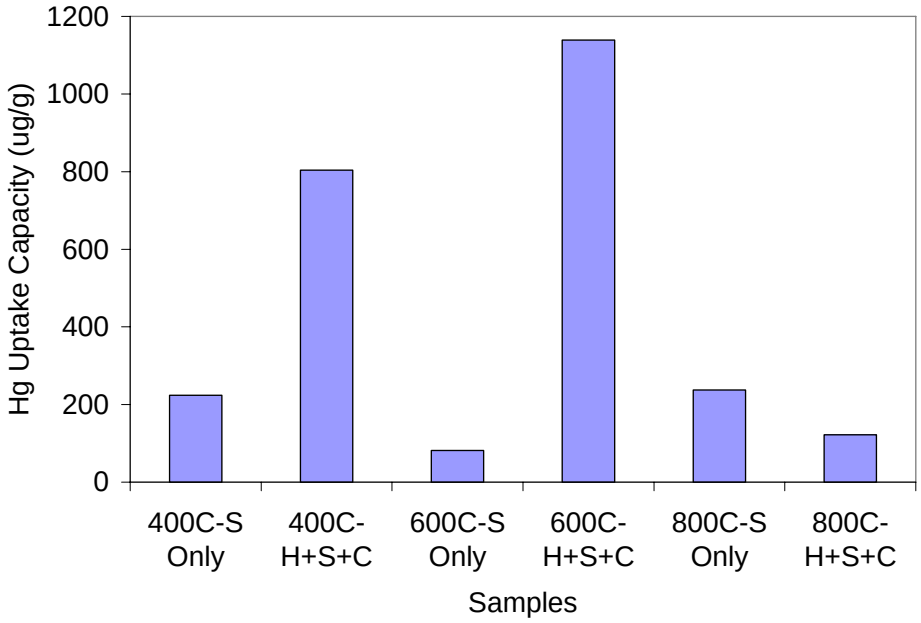

Figure 31. Effect of exposure to H_2S during heating and cooling on Hg uptake at different temperatures

Effect of different sulfur forms on Hg uptake

The correlation between mercury uptake capacity and total sulfur content is shown in Figure 32. The fairly good correlation shows the importance of sulfur content for sorbents with similar pore structure. Previous studies had proposed the effect of pore structure [110, 111, 187]. However, this study clearly showed that sulfur forms are more important for impregnated sorbents with similar pore structure.

The correlations between mercury uptake capacity and different sulfur forms are shown in Figure 33. Based on the slope of the linear correlation and the R^2 value, it seems that three forms of sulfur, namely, elemental sulfur, thiopene (typical organic sulfur on carbon surface), and sulfate, could possibly contribute to mercury uptake capacity. Elemental sulfur and organic sulfur were previously considered to be effective mercury removal agents [38]. However, sulfate also showed good correlation with mercury uptake capacity in this study.

It should be noted that the thiophene content on the samples produced in the presence of H_2S at stable temperatures only (BPL-400C-S Only, BPL-600C-S Only, and BPL-800C-S Only), increased more than three times with the increase in temperature, but the mercury uptake capacity remained unchanged. Such behavior suggests that thiophene might not be the major active site for mercury uptake although fairly good correlation was found between mercury uptake capacity and thiophene content. Comparing to the other two possible effective sulfur species, the sulfate content is very low. This also indicates that sulfate may not be the most effective sulfur forms for mercury uptake regardless of the good linear correlation between mercury uptake capacity and sulfate content.

Elemental sulfur can react with elemental mercury even at room temperature. However, not all elemental sulfur forms function equally. As described in section 4.3.2, temperature programmed reaction between H_2S and carbon surface released H_2 at temperatures around 600 °C during. This suggests the decomposition of H_2S into H_2 and S that is likely catalyzed by the carbon surface. This reaction pathway can easily create short-chain elemental sulfur species, such as S_2, S_3, and S_4, which are believed to be much more effective in Hg uptake than longer chained elemental sulfur [103, 104, 111].

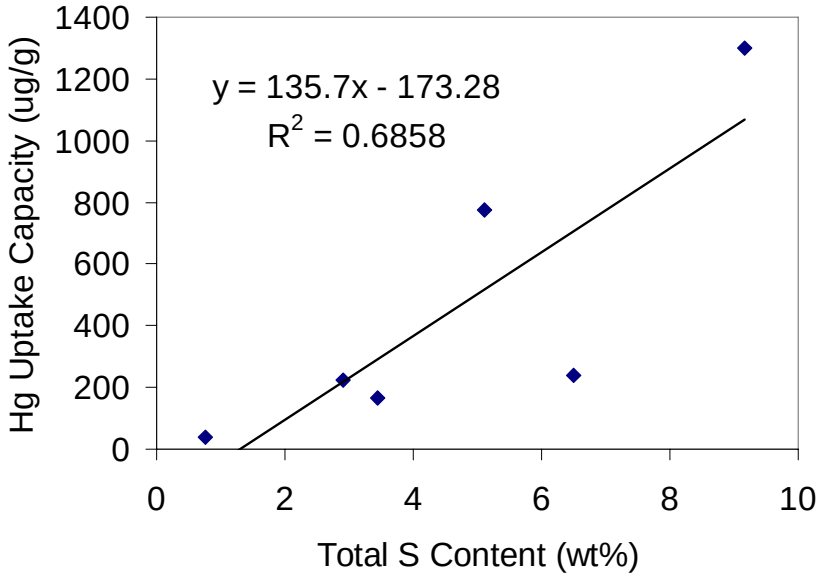

Figure 32. Correlation of Hg uptake capacity with total sulfur content for sorbent produced by sulfurization above 400 °C

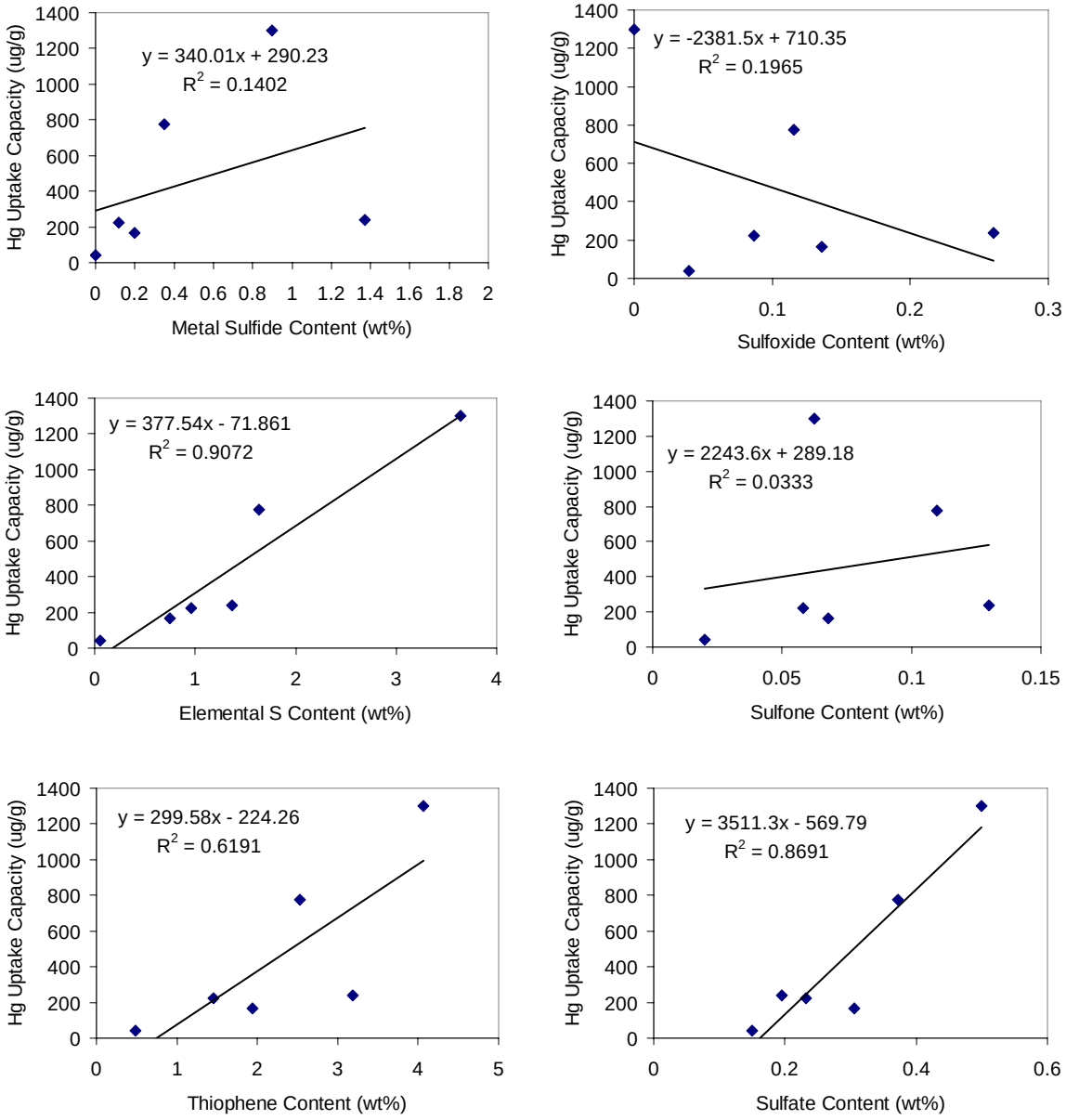

Figure 33. Correlation of Hg uptake capacity with different sulfur species on sulfurized sorbents

4.3.8 Summary

The uptake of hydrogen sulfide by carbon materials (ACFs and BPL) under dry and anoxic conditions at high temperatures (200-800 °C) was tested using a fixed bed reactor system. The uptake of hydrogen sulfide at 600 ^{o}C correlates well with the surface area of the carbon materials, indicating the formation of active sites during the formation of the pore structure. Sulfurization at higher temperatures resulted in higher sulfur content and more stable sulfur species. At temperatures below 600 °C, sulfurization is likely occurring through the addition of H_2S onto active sites enhanced by decomposition of CO_2 yielding oxygen containing functionalities, while at higher temperatures direct reaction between H_2S and the carbon occurred. The presence of H_2S during the cooling process obviously increased the ultimate sulfur content, especially with relatively unstable species. Sulfurized sorbents produced at temperatures higher than 400 °C maintained pore structures similar to that of the virgin carbon.

XPS and XAFS analysis of the sorbents produced at different temperatures and different sulfurization protocols showed that most of the produced sulfur is either organic sulfur, elemental sulfur, or metal sulfide. High temperatures promote the formation of organic sulfur, and the presence of H_2S during the cooling process increased elemental sulfur content. Hg uptake test indicates that 400-600 °C is the optimum temperature range to produce effective mercury sorbents. The presence of H_2S during the cooling process creates the most effective sulfur species for mercury binding. Elemental sulfur species are probably the most effective for capturing mercury although thiophene and sulfate content also showed good correlation with mercury uptake capacity.

4.4 OXIDATION OF H_2S ON ACFS FOR MERCURY UPTAKE

4.4.1 Structure of Raw ACFs

Figure 34(a) depicts pore size distribution of raw ACFs after grinding into powders. It is clear that the diameter of most pores in these ACFs is below 2nm. These micropores can be divided into three ranges corresponding to three peaks on Figure 34(a): small micropores ($d < 0.72$ nm), medium micropores (0.72 nm $< d < 0.90$ nm) and big micropores ($d > 0.90$ nm). As the serial number increases from ACF10 to ACF25, medium and big micropore volume (> 0.72 nm) increases while the small micropore volume (< 0.72 nm) decreases. This is not surprising because ACFs with increasing serial numbers were produced under extended activation time.

4.4.2 Sulfur Content and Distribution

Table 11 summarizes general properties of the sorbents produced in this study and their respective Hg uptake capacities. It is clear from these results that low temperature (e.g., 80 ºC) does not facilitate significant sulfur deposition through H_2S oxidation, even if a complete H_2S breakthrough was attained. Both ACF-10 and ACF-25 achieved much higher sulfur content at 150ºC. This is due to the fact that a predominant mechanism for H_2S adsorption at low temperatures is physisorption [119-121], which leads to filling of small micropores ($d < 0.72$ nm) first. As a result, the catalytic oxidation of H_2S could only take place in small micropores. This

hypothesis is supported by pore size distribution measurements shown in Figure 34 (b), which depicts changes in the pore size distribution of ACF10 after sulfur impregnation at 80 °C and 150 °C. It is clear that sulfur deposition at 80 °C is accomplished more by pore filling rather than by monolayer deposition as the loss in the small micropores is obvious, while very few medium micropores were occupied by sulfur molecules.

Table 11. Summary of sorbent properties and mercury adsorption capacity

Sample Name	S Content (wt%)	Vs (cm^3/g)	Vm (cm^3/g)	Vb (cm^3/g)	Vt (cm^3/g)	BET Surface Area** (m^2/g)	Hg Uptake Capacity (μg/g)	S Utilization Ratio (%)
ACF10-Raw	0.2	0.274	0.039	0.065	0.371	920	214	---
ACF10-80C-24hrs	6.7	0.164	0.040	0.095	0.299	710	450	0.107
ACF10-150C-24hrs	26.3	0.001	0.001	0.003	0.005	8	220	0.013
ACF25-Raw	0.2	0.263	0.101	0.489	0.741	1950	319*	---
ACF25-150C-2hrs	4.1	0.227	0.069	0.454	0.714	1880	790	0.307
ACF25-150C-6hrs	10.2	0.173	0.052	0.409	0.634	1610	480	0.075
ACF25-150C-24hrs	30.5	0.006	0.002	0.007	0.015	100	230	0.012

Vs: small micropore volume Vb: big micropore volume; Vm: medium micropore volume, Vt: total pore volume

*deviation was ±8% based on three runs. ** Pressure used: $P/P_0=1.0 \times 10^{-5} \sim 1.0$.

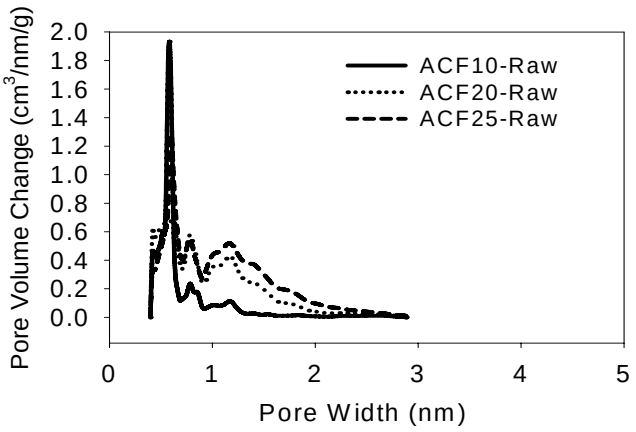

(a) Raw ACFs

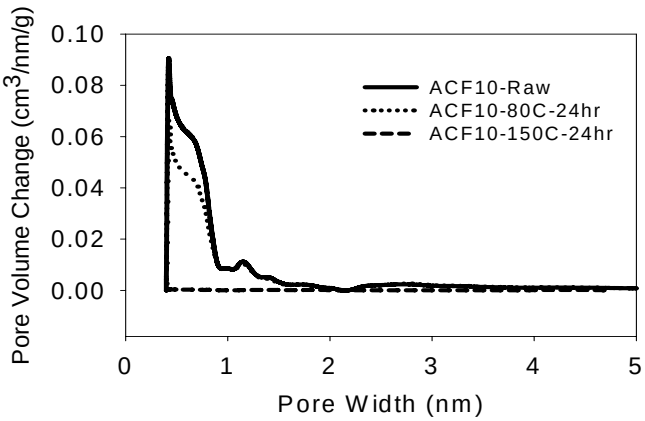

(b) ACF-10

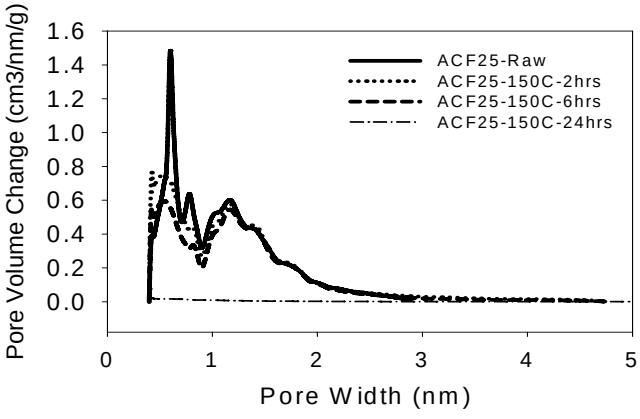

(c) ACF-25

Figure 34. Pore size distribution of ACFs before and after sulfur impregnation

Figure 34 (c) shows changes in the pore size distribution of ACF25 as a result of sulfur impregnation at 150°C for 2, 6, and 24 hours. It is clear that the initial losses in the pore volume after only 2 hours of impregnation occurred in small and medium micropores, while large micropores were not affected by sulfur deposition. The loss of small micropores was also observed by Hsi *et al.* [110, 111]. As the impregnation time was extended to 6 hours, further reduction in small and medium size micropores was observed. Reduction in the large micropore volume was observed only after the amount of sulfur deposited on the ACF surface exceeded 20 wt% after 24 hours of impregnation. A similar conclusion can be made for the data shown in Figure 34 (b) and Table 11, where the sulfur content exceeded 20 wt% before filling of large micropores was accomplished.

SEM-EDAX analysis was conducted for ACFs before and after sulfur impregnation. EDAX provided the elemental composition (wt%) of the outer layer of the ACF samples. The results obtained at 15 kV are shown in Table 12. Sulfur contents based on QMS detection, which represent the average sulfur content (wt%) of the sample, are also listed in the same table. At low temperatures (i.e., 80 ºC) and short impregnation times (i.e., 2 and 6 hours), sulfur content at the outer surface of the ACF is much lower than the bulk average. This means that sulfur tends to deposit more inside the fibers than on the outside at lower impregnation temperatures and during the initial stages of impregnation at higher temperatures. However, pore filling is not the only mechanism for sulfur deposition on ACF. Some sites at the outer surface, especially at high temperatures, were also important for sulfur deposition because the sulfur content on the outer

surface was higher than the bulk average after 24 hours of impregnation, when almost all pores are filled or blocked. In addition, sulfur is melted at a temperature of 150 °C, which may also achieve a more uniform distribution of sulfur on the carbon surface.

Table 12. Comparison of surface (EDAX) and average (QMS) sulfur content

Samples	EDAX Analysis#, wt%			Average S%, wt%*
	C	O	S	S
ACF10-Raw	97.60	2.38	0.20	0.2
ACF10-80C	96.44	2.42	1.14	6.7
ACF10-150C	62.97	2.52	34.50	26.3
ACF25-Raw	95.41	4.38	0.20	0.2
ACF25-150C-2hrs	94.95	4.03	1.02	4.1
ACF25-150C-6hrs	89.67	2.97	7.36	10.2
ACF25-150C-24hrs	61.14	4.45	34.41	30.5

*Calculated from QMS analysis.
#SEM-EDAX operation conditions: Magnification: 100, Voltage: 15kV, Scan time: 60 seconds

It is clear that pore size analysis conducted through nitrogen adsorption measurements can not determine if the loss in pore volume is due to sulfur deposition by complete filling of the pores or just blockage of the pore entrance. This question can only be answered by calculating the volume of sulfur added per gram of ACFs and comparing it with the lost pore volume. The volume of deposited sulfur can be calculated assuming that the predominant form of elemental sulfur deposited in the ACF pores is S_λ with a density of 1.96 g/cm^3 because of low temperatures used in this study [188]. Table 13 compares the loss in pore volume to the volume of impregnated sulfur. Column six of this table clearly suggests that the total pore volume lost during the impregnation process was not completely filled with sulfur. Pore blocking must account for a

significant fraction of the lost pore volume. The lower temperature resulted in a higher ratio of pore filling. This further supports the hypothesis that pore filling is the dominant mechanism for sulfur deposition at low temperature. At 150 ºC, all samples showed that less than 50% of the lost pore volume was filled with sulfur. This indicates that most of the pores were blocked, rather than filled. Comparing the volume of sulfur added through impregnation with the loss in volume of medium and big micropores shows that some sulfur must be added into small micropores (SEM-EDAX showed that the excess sulfur was not on the outer surface, Table 12) because it is not possible to have over 100% filling of the pores for ACF10-80C and ACF10-150C. This result suggests that impregnated sulfur can not be entirely in the form of S_8 because of size restriction (see text bellow) for the entrance of these large molecules into small micropores. It is more likely that, H_2S and O_2, which are much smaller molecules, first entered into small micropores and were then oxidized in-situ.

Table 13. Comparison of the loss in pore volume and the volume of impregnated sulfur

Samples	Average S%* (Wt%)	S added (mg/g raw ACF)	Volume of S added (cm^3)	Vt Loss (cm^3)	% of Lost Vt filled (%)	Lost Vb+Vm (cm^3)	% of Lost Vm+Vb filled (%)
ACF10-80C	6.7	71.8	0.037	0.05	73	0.003	1078
ACF10-150C	26.3	356.9	0.182	0.36	50	0.143	127
ACF25-150C-2hrs	4.1	42.8	0.022	0.11	20	0.067	33
ACF25-150C-6hrs	10.2	113.6	0.058	0.15	39	0.062	93
ACF25-150C-24hrs	30.5	438.8	0.224	0.83	27	0.452	50

Vb: big micropore volume; Vm: medium micropore volume, Vt: total pore volume
Assume all sulfur in S_8 form with a density of 1.96 g/cm^3

According to Meyer [189], the sulfur at 150 °C should be predominantly in the S_λ form, which is a ring of eight sulfur atoms. Assuming that S_λ is a spherical sulfur allotrope, its diameter is calculated to be 0.73 nm based on the sulfur density. Hsi et al [110], also reported a diameter of 0.76 to 0.84 nm depending if the molecule exists as a ring or as a chain. Figure 34 (a) shows that ACF25-150C-2hrs and ACF25-150C-6hrs actually developed more small micropores with diameter below 0.75nm. This is most probably because the sulfur molecules plugged small micropores with diameter larger than that of one sulfur molecule but smaller than that of two.

4.4.3 Stability of Sulfur

Stability of sulfur on the carbon surface is important for practical application since the temperature of mercury laden gas streams is usually above 100 °C. Figure 35 shows TGA analysis of ACF10 before and after sulfur impregnation at 80 and 150 °C (it can be assumed that ACF20 and ACF25 impregnated at 150ºC would exhibit similar behavior). After heating to 800ºC, the raw ACF10 lost less than 2% of its weight, while ACF10-80C and ACF10-150C showed weight loss of 6 and 17 %, respectively. These data show that not all the sulfur impregnated on the ACF surface is removed by heating to 800 ºC in an inert environment (elemental sulfur has a melting point around 119 °C and a boiling point about 444 °C). Such behavior is reasonable because some of the sulfur may be embedded into the carbon structure to form C-S complexes. Puri *et al.* [143] reported that C-S complexes formed by the reactions between various sulfur containing gases, including S, H_2S, SO_2 and CS_2, and activated carbon are very stable and that heating the complex up to 600 °C could not remove all the sulfur impregnated on

the carbon surface. Although it is not directly proven in this study, it can be expected that the sulfur vapor created during thermal gravimetric analysis can react with the carbon surface to form these strong bonds at higher temperatures.

The derivative weight loss curve (Figure 35 (b)) shows that there are two weight-loss peaks that appear between 200-300 ºC and between 400-500 ºC. The two peaks may represent different bond strength between the deposited sulfur and carbon structure of the fiber. Figure 35 also shows that the increase in sulfur impregnation temperature results in greater area for the second peak. Such behavior is expected because higher temperature provides greater energy for creating stronger bonds. Another observation from Figure 35 is that the elemental sulfur loss occurred at a temperature that is much higher than any of the temperatures used during the impregnation process. Such behavior can be explained by the strength of the interaction between carbon and sulfur and by the porous structure of the sorbent that helps to retain deposited sulfur. Such behavior is beneficial for the mercury removal process as the adsorbed mercury will not be easily released from the sorbent surface if this result can be extrapolated to realistic mercury removal conditions.

Using the method described before [168], the activation energy can be estimated based on the results shown in Figure 36. Figure 36 (a) shows the weight loss of ACF10-150C-24hrs at different heating rates. From the slope of the line correlating –logB vs 1/T, it was estimated that the activation energy of the decomposition of the impregnated sulfur on ACF10-150C-24hr is 90.0 kJ/mol (elemental sulfur sublimation energy is 16.28 kJ/mol, Appendix C, Table 17). Compared to a typical C-S chemical bond energy of about 272 kJ/mol [190], this low activation

energy indicates that the sulfur lost during TGA analysis did not form chemical bonds with the carbon surface but is likely bound to the sulfur that remained on the ACF surface at the end of the TGA experiment.

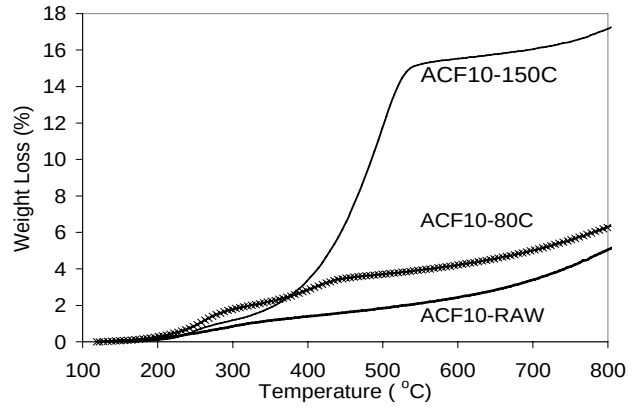

(a)

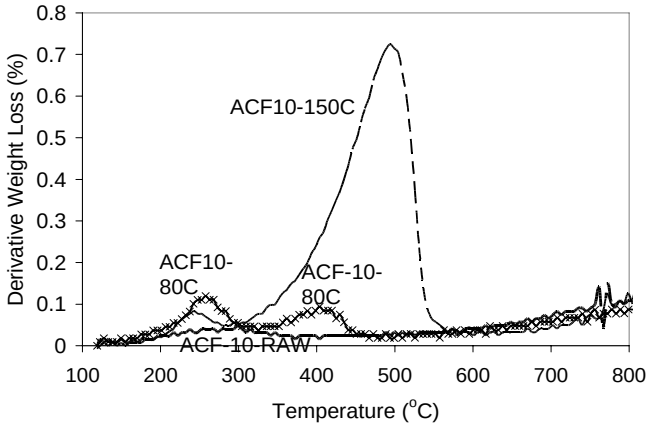

(b)

Figure 35. TGA analysis of ACF-10 before and after sulfur impregnation: (a) total weight loss, (b) derivative weight loss

(Sample weight: ~15 mg, nitrogen flow rate: 40 ml/min, heating profile: 120 °C for 2 hrs, ramp from 120 °C to 800 °C at 10 ºC/min)

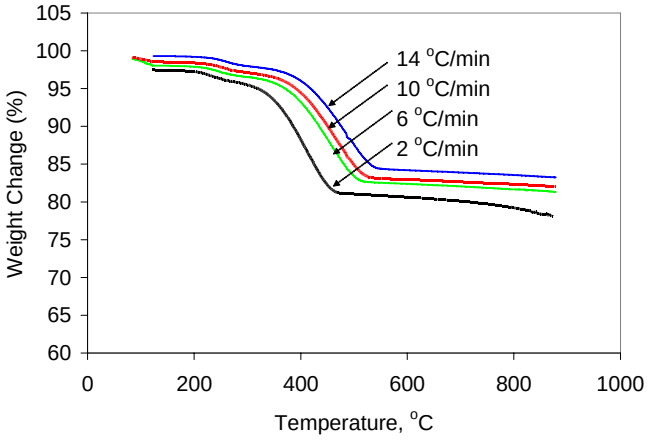

(a)

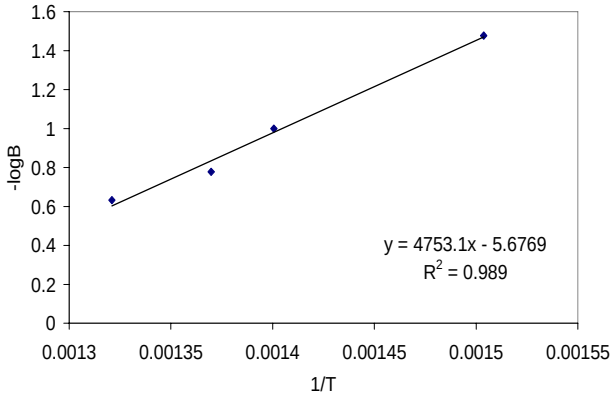

(b)

Figure 36. Estimation of the activation energy for desorption of impregnated sulfur on ACF10-150C-24hrs: (a) weight loss at different heating rates; (b) plot of –logB vs 1/T

(Sample weight: ~18 mg, Nitrogen flow rate: 20 ml/min, Heating profile: 120°C for 2 hrs, ramp from 120°C to 800°C at 10ºC/min)

4.4.4 Forms of Sulfur

In order to obtain information on the forms of sulfur on the carbon surface, the QMS 300 was coupled with the TGA 7 to simultaneously monitor the sulfur loss and species released from the ACFs. For this study, a slow nitrogen flow of 12 ml/min and a much higher heating rate of 60 °C/min were employed.

Gases exiting the TGA were analyzed by the QMS 300 and the following AMUs (atomic mass units) were monitored: 16 (O), 18 (H_2O), 28 (CO/N_2), 32 (O_2/S), 34 (H_2S), 44 (CO_2), 48(SO), 64 (SO_2/S_2), 96 (S_3), 128(S_4). It was found that major species emitted from ACF10-Raw and ACF10-150C were O_2, CO_2, and SO_2. Also, condensed elemental sulfur was clearly observed in the tube at the exit of the TGA furnace and no peaks associated with elemental sulfur were detected by the QMS because of the condensation.

During the TPD (TGA-QMS) analysis, oxygen (possibly from the carbon surface) was released from the carbon surface. For ACF10-raw, only CO_2 was observed, while for ACF10-150C, both SO_2 and CO_2 were released (Figure 37). These results can not confirm whether the released sulfur was originally retained on the carbon surface as SO_2 or in some other form. Therefore, these results were combined with XPS study to determine the origin of the SO_2 during heating.

The characteristic XPS spectra for ACF-25 before and after sulfur impregnation are shown on Figure 38(a). Based on the standard library spectra, the following binding energy data are relevant for this experimental system: around 164.05eV for free elemental sulfur, 161.8-162.6eV for chemisorbed sulfur, and higher than 167eV for oxidized sulfur. Unbound organic sulfur

species, like thiophene, also show peaks around 164 eV. However, in the presence of oxygen, the generation of these organic species is highly questionable. Figure 38(a) shows that sulfur on ACF surface is present mainly in free elemental form with negligible amounts of oxidized sulfur forms. Figure 38(b) shows that the oxygen intensity on ACF surface increased, but not as significant as that of sulfur.

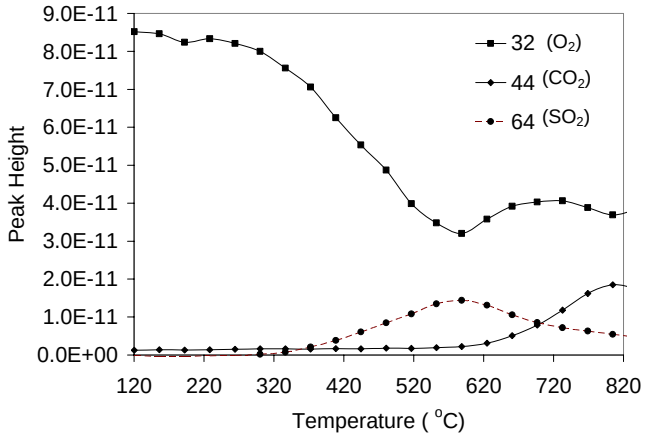

Figure 37. TPD of ACF10-150C

(Heating rate: 60°C/min, pure nitrogen flow rate: 12 ml/min. Samples were dried at 120°C for 2 hours before analysis. Monitored AMUs by QMS: 16,18,28,32,34,44,48,96,128)

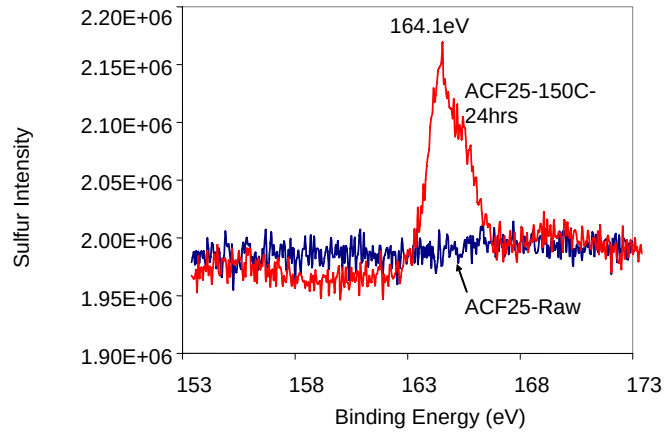

(a)

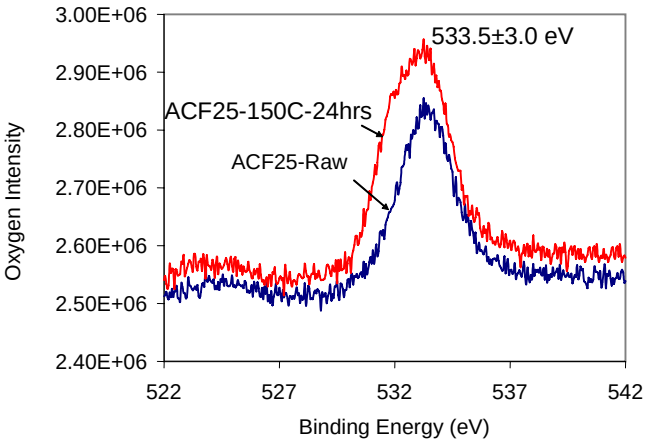

(b)

Figure 38. XPS Spectrum of ACF25 before and after sulfur impregnation: (a) sulfur intensity and (b) oxygen intensity

Combining all the observations discussed above, it can be concluded that impregnated sulfur on the carbon surface is mainly present in elemental form. Upon heating the impregnated sorbent, chemisorbed oxygen was released through decomposition of surface functionalities and combined with sulfur to form SO_2 that was observed in the effluent gas during TPD.

It is important to note that contrary to other studies, which found that the major products created during H_2S oxidation on activated carbon surface were both elemental and oxidized sulfur (i.e. sulfuric acid) [126, 127, 162], this study was conducted under dry conditions. Furthermore, the samples used in this study were exposed to relatively high temperatures, which prevented significant retention of water vapor on the carbon surface.

4.4.5 Impact of Sulfur Content on Mercury Adsorption

Mercury uptake capacity of all adsorbents used in this study as a function of sulfur content is depicted on Figure 39. It is clear that higher sulfur content does not necessarily lead to greater mercury uptake. Figure 39 and Table 11 suggest that the sulfur content of around 4% deposited at 150 ºC produced a sorbent with the highest mercury capacity. Further increase in sulfur content hinders mercury uptake because the excess sulfur blocks or fills the pores of the sorbent, which are required for mercury adsorption. Similar behavior was observed before [105, 109]. Sulfur utilization ratio was defined as the ratio of the molar amount of sulfur combined with mercury to the total molar amount of impregnated sulfur. The sulfur utilization ratios were calculated and included into Table 11. The low utilization ratios show that most of the sulfur did not react with mercury. Sulfur utilization ratio decreased with a decrease in pore volume, which is likely due reduced accessibility for the reaction with mercury.

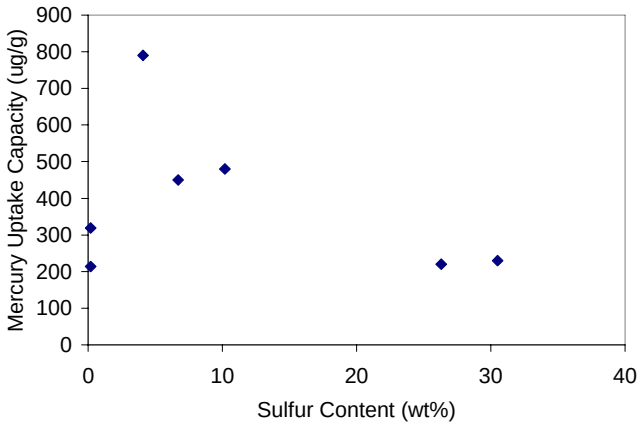

Figure 39. Correlation of sulfur content with Hg uptake capacity for sorbents produced through H_2S oxidation

(Refer to Table 11 for sorbents propterties)

Realizing that both sulfur content and pore structure of the sorbent are important, it is likely that the sorbent impregnated with a sulfur monolayer would offer best performance for mercury uptake. It is reasonable to suggest that sulfur which deposits on the sorbent surface in the second layer would block the access to the first layer and, at the same time, reduce the pore volume of the sorbent.

4.4.6 Impact of Pore Volume and Surface Area on Mercury Adsorption

The effects of pore volume and surface area were analyzed separately for raw ACFs and for ACF25 impregnated with sulfur. The pores were divided into three groups as described earlier: small micropores, medium micropores and big micropores. Pore volume and surface area of each group were determined from surface area analysis. These values were correlated with observed mercury uptake using linear regression and the slope of the linear fit to experimental

data (value of the coefficient b in the expression $q_{Hg} = a + bx$) indicates the significance of a given parameter for Hg uptake. Sulfur impregnated ACFs were analyzed separately from virgin ACFs due to the important contribution of impregnated sulfur on mercury uptake. These analyses were done in an attempt to find the most important pore size region for Hg uptake by virgin and impregnated ACFs.

Table 14 shows the effect of pore volume on Hg uptake capacity of the raw ACFs. V_b, V_s+V_m, V_m+V_b, and the total pore volume all showed good correlation with Hg uptake. Although V_s+V_m has the highest b value, its R^2 is much smaller than that of the others. It appears that medium and big micropores contribute the most to Hg uptake. Because small micropores do not represent a major contribution to mercury uptake by virgin ACFs, it can be concluded that mercury adsorption on virgin ACFs at 140 ^oC is not achieved through physisorption [191]. This finding supports previous suggestion that mercury uptake by carbonaceous sorbents at 140 ^oC is mainly due to chemisorption [192]. As shown in Table 15, attempts to correlate fractions of surface area associated with small, medium and big micropores with mercury uptake support the conclusions discussed above because the surface area of medium and big micropores (S_m+S_b) provided the best correlation with Hg uptake.

In addition to the impacts of surface morphology that were investigated in this study, it is important to consider the impact of surface chemistry on mercury uptake [99, 100]. Attempts to correlate the pore volume and surface area of sulfur impregnated ACF25 and mercury uptake resulted in fairly small R^2 values, which suggests that factors other than surface morphology affect Hg uptake. This conclusion is expected because HgS formation is believed to be the dominant mechanism for mercury uptake by sulfur impregnated sorbents.

Table 14. Effect of pore volume of raw ACFs on Hg uptake capacity

Sample Name	Vs (cm^3/g)	Vm (cm^3/g)	Vb (cm^3/g)	Vs+Vm (cm^3/g)	Vm+Vb (cm^3/g)	Total (cm^3/g)	Hg Uptake Capacity (μg/g)
ACF-10-Raw	0.274	0.039	0.065	0.313	0.104	0.378	214
ACF-20-Raw	0.258	0.104	0.329	0.362	0.433	0.691	271
ACF-25-Raw	0.263	0.101	0.489	0.364	0.59	0.853	319
Slope, b	-4544	246.7	244.5	1646	209.5	215.8	
Coefficient, R^2	0.501	0.757	0.992	0.819	0.977	0.983	

Table 15. Effect of surface area of raw ACFs on Hg uptake capacity

Sample Name	Ss (m^2/g)	Sm (m^2/g)	Sb (m^2/g)	Ss+Sm (m^2/g)	Sm+Sb (m^2/g)	Total (m^2/g)	Hg Uptake Capacity (μg/g)
ACF-10-Raw	485	528	196	1012	724	920	214
ACF-20-Raw	578	388	762	966	1150	1453	271
ACF-25-Raw	398	533	973	931	1506	1950	319
Slope, b	-2.65	-0.01	0.128	-1.29	0.13	0.10	
Coefficient, R^2	0.215	0.003	0.957	0.999	1	0.999	

4.4.7 Summary

Impregnation of sulfur onto the activated carbon fiber surface through H_2S oxidation was studied at temperatures lower than 150°C followed by the mercury uptake test in nitrogen. Sulfur was impregnated mainly as elemental sulfur and the amount of sulfur deposited on the ACF increased with an increase in impregnation temperature; higher temperature leads to more uniform sulfur distribution inside the sorbent pores. More sulfur was found in the internal pores

than on the external surface layer; the impregnation process can be explained by a combination of pore filling and monolayer adsorption, with the former mechanism predominating at low temperatures. In the absence of sulfur, the mercury adsorption capacity can be correlated with surface area and pore volume with medium (0.72nm < d < 0.90nm) and big micropores (d > 0.90nm) being more important for mercury uptake.

5.0 SUMMARY AND CONCLUSIONS

Both mercury and hydrogen sulfide are air pollutants in need of serious attention. Based on the concept of industrial ecology, this study investigated hydrogen sulfide adsorption/oxidation onto carbon surfaces and its application in mercury pollution control. A fixed bed reactor system was used to study adsorption/sulfurization/oxidation of hydrogen sulfide by activated carbon fibers (ACFs) and activated carbons. The carbon surface chemistry was characterized before and after adsorption/sulfurization/oxidation by various techniques including BET, SEM-EDAX, sulfur analysis, XPS, XANES, TGA, TPD, Boehm tiration, and so on. The produced sorbents were then tested for mercury uptake in the same fixed bed reactor system. Through this study, the following conclusions were obtained:

H_2S Adsorption on ACFs and Activated Carbons

- Adsorption of hydrogen sulfide on carbon surfaces at low temperatures under dry and anoxic conditions was found to be affected by both pore structure and surface chemistry. Reversible adsorption (or physical adsorption) was mainly affected by the pore structure, with smaller pores enhancing physical adsorption. On the other hand, irreversible adsorption (or chemisorption) is mainly affected by the carbon surface chemistry.

- Chemical fixation of hydrogen sulfide is an important pathway, especially after surface treatment. Both air oxidation and heat treatment enhanced retention of hydrogen sulfide on the carbon surface, which means both addition and removal of oxygen at carbon surface improve hydrogen sulfide retention.

- The retained amount of hydrogen sulfide correlated well with the amount of basic functionalities on the raw ACFs and virgin activated carbon surfaces, indicating the importance of acid-base interactions in chemisorption of hydrogen sulfide under dry and anoxic conditions.

- Hydrogen sulfide retention did not increase linearly with the temperature for heat treatment in argon, indicating the basic functionalities are more important than the graphite structure for hydrogen sulfide uptake.

Sulfurization on ACFs and BPL Carbon

- Sulfurization at higher temperatures resulted in higher sulfur content, which may be due to decomposition of more oxygen containing functionalities. Experimental results suggested that the uptake of H_2S was facilitated through substitution of the surface oxygen or active carbon atoms. Sulfur species produced at higher temperatures are more stable and high temperatures promote the formation of organic sulfur.

- The presence of H_2S during the cooling process obviously increased the ultimate sulfur content, especially relatively unstable sulfurous species. XANES results proved that the presence of H_2S during the cooling process increased mainly elemental sulfur content.

- At temperatures below 600 °C, sulfurization most likely occurred through the addition of H_2S onto active sites enhanced by decomposition of CO_2 yielding oxygen containing functionalities; while at higher temperatures decomposition of H_2S and direct reaction with carbon structure occurred.

- Surface chemistry was very important for sulfurized sorbents produced at temperatures above 400 °C, which had similar pore structures. Effective mercury sorbents were produced at Hg 600 °C with the presence of hydrogen sulfide during the cooling process.

- Elemental sulfur species are probably the most effective for capturing mercury although thiophene and sulfate content also showed good correlation with mercury uptake capacity.

H_2S Oxidation on ACFs

- Oxidation of H_2S on ACFs at lower temperature range (<150 °C) generated mainly elemental sulfur and the amount of sulfur deposited on the ACF increased with an increase in impregnation temperature; higher temperature leads to more uniform sulfur distribution inside the sorbent pores.

- More sulfur was found in the internal pores than on the external surface layer; the impregnation process can be explained by a combination of pore filling and monolayer adsorption, with the former mechanism predominating at low temperatures.

- The mercury uptake capacity did not correlate linearly with the sulfur content of the sorbents produced through oxidation because of the blockage of the pore structure.

- In the absence of sulfur, the mercury adsorption capacity can be correlated with surface area and pore volume. Experimental results suggested that medium (0.72nm < d < 0.90nm) and big micropores (d > 0.90nm) are very important for mercury uptake.

6.0 ENGINEERING SIGNIFICANCE OF THIS STUDY

6.1 DIRECT ENGINEERING APPLICATIONS

This study focused on the interaction between hydrogen sulfide and carbonaceous surfaces, mainly for the development of mercury sorbents. The findings of this study apply directly to both H_2S removal and vapor-phase mercury removal by carbonaceous sorbents. For both applications, it is important to optimize the sorbent performance in terms of pore structure and surface chemistry.

For the removal of low concentration of H_2S at low temperature, such as indoor air pollution control, sorbents with small pores are superior because of high uptake capacity and ease of regeneration. However, for the removal of high concentration H_2S, such as natural gas sweetening, higher surface area and pore volume are more important parameters for sorbent selection.

In some cases, chemisorption is preferred to prevent desorption of contaminants or impurities due to fluctuations in operating conditions. For example, production of high purity gases, such as fuel cell feed gas, requires removal of H_2S to ppb levels. Good performance of gas sensors requires high reactivity and high selectivity. This study suggests that creation of more basic active sites, especially more basic surface functionalities, will improve the chemisorption of acidic gas species such as H_2S onto the carbon surface. The creation of more basic active sites can be

achieved through ammonia treatment or heat treatment. Removal of H_2S from high temperature gas streams requires improvements in the carbon surface chemistry too. Higher chemisorption capacity can be achieved by creating more basic active sites.

Sulfurization of carbon surfaces can produce sorbents or catalysts with different sulfur containing surface functionalities, especially for the production of mercury sorbents. It is found that sulfur content, sulfur distribution, and sulfur forms can be controlled by changing the impregnation temperature and impregnation protocols. Higher temperature helps to strongly bind more sulfur species, especially organic sulfur, to the carbon surface. In addition, higher temperature facilitates more uniform sulfur distribution. Mercury sorbents of high performance require high surface area, pore size/volume, and well distributed short-chained elemental sulfur. Such sorbents can be produced by sulfurization of carbon surface at 600 °C with exposure of H_2S during the cooling process.

Good mercury sorbents can also be produced by oxidation of H_2S on ACF-25 at 150 °C for 2 hours. This is because the major sulfur species, elemental sulfur, was formed mainly through the monolayer adsorption, thereby retaining the pore structure of the original sorbent.

The results of this study revealed the nature of chemisorption of H_2S onto carbon surface, implying that carbon surface with high density of basic surface functionalities can serve as excellent sorbents for H_2S.

6.2 GENERAL IMPLICATIONS

Besides the direct application of the findings mentioned above, this study helps to understand some surface phenomena in general, which are beyond practical applications. The following conclusions can possibly be extended to other fields:

This study clarifies that adsorption onto porous materials is generally composed of chemisorption and physisorption, the relative contribution of the two processes are associated with the pore structure and surface chemistry, as well as experimental conditions.

The findings of this study help to understand the complexities of carbon surface chemistry, especially the importance of oxygen containing surface functionalities (both acidic and basic) and the active sites formed after decomposition of these functionalities. The results indicate that oxidation followed by heat treatment may be a good method of generating active sites for special applications. This study also helps to understand the nature of carbon basicity.

This study implies the electrical nature of the interaction between H_2S and active sites on carbonaceous surface. The Lewis acid-base interaction can possibly be extended to the interaction between other gas molecules and other surfaces. Further study can facilitate general sorbents and catalysts development.

7.0 RECOMMENDATIONS FOR FUTURE WORK

Starting from a practical pollution control problem, the project focused on the carbon surface chemistry. Surface science is an interdisciplinary study involving chemistry, physics, engineering, and many other fields. Rapid developments in these fields can help to understand the puzzle of carbon surface chemistry.

Quantum mechanics theory has shown its success in explaining many experimental observations with different surfaces. It is important to introduce this powerful tool to facilitate the understanding of carbon surface chemistry as well. Theoretical calculation on the effect of carbon surface chemistry on H_2S chemisorption and mercury uptake is important in better explaining the observations made in this study. Theoretical models should include the carbon basal planes, oxygen containing functionalities, sulfur containing functionalities and metals in order to achieve better understanding of these complex systems.

The nature of carbon basicity also needs theoretical explanation. Better understanding of the origin of carbon basicity will enhance the application of carbon materials in adsorption, catalysis and many other areas. Modification and characterization of carbon surface chemistry is becoming a new area of strong research interest.

For practical applications, the following topics are found to be interesting and worth pursuing:

- The effect of carbon surface chemistry on selective H_2S oxidation, especially on ways to improve the selectivity to elemental sulfur by modifying the carbon surface chemistry;

- Systematic work on the effect of pore structure and carbon surface chemistry on the decomposition of H_2S into H_2 and S_x.

APPENDIX A

ADDITIONAL FIGURES

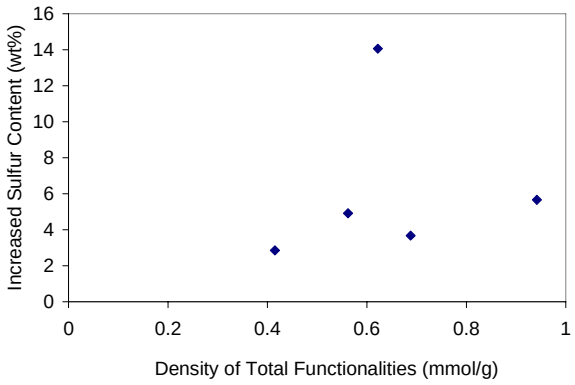

(a)

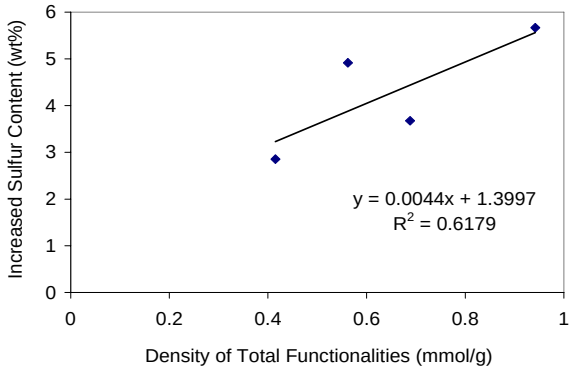

(b)

Figure 40. Correlation of total functionalities with increased sulfur content: (a) with Centaur, (b) without Centaur

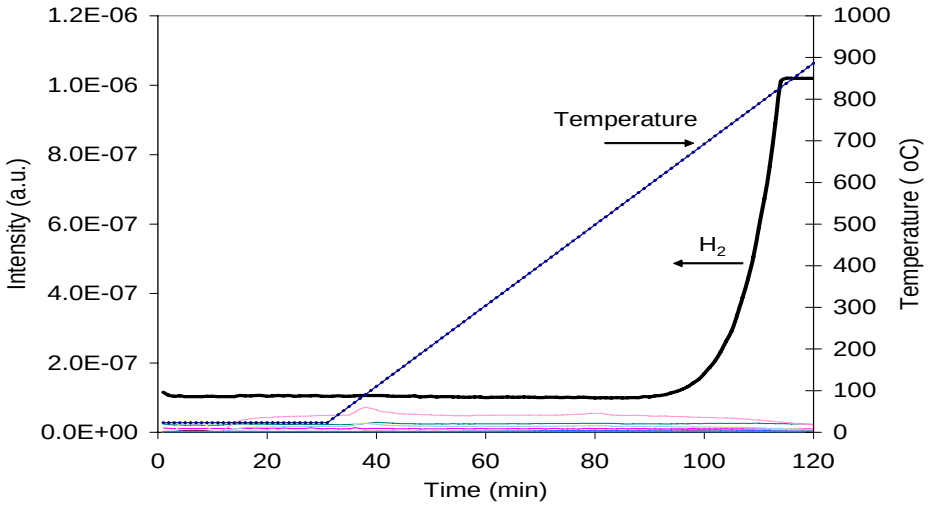

Figure 41. Hydrogen generation during temperature programmed reaction

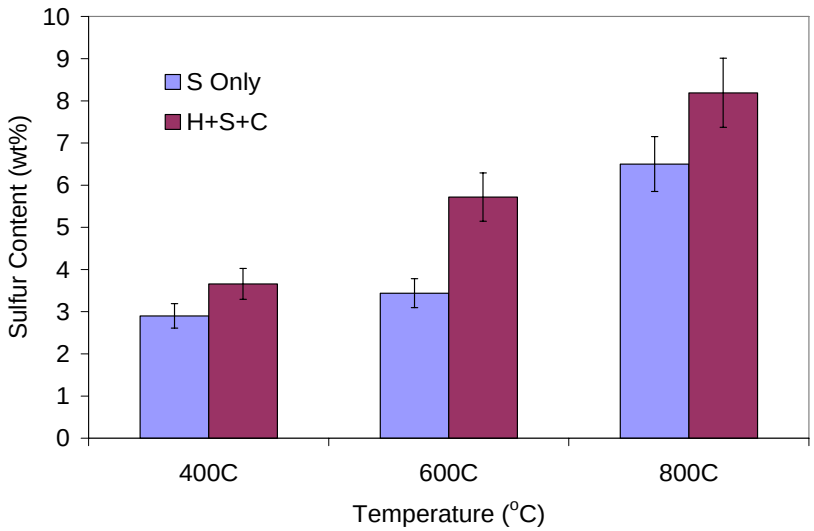

Figure 42. Effect of sulfurization protocol at different temperatures

(Carbon amount: 0.5 g, H_2S concentration: 3000 ppm, sulfurization time: 6 hours)

APPENDIX B

PHYSICAL PROPERTIES OF CHEMICALS

Table 16. Physical properties of chemicals *

	Mercury (Hg)	Hydrogen Sulfide (H_2S)	Elemental Sulfur (S_x)
Molecular Weight (g/mol)	200.59	34.08	32.07
Melting Point (Tm, K)	234.17	187.65	388.36
Boiling Point (Tb, K)	629.73	212.45	717.75
Critical Point (Tc, K)	1750	---	1314
Density (g/cm^3)	13.53 at 293K	1.539 g/l	1.96 (monoclinic) 2.07 (rhombic)

* All the data are from: *Lide D. R., CRC Handbook of Chemistry and Physics, 74th edition, 1994, Boca Raton: CRC press.*

APPENDIX C

ELEMENTAL SULFUR SUBLIMATION ENERGY CALCULATION

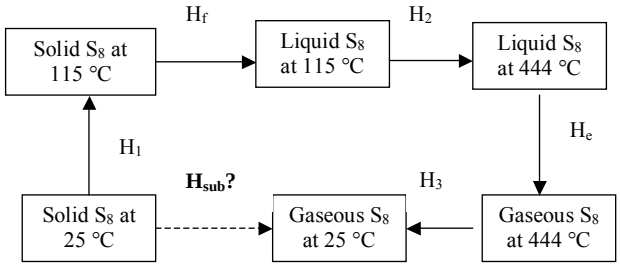

Table 17. Elemental Sulfur sublimation energy calculation at 298 K*

Cp Regression Coefficients					Phase	Starting Temperature	Ending Temperature	Heat	NOTE
A	B	C	D	E		(K)	(K)	(J/mol)	
2.003	1.20E-01	-1.62E-04			Solid	298.00	388.36	2169	Heating Up Solid, H_1
					S-L			1727	Heat of Fusion, H_f
108.05	-2.37E-01	2.27E-04	-6.00E-08		Liquid	388.36	717.82	12279	Heating Up Liquid, H_2
					L-G			9620	Heat of Evaporation, H_e
24.624	-5.04E-03	2.42E-06	-4.22E-10	2.52E-14	Gas	717.82	298.00	-9514	Cooling Gas, H_3
								16280	Heat of Sublimation, summation of the above.

*All data from *Yaws, C. L., "Chemical Properties Handbook", McGraw-Hill, 1999*
** Formula for Cp calculation: $Cp=A+BT+CT^2+DT^3+ET^4$

Therefore, the sublimation energy of S_8 at 298 K is 16.28 kJ/mol.

BIBLIOGRAPHY

1. Yoshida, M., Elemental and inorganic mercury poisoning. *Japanese Journal of Toxicology and Environmental Health* **1998,** 44 (3), 168-181.

2. Akagi, H.; Naganuma, A., Human exposure to mercury and the accumulation of methylmercury that is associated with gold mining in the Amazon Basin, Brazil. **2000,** 46 (5), 323-328.

3. Boffetta, P.; Merler, E.; Vainio, H., Carcinogenicity of Mercury and Mercury-Compounds. *Scandinavian Journal of Work Environment & Health* **1993,** 19 (1), 1-7.

4. Boyd, A. S.; Seger, D.; Vannucci, S.; Langley, M.; Abraham, J. L.; King, L. E., Mercury exposure and cutaneous disease. *Journal of the American Academy of Dermatology* **2000,** 43 (1), 81-90.

5. Ratcliffe, H. E.; Swanson, G. M.; Fischer, L. J., Human exposure to mercury: A critical assessment of the evidence of adverse health effects. *Journal of Toxicology and Environmental Health* **1996,** 49 (3), 221-270.

6. Asano, S.; Eto, K.; Kurisaki, E.; Gunji, H.; Hiraiwa, K.; Sato, M.; Sato, H.; Hasuike, M.; Hagiwara, N.; Wakasa, H., Acute inorganic mercury vapor inhalation poisoning. *Pathology International* **2000,** 50 (3), 169-174.

7. Tchounwou, P. B.; Ayensu, W. K.; Ninashvili, N.; Sutton, D., Environmental exposure to mercury and its toxicopathologic implications for public health. *Environmental Toxicology* **2003,** 18 (3), 149-175.

8. Nriagu, J. O.; Pacyna, J. M., Quantitative Assessment of Worldwide Contamination of Air, Water and Soil by Trace Metals. *Nature* **1988,** 333 (12), 134-139.

9. USEPA *Mercury Study Report to Congress*; 1997.

10. Chang, R.; Offen, G., Mercury Emission Control Technologies: An EPRI Synopsis. *Power Engineering* **1995,** 99 (11), 51-57.

11. Brenneman, K. A.; James, R. A.; Gross, E. A.; Dorman, D. C., Olfactory neuron loss in adult male CD rats following subchronic inhalation exposure to hydrogen sulfide. *Toxicologic Pathology* **2000,** 28 (2), 326-333.

12. Guidotti, T. L., Occupational Exposure to Hydrogen-Sulfide in the Sour Gas-Industry - Some Unresolved Issues. *International Archives of Occupational and Environmental Health* **1994,** 66 (3), 153-160.

13. Dorman, D. C.; Moulin, F. J. M.; McManus, B. E.; Mahle, K. C.; James, R. A.; Struve, M. F., Cytochrome oxidase inhibition induced by acute hydrogen sulfide inhalation: Correlation with tissue sulfide concentrations in the rat brain, liver, lung, and nasal epithelium. *Toxicological Sciences* **2002,** 65 (1), 18-25.

14. Hendrickson, R. G.; Chang, A.; Hamilton, R. J., Co-worker fatalities from hydrogen sulfide. *American Journal of Industrial Medicine* **2004,** 45 (4), 346-350.

15. Nikkanen, H. E.; Burns, M. M., Severe hydrogen sulfide exposure in a working adolescent. *Pediatrics* **2004,** 113 (4), 927-929.

16. Milby, T. H.; Baselt, R. C., Hydrogen sulfide poisoning: Clarification of some controversial issues. *American Journal of Industrial Medicine* **1999,** 35 (2), 192-195.

17. Agency for Toxic Substances and Disease Registry *Toxicological profile for hydrogen sulfide*; U.S. Department of Health and Human Services, Public Health Service: Atlanta, GA, 1999; 139-144.

18. Graede, T. E., Haukins D. T., Claxton L. D., *Atmospheric Chemcial Compounds: Sources, Occurence, and Bioassay*. Academic Press: NY, 1986.

19. Cal, M. P.; Strickler, B. W.; Lizzio, A. A.; Gangwal, S. K., High temperature hydrogen sulfide adsorption on activated carbon II. Effects of gas temperature, gas pressure and sorbent regeneration. *Carbon* **2000,** 38 (13), 1767-1774.

20. Cal, M. P.; Strickler, B. W.; Lizzio, A. A., High temperature hydrogen sulfide adsorption on activated carbon I. Effects of gas composition and metal addition. *Carbon* **2000,** 38 (13), 1757-1765.

21. Swisher, J. H., Yang, J., Gupta, R. P., Attrition-resistant zinc titanate sorbent for sulfur. *Ind. Eng. Chem. Res.* **1995,** 34 (4), 4463–4471.

22. Khare, G. P.; Delzer, G. A.; Kubicek, D. H.; Greenwood, G. J., Hot gas desulfurization with Phillips Z-sorb sorbent in moving bed and fluidized bed reactors. **1995,** 14 (3), 146-150.

23. Adamson, A. W., *Physical Chemistry of Surfaces*. Wiley-Interscience Publication: New York, 1982.

24. Lüth, H., *Solid Surfaces, Interfaces and Thin Films*. Springer Verlag: Heidelberg, 2001.

25. Vidali, G.; Ihm, G.; Kim, H.-Y.; Cole, M. W., Potentials of physical adsorption. *Surface Science Reports* **1991,** 12, 133-166.

26. Suzuki, M., *Adsorption engineering*. Kodansha; Elsevier: Tokyo; Amsterdam; New York, 1990.

27. Spencer, N. D.; Moore, J. H., *Encyclopedia of chemical physics and physical chemistry*. Institute of Physics Pub.: Bristol; Philadelphia, 2001.

28. Duong, D. D., *Adsorption analysis-- equilibria and kinetics*. Imperial College Press; Distributed by World Scientific Pub.: London; Singapore; River Edge, NJ, 1998.

29. Dubinin, M. M.; Polyakov, N. S.; Kadlez, O.; Kataeva, L. I.; Petukhova, G. A., Heterogeneous Microporous Structures and Adsorption Properties of Carbon Adsorbents.12. Porous Structure and Adsorption Properties of Active Carbons. *Russian Chemical Bulletin* **1993,** 42 (8), 1304-1308.

30. Nguyen, C.; Do, D. D., The Dubinin-Radushkevich equation and the underlying microscopic adsorption description. *Carbon* **2001,** 39 (9), 1327-1336.

31. Tovbin, Y. K., The volume of micropores and the Dubinin-Radushkevich equation. *Russian Chemical Bulletin* **1998,** 47 (4), 637-643.

32. Polyakov, N. S.; Dubinin, M. M.; Kataeva, L. I.; Petuhova, G. A., Porous Structure and Adsorption Properties of Active-Carbon. *Pure and Applied Chemistry* **1993,** 65 (10), 2189-2192.

33. Mangun, C. L.; Daley, M. A.; Braatz, R. D.; Economy, J., Effect of pore size on adsorption of hydrocarbons in phenolic-based activated carbon fibers. *Carbon* **1998,** 36 (1-2), 123-129.

34. Pierson, H. O., *Handbook of carbon, graphite, diamond and fullerenes*. Noyes Publications: Park Ridge, NJ, USA, 1993.

35. Lahaye, J., The chemistry of carbon surfaces. *Fuel* **1998,** 77 (6), 543-547.

36. Montes-Moran, M. A.; Suarez, D.; Menendez, J. A.; Fuente, E., On the nature of basic sites on carbon surfaces: An overview. *Carbon* **2004,** 42 (7), 1219-1225.

37. Boehm, H. P., Some Aspects of the Surface-Chemistry of Carbon-Blacks and Other Carbons. *Carbon* **1994,** 32 (5), 759-769.

38. Figueiredo, J. L.; Pereira, M. F. R.; Freitas, M. M. A.; Orfao, J. J. M., Modification of the surface chemistry of activated carbons. *Carbon* **1999,** 37 (9), 1379-1389.

39. Boehm, H. P., Surface oxides on carbon and their analysis: a critical assessment. *Carbon* **2002,** 40 (2), 145-149.

40. Donnet, J. B.; Custodero, E.; Wang, T. K.; Hennebert, G., Energy site distribution of carbon black surfaces by inverse gas chromatography at finite concentration conditions. *Carbon* **2002,** 40 (2), 163-167.

41. Zielke, U.; Huttinger, K. J.; Hoffman, W. P., Surface-oxidized carbon fibers.1. Surface structure and chemistry. *Carbon* **1996,** 34 (8), 983-998.

42. Pradhan, B. K.; Sandle, N. K., Effect of different oxidizing agent treatments on the surface properties of activated carbons. *Carbon* **1999,** 37 (8), 1323-1332.

43. Ania, C. O.; Parra, J. B.; Pis, J. J., Influence of oxygen-containing functional groups on active carbon adsorption of selected organic compounds. *Fuel Processing Technology* **2002,** 79 (3), 265-271.

44. Lakshminarayanan, P. V.; Toghiani, H.; Pittman, C. U., Nitric acid oxidation of vapor grown carbon nanofibers. *Carbon* **2004,** 42 (12-13), 2433-2442.

45. Moreno-Castilla, C.; Carrasco-Marin, F.; Maldonado-Hodar, F. J.; Rivera-Utrilla, J., Effects of non-oxidant and oxidant acid treatments on the surface properties of an activated carbon with very low ash content. *Carbon* **1998,** 36 (1-2), 145-151.

46. Chen, J. P.; Wu, S. N., Acid/base-treated activated carbons: Characterization of functional groups and metal adsorptive properties. *Langmuir* **2004,** 20 (6), 2233-2242.

47. Chiang, H. L.; Huang, C. P.; Chiang, P. C., The surface characteristics of activated carbon as affected by ozone and alkaline treatment. *Chemosphere* **2002,** 47 (3), 257-265.

48. Boudou, J. P.; Martinez-Alonzo, A.; Tascon, J. M. D., Introduction of acidic groups at the surface of activated carbon by microwave-induced oxygen plasma at low pressure. *Carbon* **2000,** 38 (7), 1021-1029.

49. Boudou, J. P.; Paredes, J. I.; Cuesta, A.; Martinez-Alonso, A.; Tascon, J. M. D., Oxygen plasma modification of pitch-based isotropic carbon fibres. *Carbon* **2003,** 41 (1), 41-56.

50. Pittman, C. U.; Jiang, W.; Yue, Z. R.; Gardner, S.; Wang, L.; Toghiani, H.; Leon, C., Surface properties of electrochemically oxidized carbon fibers. *Carbon* **1999,** 37 (11), 1797-1807.

51. Pittman, C. U.; Jiang, W.; Yue, Z. R.; Leon, C., Surface area and pore size distribution of microporous carbon fibers prepared by electrochemical oxidation. *Carbon* **1999,** 37 (1), 85-96.

52. Yue, Z. R.; Jiang, W.; Wang, L.; Gardner, S. D.; Pittman, C. U., Surface characterization of electrochemically oxidized carbon fibers. *Carbon* **1999,** 37 (11), 1785-1796.

53. Muller, E. A.; Gubbins, K. E., Molecular simulation study of hydrophilic and hydrophobic behavior of activated carbon surfaces. *Carbon* **1998,** 36 (10), 1433-1438.

54. Phillips, J.; Kelly, D.; Radovic, L.; Xie, F., Microcalorimetric study of the influence of surface chemistry on the adsorption of water by high surface area carbons. *Journal of Physical Chemistry B* **2000,** 104 (34), 8170-8176.

55. Dubinin, M. M.; Nikolaev, K. M.; Petukhova, G. A.; Polyakov, N. S., Adsorption of water vapor and microporous structures of carbon adsorbents. 18. Effect of active carbon surface chemistry on water-vapor adsorption. *Izvestiya Akademii Nauk SSSR, Seriya Khimicheskaya* **1991,** (1), 35-40.

56. Lopez-Ramon, M. V.; Stoeckli, F.; Moreno-Castilla, C.; Carrasco-Marin, F., Specific and non-specific interactions of water molecules with carbon surfaces from immersion calorimetry. *Carbon* **2000,** 38 (6), 825-829.

57. McCallum, C. L.; Bandosz, T. J.; McGrother, S. C.; Muller, E. A.; Gubbins, K. E., A molecular model for adsorption of water on activated carbon: Comparison of simulation and experiment. *Langmuir* **1999,** 15 (2), 533-544.

58. Garcia, T.; Murillo, R.; Cazorla-Amoros, D.; Mastral, A. M.; Linares-Solano, A., Role of the activated carbon surface chemistry in the adsorption of phenanthrene. *Carbon* **2004,** 42 (8-9), 1683-1689.

59. Szymanski, G. S.; Karpinski, Z.; Biniak, S.; Swiatkowski, A., The effect of the gradual thermal decomposition of surface oxygen species on the chemical and catalytic properties of oxidized activated carbon. *Carbon* **2002,** 40 (14), 2627-2639.

60. Quinlivan, P. A.; Li, L.; Knappe, D. R. U., Effects of activated carbon surface chemistry and pore structure on the adsorption of methyl tertiary-butyl ether and trichloroethene from natural water. *Proceedings - Annual Conference, American Water Works Association* **2001**, 2037-2050.

61. Al-Degs, Y.; Khraisheh, M. A. M.; Allen, S. J.; Ahmad, M. N., Effect of carbon surface chemistry on the removal of reactive dyes from textile effluent. *Water Research* **2000,** 34 (3), 927-935.

62. Terzyk, A. P., Further insights into the role of carbon surface functionalities in the mechanism of phenol adsorption. *Journal Of Colloid And Interface Science* **2003,** 268 (2), 301-329.

63. Ania, C. O.; Parra, J. B.; Pis, J. J., Oxygen-induced decrease in the equilibrium adsorptive capacities of activated carbons. *Adsorption Science & Technology* **2004,** 22 (4), 337-351.

64. Pittman, C. U.; He, G. R.; Wu, B.; Gardner, S. D., Chemical modification of carbon fiber surfaces by nitric acid oxidation followed by reaction with tetraethylenepentamine. *Carbon* **1997,** 35 (3), 317-331.

65. Mangun, C. L.; Benak, K. R.; Economy, J.; Foster, K. L., Surface chemistry, pore sizes and adsorption properties of activated carbon fibers and precursors treated with ammonia. *Carbon* **2001,** 39 (12), 1809-1820.

66. Bagreev, A.; Menendez, J. A.; Dukhno, I.; Tarasenko, Y.; Bandosz, T. J., Oxidative adsorption of methyl mercaptan on nitrogen-enriched bituminous coal-based activated carbon. *Carbon* **2005,** 43 (1), 208-210.

67. Xiao, B.; Boudou, J. P.; Thomas, K. M., Reactions of nitrogen and oxygen surface groups in nanoporous carbons under inert and reducing atmospheres. *Langmuir* **2005,** 21 (8), 3400-3409.

68. Perez-Cadenas, A. F.; Maldonado-Hodar, F. J.; Moreno-Castilla, C., On the nature of surface acid sites of chlorinated activated carbons. *Carbon* **2003,** 41 (3), 473-478.

69. Dastgheib Seyed, A.; Karanfil, T., Adsorption of oxygen by heat-treated granular and fibrous activated carbons. *Journal of colloid and interface science* **2004,** 274 (1), 1-8.

70. Menendez, J. A.; Phillips, J.; Xia, B.; Radovic, L. R., On the modification and characterization of chemical surface properties of activated carbon: In the search of carbons with stable basic properties. *Langmuir* **1996,** 12 (18), 4404-4410.

71. Puri, B. R., Surface Complexes on Carbon. In *Physics and Chemistry of Carbon*, Walker, P. L., Marcel Dekker, Inc.: New York, 1970; 6, 191-282.

72. Puri, B. R.; Hazra, R. S., Carbon-Sulfur Surface Complex on Charcoal. *Carbon* **1971,** 9, 123-134.

73. Menendez, J. A.; Suarez, D.; Fuente, E.; Montes-Moran, M. A., Contribution of pyrone-type structures to carbon basicity: Theoretical evaluation of the pK(a) of model compounds. *Carbon* **1999,** 37 (6), 1002-1006.

74. Suarez, D.; Menendez, J. A.; Fuente, E.; Montes-Moran, M. A., Contribution of pyrone-type structures to carbon basicity: An ab initio study. *Langmuir* **1999,** 15 (11), 3897-3904.

75. El-Sayed, Y.; Bandosz, T. J., Acetaldehyde adsorption on nitrogen-containing activated carbons. *Langmuir* **2002,** 18 (8), 3213-3218.

76. Jia, Y. F.; Xiao, B.; Thomas, K. M., Adsorption of metal ions on nitrogen surface functional groups in activated carbons. *Langmuir* **2002,** 18 (2), 470-478.

77. Montes-Moran, M. A.; Menendez, J. A.; Fuente, E.; Suarez, D., Contribution of the basal planes to carbon basicity: An ab initio study of the H3O+-pi interaction in cluster models. *Journal Of Physical Chemistry B* **1998,** 102 (29), 5595-5601.

78. Darmstadt, H.; Roy, C., Surface spectroscopic study of basic sites on carbon blacks. *Carbon* **2003,** 41 (13), 2662-2665.

79. Hattori, H., Solid base catalysts: generation of basic sites and application to organic synthesis. *Applied Catalysis A-General* **2001,** 222 (1-2), 247-259.

80. Barton, S. S.; Evans, M. J. B.; Halliop, E.; MacDonald, J. A. F., Acidic and basic sites on the surface of porous carbon. *Carbon* **1997,** 35 (9), 1361-1366.

81. Fuente, E.; Menendez, J. A.; Suarez, D.; Montes-Moran, M. A., Basic surface oxides on carbon materials: A global view. *Langmuir* **2003,** 19 (8), 3505-3511.

82. Dandekar, A.; Baker, R. T. K.; Vannice, M. A., Characterization of activated carbon, graphitized carbon fibers and synthetic diamond powder using TPD and drifts. *Carbon* **1998,** 36 (12), 1821-1831.

83. Phillips, J., Creating "basic" carbon surfaces. *Energeia* **1996,** 7 (5), 1-4.

84. Laine, N. R.; Vastola, F. J.; Walker, P. L., Jr., The importance of active surface area in the carbon-oxygen reaction. *Journal of Physical Chemistry* **1963,** 67 (10), 2030-4.

85. Darmstadt, H.; Cao, N. Z.; Pantea, D. M.; Roy, C.; Summchen, L.; Roland, U.; Donnet, J. B.; Wang, T. K.; Peng, C. H.; Donnelly, P. J., Surface activity and chemistry of thermal carbon blacks. *Rubber Chemistry And Technology* **2000,** 73 (2), 293-309.

86. Menendez, J. A.; Menendez, E. M.; Garcia, A.; Parra, J. B.; Pis, J. J., Thermal treatment of active carbons: A comparison between microwave and electrical heating. *Journal Of Microwave Power And Electromagnetic Energy* **1999,** 34 (3), 137-143.

87. Nabais, J. M. V.; Carrott, P. J. M.; Carrott, M.; Menendez, J. A., Preparation and modification of activated carbon fibres by microwave heating. *Carbon* **2004,** 42 (7), 1315-1320.

88. Daley, M. A.; Mangun, C. L.; DeBarr, J. A.; Riha, S.; Lizzio, A. A.; Donnals, G. L.; Economy, J., Adsorption of SO2 onto oxidized and heat-treated activated carbon fibers (ACFS). *Carbon* **1997,** 35 (3), 411-417.

89. Leon y Leon, C. A.; Radovic, L., Interfacial chemistry and electrochemistry of carbon surfaces. In *Chemistry and Physics of Carbon*, Thrower, P. A., Marcel Dekker, Inc.: New York, 1994; 24, 213-310.

90. Leon y Leon, C. A.; Solar, J. M.; Calemma, V.; Radovic, L. R., Evidence For The Protonation Of Basal-Plane Sites On Carbon. *Carbon* **1992,** 30 (5), 797-811.

91. Chang, M. B.; Wu, H. T.; Huang, C. K., Evaluation on speciation and removal efficiencies of mercury from municipal solid waste incinerators in Taiwan. *Science of the Total Environment* **2000,** 246 (2-3), 165-173.

92. Brna, T. G. *Toxic Metal Emissions from MWCs and Their Control*, Municipal Waste Combustion: Papers and Abstracts from the Second Annual International Conference, Tampa, FL, April 15-19, 1991.

93. Licata, A., Balles, E., Dougherty, J. *Coal-fired power plant mercury control by injecting sodium tetrsulfide*, Power Gen 2003, Las Vegas, NV, 2003.

94. Felsvang, K.; Gleiser, R.; Juip, G.; Nielsen, K. K., Activated Carbon Injection in Spray Dryer Esp/Ff for Mercury and Toxics Control. *Fuel Processing Technology* **1994,** 39 (1-3), 417-430.

95. Flora, J. R. V.; Hargis, R. A.; O'Dowd, W. J.; Pennline, H. W.; Vidic, R. D., Modeling sorbent injection for mercury control in baghouse filters: II - Pilot-scale studies and model evaluation. *Journal of the Air & Waste Management Association* **2003,** 53 (4), 489-496.

96. R. Chang, D. O., Developing Mercury Removal Methods for Power Plants. *EPRI Journal* **1994**, 46.

97. Biswas, P.; Senior, C.; Chang, R.; Vidic, R.; Laudal, D.; Brown, T., Mercury measurement and its control: What we know, have learned, and need to further investigate. *Journal of the Air & Waste Management Association* **1999,** 49 (12), 1469-1473.

98. Carey, T. R.; Hargrove, C. W.; Richardson, C. F.; Chang, R., Factors affecting mercury control in utility flue gas using activated carbon. *Journal of the Air & Waste Management Association* **1998,** 48 (12), 1166-1174.

99. Krishnan, S. V.; Gullett, B. K.; Jozewicz, W., Sorption of elemental mercury by activated carbons. *Environmental Science & Technology* **1994,** 28 (8), 1506-1512.

100. Li, Y. H.; Lee, C. W.; Gullett, B. K., Importance of activated carbon's oxygen surface functional groups on elemental mercury adsorption. *Fuel* **2003,** 82 (4), 451-457.

101. McLaughlin, J. B. Activated carbon adsorption for the removal of mercury from flue gas emissions. Thesis MS --University of Pittsburgh, Pittsburgh, PA, 1995.

102. Vidic, R. D.; Siler, D. P., Vapor-phase elemental mercury adsorption by activated carbon impregnated with chloride and chelating agents. *Carbon* **2001,** 39 (1), 3-14.

103. Liu, W.; Vidic, R. D.; Brown, T. D., Optimization of sulfur impregnation protocol for fixed bed application of activated carbon-based sorbents for gas-phase mercury removal. *Environmental Science & Technology* **1998,** 32 (4), 531-538.

104. Liu, W.; Vidic, R. D.; Brown, T. D., Optimization of high temperature sulfur impregnation on activated carbon for permanent sequestration of elemental mercury vapors. *Environmental Science & Technology* **2000,** 34 (3), 483-488.

105. Shinha, R. K. W., P. L., Removal of mercury by sulfurized carbons. *Carbon* **1972,** 10, 754-756.

106. Otani, Y. E., H.; Kanooka, C.; Uchiwa,I.; Nishino, H., Removal of mercury vapor from air with sulfur-impregnated adsorbents. *Environmental Science & Technology* **1988,** 22, 708-711.

107. Korpiel, J. A. Effect of sulfur impregnation method on activated carbon adsorption of vapor-phase mercury. Thesis, MS --University of Pittsburgh, Pittsburgh, PA, 1996.

108. Korpiel, J. A., Vidic, R.D., Effect of sulfur impregnation method on activated carbon uptake of gas-phase mercury. *Environmental Science & Technology* **1997,** 31 (8), 2319-2325.

109. Kwon, S.; Vidic, R. D., Evaluation of two sulfur impregnation methods on activated carbon and bentonite for the production of elemental mercury sorbents. *Environmental Engineering Science* **2000,** 17 (6), 303-313.

110. Hsi, H. C.; Rood, M. J.; Rostam-Abadi, M.; Chen, S. G.; Chang, R., Mercury adsorption properties of sulfur-impregnated adsorbents. *Journal of Environmental Engineering-Asce* **2002,** 128 (11), 1080-1089.

111. Hsi, H. C.; Rood, M. J.; Rostam-Abadi, M.; Chen, S. G.; Chang, R., Effects of sulfur impregnation temperature on the properties and mercury adsorption capacities of activated carbon fibers (ACFs). *Environmental Science & Technology* **2001,** 35 (13), 2785-2791.

112. Hsi, H. C.; Chen, S. G.; Rostam-Abadi, M.; Rood, M. J.; Richardson, C. F.; Carey, T. R.; Chang, R., Preparation and evaluation of coal-derived activated carbons for removal of mercury vapor from simulated coal combustion flue gases. *Energy & Fuels* **1998,** 12 (6), 1061-1070.

113. Lee, S. H.; Park, Y. O., Gas-phase mercury removal by carbon-based sorbents. *Fuel Processing Technology* **2003,** 84 (1-3), 197-206.

114. Daza, L.; Mendioroz, S.; Pajares, J. A., Influence of texture and chemical composition on sulphur deposition onto sepiolites. *Applied Clay Science* **1989,** 4 (5-6), 389-402.

115. Daza, L.; Mendioroz, S.; Pajares, J. A., Mercury elimination from gaseous streams. *Applied Catalysis B: Environmental* **1993,** 2, 277-287.

116. Guijarro, M. I.; Mendioroz, S.; Munoz, V., Effect of morphology of sulfurized materials in the retention of mercury from gas streams. *Industrial & Engineering Chemistry Research* **1998,** 37 (3), 1088-1094.

117. Dubinin, M. M., Physical adsorption of gases and vapors in micropores. *Progress in Surface and Memberane Science* **1975,** 9, 1-70.

118. Dubinin, M. M., Fundamentals of the Theory of Adsorption of Micropores of Carbon Adsrobents: Characteristics of their Adsorption Properties and Microporous Structures. *Carbon* **1989,** 27 (3), 457-467.

119. Boki, K.; Tanada, S., Adsorption of hydrogen sulfide on activated carbon. *Chem. Pharm. Bull.* **1980,** 28 (4), 1270-1275.

120. Aranovich, G. L.; Donohue, M. D., Adsorption-Isotherms for Microporous Adsorbents. *Carbon* **1995,** 33 (10), 1369-1375.

121. Lee, W. H.; Reucroft, P. J., Vapor adsorption on coal- and wood-based chemically activated carbons - (III) - NH_3 and H_2S adsorption in the low relative pressure range. *Carbon* **1999,** 37 (1), 21-26.

122. Lee, W. H.; Reucroft, P. J., Vapor adsorption on coal- and wood-based chemically activated carbons - (II) - adsorption of organic vapors. *Carbon* **1999,** 37 (1), 15-20.

123. Lee, W. H.; Reucroft, P. J., Vapor adsorption on coal- and wood-based chemically activated carbons - (I) - Surface oxidation states and adsorption of H_2O. *Carbon* **1999,** 37 (1), 7-14.

124. Bagreev, A.; Adib, F.; Bandosz, T. J., Initial heats of H_2S adsorption on activated carbons: Effect of surface features. *Journal of Colloid and Interface Science* **1999,** 219 (2), 327-332.

125. Bagreev, A.; Bandosz, T. J., Study of hydrogen sulfide adsorption on activated carbons using inverse gas chromatography at infinite dilution. *Journal of Physical Chemistry B* **2000,** 104 (37), 8841-8847.

126. Bandosz, T. J., On the adsorption/oxidation of hydrogen sulfide on activated carbons at ambient temperatures. *Journal of Colloid and Interface Science* **2002,** 246 (1), 1-20.

127. Bandosz, T. J., Effect of pore structure and surface chemistry of virgin activated carbons on removal of hydrogen sulfide. *Carbon* **1999,** 37 (3), 483-491.

128. Bandosz, T.; Askew, S.; Kelly, W. R.; Bagreev, A.; Adib, F.; Turk, A., Biofiltering action on hydrogen sulfide by unmodified activated carbon in sewage treatment plants. *Water Science and Technology* **2000,** 42 (1-2), 399-401.

129. Mikhalovsky, S. V.; Zaitsev, Y. P., Catalytic properties of activated carbons.1. Gas-phase oxidation of hydrogen sulphide. *Carbon* **1997,** 35 (9), 1367-1374.

130. Pieplu, A.; Saur, O.; Lavalley, J. C.; Legendre, O.; Nedez, C., Claus catalysis and H_2S selective oxidation. *Catalysis Reviews-Science and Engineering* **1998,** 40 (4), 409-450.

131. Bagreev, A.; Bandosz, T. J., A role of sodium hydroxide in the process of hydrogen sulfide adsorption/oxidation on caustic-impregnated activated carbons. *Industrial & Engineering Chemistry Research* **2002,** 41 (4), 672-679.

132. Chiang, H. L.; Tsai, J. H.; Tsai, C. L.; Hsu, Y. C., Adsorption characteristics of alkaline activated carbon exemplified by water vapor, H_2S, and CH3SH gas. *Separation Science and Technology* **2000,** 35 (6), 903-918.

133. Tsai, J. H.; Jeng, F. T.; Chiang, H. L., Removal of H_2S from exhaust gas by use of alkaline activated carbon. *Adsorption-Journal of the International Adsorption Society* **2001,** 7 (4), 357-366.

134. Przepiorski, J.; Oya, A., K_2CO_3-loaded deodorizing activated carbon fibre against H_2S gas: Factors influencing the deodorizing efficiency and the regeneration method. *Journal of Materials Science Letters* **1998,** 17 (8), 679-682.

135. Przepiorski, J.; Yoshida, S.; Oya, A., Structure of K_2CO_3-loaded activated carbon fiber and its deodorization ability against H_2S gas. *Carbon* **1999,** 37 (12), 1881-1890.

136. Wu, Q. F.; Yakshinskiy, B. V.; Madey, T. E., Adsorption and decomposition of H_2S on UO_2(001). *Surface Science* **2003,** 523 (1-2), 1-11.

137. Rodriguez, J. A.; Maiti, A., Adsorption and decomposition of H_2S on MgO(100), NiMgO(100), and ZnO(0001) surfaces: A first-principles density functional study. *Journal of Physical Chemistry B* **2000,** 104 (15), 3630-3638.

138. Nelen, L. M.; Fuller, K.; Greenlief, C. M., Adsorption and decomposition of H_2S on the Ge(100) surface. *Applied Surface Science* **1999,** 150 (1-4), 65-72.

139. Hung, W. H.; Chen, H. C.; Chang, C. C.; Hsieh, J. T.; Hwang, H. L., Adsorption and decomposition of H_2S on InP(100). *Journal of Physical Chemistry B* **1999,** 103 (18), 3663-3668.

140. Puri, B. R., Jain, C. M., Hazra, R. S., *Journal of Indian Chemical Society* **1966,** 43 (67).

141. Blayden, H. E., Patrick, J. W., Solid Complexes of Carbon and Sulfur- I. Sulfurized Polymer Carbons. *Carbon* **1967,** 5, 533-544.

142. Valenzuela Calahorro, C.; Macias Garcia, A.; Bernalte Carcia, A.; Gomez Serrano, V., Study of Sulfur Introduction In Activated Carbon. *Carbon* **1990,** 28, 321-335.

143. Puri, B. R., *Surface Complexes on Carbon*. Marcel Dekker, Inc.: New York, 1970.

144. Sugawara, K.; Enda, Y.; Kato, T.; Sugawara, T.; Shirai, M., Effect of hydrogen sulfide on organic sulfur behavior in coal and char during heat treatments. *Energy & Fuels* **2003,** 17 (1), 204-209.

145. Ozaki, J.; Yoshimoto, Y.; Oya, A.; Takarada, T.; Kuzunetsov, V. V.; Ismagilov, Z. R., H_2S decomposition activity of TS carbon derived from furan resin. *Carbon* **2001,** 39 (10), 1611-1612.

146. Kok, M. D.; Schouten, S.; Damste, J. S. S., Formation of insoluble, nonhydrolyzable, sulfur-rich macromolecules via incorporation of inorganic sulfur species into algal carbohydrates. *Geochimica et Cosmochimica Acta* **2000,** 64 (15), 2689-2699.

147. van Dongen, B. E.; Schouten, S.; Sinninghe Damsté, J. S., Sulfurization of carbohydrates results in a sulfur-rich, unresolved complex mixture in kerogen pyrolysates. *Energy & Fuels* **2003,** 17 (4), 1109-1118.

148. Trofimov, B. A.; Skotheim, T. A.; Mal'kina, A. G.; Sokolyanskaya, L. V.; Myachina, G. F.; Korzhova, S. A.; Vakul'skaya, T. I.; Kovalev, I. P.; Mikhailik, Y. V.; Boguslavskii, L. I., Sulfurization of polymers 3. Paramagnetic and redox properties of sulfurized polyethylene. *Russian Chemical Bulletin* **2000,** 49 (5), 870-873.

149. Trofimov, B. A.; Skotheim, T. A.; Mal'kina, A. G.; Sokolyanskaya, L. V.; Myachina, G. F.; Korzhova, S. A.; Stoyanov, E. S.; Kovalev, I. P., Sulfurization of polymers 2. Polythienothiophene and related structures from polyethylene and elemental sulfur. *Russian Chemical Bulletin* **2000,** 49 (5), 863-869.

150. Filik, J.; Lane, I. M.; May, P. W.; Pearce, S. R. J.; Hallam, K. R., Incorporation of Sulfur into Hydrogenated Amorphous Carbon Films. *Diamond and Related Materials* **2004,** 13, 1377-1384.

151. Kim, M.; Cho, S.; Lee, Y. K.; Boo, J.-H., Characterization of polymer-like thin films deposited on silicon and glass substrates using PECVD method. *Thin solid films* **2004,** 30, 592-598.

152. Saleh, J. M., Interaction of sulfur compounds with palladium. *Transactions of the Faraday Society* **1970,** 66 (1), 242-50.

153. Ghosh, T. K., Tollefson, E.L., Kinetics and Reaction Mechanism of Hydrogen Sulfide Oxidation over Activated Carbon in the Temperature Range of 125-200°C. *The Canadian Journal of Chemical Engineering* **1986,** 64, 969-976.

154. Sreeramamurthy, R., Menon, P.G., Oxidation of H_2S on Active Carbon Catalyst. *Journal of Catalysis* **1974,** 37, 287-296.

155. Steijns, M., Derks, F., Verloop, A., Mars, P., *Journal of Catalysis* **1976,** 2, 87-96.

156. Coskun, I.; Tollefson, E. L., Oxidation of Low Concentrations of Hydrogen Sulfide over Activated Carbon. *The Canadian Journal of Chemical engineering* **1980,** 58, 72-76.

157. Klein, J., Henning, K., Catalytic Oxidation of Hydrogen Sulphide on Activated Carbons. *Fuel* **1984,** 63, 1064-1067.

158. Mikhalovsky, S. V. Z., Y. P., Catalytic properties of activated carbons. I. Gas-phase oxidation of hydrogen sulfide. *Carbon* **1997,** 35 (9), 1367-1374.

159. Bagreev, A.; Bandosz, T. J., H_2S adsorption/oxidation on unmodified activated carbons: importance of prehumidification. *Carbon* **2001,** 39 (15), 2303-2311.

160. Bagreev, A.; Rahman, H.; Bandosz, T. J., Thermal regeneration of a spent activated carbon previously used as hydrogen sulfide adsorbent. *Carbon* **2001,** 39 (9), 1319-1326.

161. Yan, R.; Liang, D. T.; Tsen, L.; Tay, J. H., Kinetics and mechanisms of H_2S adsorption by alkaline activated carbon. *Environmental Science & Technology* **2002,** 36 (20), 4460-4466.

162. Yan, R.; Chin, T.; Ng, Y. L.; Duan, H.; Liang, D. T.; Tay, J. H., Influence of surface properties on the mechanism of H_2S removal by alkaline activated carbons. *Environmental Science & Technology* **2004,** 38 (1), 316-323.

163. Hayes, J. S. J. *Novoloid Nonwovens*, Nonwoven Symposium, Atlanta, GA, 1985.

164. Pelekani, C.; Snoeyink, V. L., Competitive adsorption between atrazine and methylene blue on activated carbon: the importance of pore size distribution. *Carbon* **2000,** 38 (10), 1423-1436.

165. Mangun, C. L.; DeBarr, J. A.; Economy, J., Adsorption of sulfur dioxide on ammonia-treated activated carbon fibers. *Carbon* **2001,** 39 (11), 1689-1696.

166. Foster, K. L.; Fuerman, R. G.; Economy, J.; Larson, S. M.; Rood, M. J., Adsorption Characteristics of Trace Volatile Organic-Compounds in Gas Streams onto Activated Carbon-Fibers. *Chemistry of Materials* **1992,** 4 (5), 1068-1073.

167. Zhu, Z. H.; Radovic, L. R.; Lu, G. Q., Effects of acid treatments of carbon on N2O and NO reduction by carbon-supported copper catalysts. *Carbon* **2000,** 38 (3), 451-464.

168. Flynn, J. H.; Wall, L. A., A Quick, Direct Method for the Determination of Activation Energy from Thermogravimetric Data. *Polymer Letters* **1966,** 4, 323-328.

169. Boehm, H. P., Functional Groups on the Surfaces of Solids. *Angewandte Chemie International Edtion* **1966,** 5 (6), 533-622.

170. Boehm, H. P.; Diehl, E.; Heck, W.; Sappok, R., Surface Oxides of Carbon. *Angewandte Chemie International Edtion* **1964,** 3 (10), 669-677.

171. Huffman, G. P.; Ganguly, B.; Zhao, J.; Rao, K.; Shah, N.; Feng, Z.; Huggins, F. E.; Taghiei, M. M.; Lu, F. L.; Wender, I.; Pradhan, V. R.; Tierney, J. W.; Seehra, M. S.; Ibrahim, M. M.; Shabtai, J.; Eyring, E. M., Structure And Dispersion Of Iron-Based Catalysts For Direct Coal-Liquefaction. *Energy & Fuels* **1993,** 7 (2), 285-296.

172. Taghiei, M. M.; Huggins, F. E.; Shah, N.; Huffman, G. P., Insitu X-Ray Absorption Fine-Structure Spectroscopy Investigation Of Sulfur Functional-Groups In Coal During Pyrolysis And Oxidation. *Energy & Fuels* **1992,** 6 (3), 293-300.

173. Huffman, G. P.; Shah, N.; Taghiei, M. M.; Lu, F. L.; Huggins, F. E., Quantitative-Analysis Of Sulfur Functional Forms And Reactions By Xafs Spectroscopy. *Abstracts Of Papers Of The American Chemical Society* **1991,** 202, 56-FUEL.

174. Bouzaza, A.; Laplanche, A.; Marsteau, S., Adsorption-oxidation of hydrogen sulfide on activated carbon fibers: effect of the composition and the relative humidity of the gas phase. *Chemosphere* **2004,** 54 (4), 481-488.

175. Bashkova, S.; Bagreev, A.; Bandosz, T. J. *Catalytic properties of activated carbon surface in the process of adsorption/oxidation of methyl mercaptan*, Carbon 2004, Providence, RI, 2004.

176. Olson, E. S.; Laumb, J. D.; Benson, S. A.; Dunham, G. E.; Sharma, R. K.; Mibeck, B. A.; Miller, S. J.; Holmes, M. J.; Pavlish, J. H., Chemical mechanisms in mercury emission control technologies. *Journal De Physique Iv* **2003,** 107, 979-982.

177. Uranowski, L. J.; Tessmer, C. H.; Vidic, R. D., The effect of surface metal oxides on activated carbon adsorption of phenolics. *Water Research* **1998,** 32 (6), 1841-1851.

178. Liu, W. Development of novel adsorbents for the control of vapor-phase mercury emissions. Ph. D. Thesis, University of Pittsburgh, Pittsburgh, PA USA, 1999.

179. Hayden, R. A.; Butterworth, S. L. Process for regenerating nitrogen-treated carbonaceous chars used for hydrogen sulfide removal. US Patent 5,494,869, 1994.

180. Matviya, T. M.; Hayden, R. A. Catalytic carbon. US Patent 5,356,849, 1994.

181. Bagreev, A.; Menendez, J. A.; Dukhno, I.; Tarasenko, Y.; Bandosz, T. J., Bituminous coal-based activated carbons modified with nitrogen as adsorbents of hydrogen sulfide. *Carbon* **2004,** 42 (3), 469-476.

182. Arenillas, A.; Drage, T. C.; Smith, K.; Snape, C. E., CO_2 removal potential of carbons prepared by co-pyrolysis of sugar and nitrogen containing compounds. *Journal Of Analytical And Applied Pyrolysis* **2005,** 74 (1-2), 298-306.

183. Yan, J. D.; Yang, J. L.; Liu, Z. Y., SH radical: The key intermediate in sulfur transformation during thermal processing of coal. *Environmental Science & Technology* **2005,** 39 (13), 5043-5051.

184. Puri, B. R., R. S. Hazra, Carbon-Sulfur Surface Complex on Charcoal. *Carbon* **1971,** 9, 123-134.

185. Leon y Leon, C. A.; Radovic, L. R., *Intefacial chemistry and electrochemistry of carbon surfaces*. Marcel Dekker, Inc.: New York, NY, 1994; 24, p 213-310.

186. Alqahtany, H.; Chiang, P. H.; Eng, D.; Stoukides, M.; Robbat, A., Electrocatalytic Decomposition of Hydrogen-Sulfide. *Catalysis Letters* **1992,** 13 (3), 289-295.

187. Daza, L.; Mendioroz, S.; Pajares, J. A., Mercury Elimination From Gaseous Streams. *Applied Catalysis B-Environmental* **1993,** 2 (4), 277-287.

188. JBerkowitz, J., Molecular Composition of Sulfur Vapor. In *Elemental Sulfur (Book), Interscience Publishers, NY*, Meyer, B., 1965; 125-160.

189. Meyer, B., Preparation and Properties of Sulfur Allotropes. In *Elemental Sulfur*, Meyer, B., Interscience Publishers: 1965; 71-94.

190. Sanderson, R. T., *Chemical Bonds and Bond Energy*. Academic Press: New York, 1976.

191. Dubinin, M. M., The Potential Theory of Adsorption of Gases and Vapors for Adsorbents with Energetically Nonuniform Surfaces. *Chemical Reviews* **1960,** 60 (2), 235-241.

192. Kwon, S.; Borguet, E.; Vidic, R. D., Impact of surface heterogeneity on mercury uptake by carbonaceous sorbents under UHV and atmospheric pressure. *Environmental Science & Technology* **2002,** 36 (19), 4162-4169.